Virginia Kendall 250

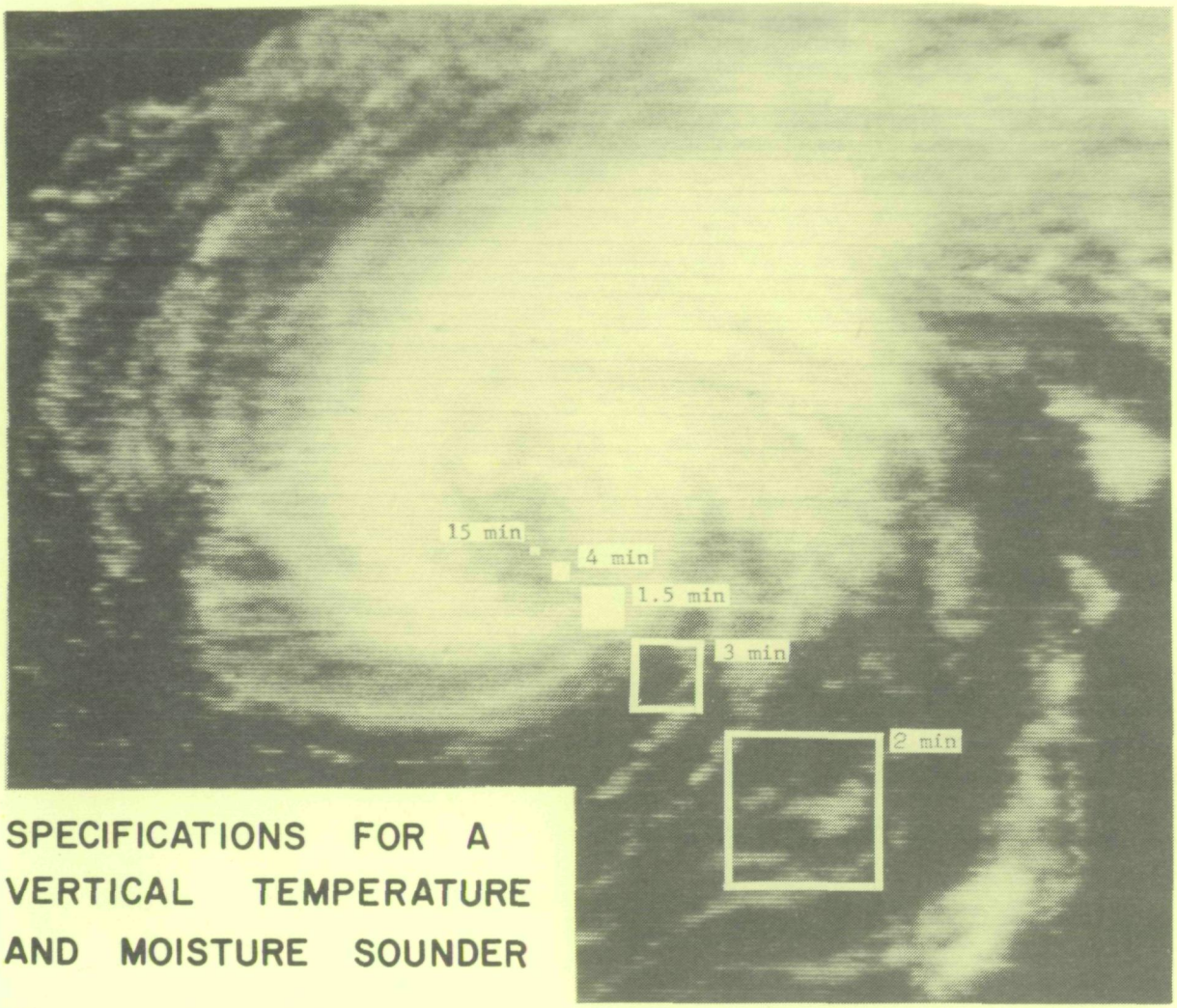

SPECIFICATIONS FOR A VERTICAL TEMPERATURE AND MOISTURE SOUNDER

FOR THE SYNCHRONOUS METEOROLOGICAL SATELLITES

A REPORT FROM THE

SPACE SCIENCE AND ENGINEERING CENTER

SMS SOUNDER SPECIFICATION

Final Report Under Extended NASA Contract NAS5-21607

V. E. Suomi (Principal Investigator)
L. A. Sromovsky (Project Manager)
R. J. Krauss
A. J. Stamm

Space Science and Engineering Center
University of Wisconsin
1225 West Dayton Street
Madison, Wisconsin

30 April 1972

THIS IS A NEW REPORT, UNDER THE EXTENDED NASA CONTRACT NAS5-21607, WHICH SUPERSEDES, AND SUBSTANTIALLY DIFFERS FROM, ALL OTHERS DESCRIBING SMS MODIFICATIONS FOR SOUNDING. IMPORTANT SIMPLIFICATIONS OF THE SOUNDER DESIGN HAVE BEEN MADE WITHOUT SERIOUS DEGRADATIONS OF PERFORMANCE. SPECIFICALLY, THE PRESENT DESIGN REQUIRES ONLY ONE FILTER WHEEL, INSTEAD OF TWO, AND A SINGLE FIXED RELAY LENS SYSTEM, INSTEAD OF A TWO LENS TURRET.

COVER: The cover photograph of Hurricane Ginger is an enlargement of an ATS 3 image from 28 September 1971. The superimposed squares indicate typical sounding resolution capabilities of the proposed SMS modifications. The solid squares, and corresponding times, apply to the fixed latitude mode of scanning and the open squares apply to a reduced frame amplitude (1.2% of full disc) mode of scanning. For a detail discussion of the full range of capabilities see Sections III and IV, especially Figure 10.

TABLE OF CONTENTS

I. INTRODUCTION

This report is a specification document for a vertical temperature and moisture sounder applicable to the Visible and Infrared Spin-Scan Radiometer (VISSR) to be flown on the Synchronous Meteorological Satellites (SMS). Work on this specification was performed by the University of Wisconsin Space Science and Engineering Center (SSEC) for NASA/GSFC under contract NAS 5-21607. This effort has been governed by two major objectives: meteorological utility and instrumental simplicity. The time continuity of geosynchronous observations together with the built in growth potential of the VISSR and SMS systems has made it possible to meet both objectives without seriously compromising either.

SMS SOUNDER CAPABILITIES

Temperature and water vapor soundings every 200 to 400 km at a rate of up to one every hour for each grid point would be possible with the modified SMS under normal operation. This grid spacing is comparable to that of the weather information gathering system in the continental U. S. (a relatively data rich region). Since this would also apply to currently data poor regions such as the oceans, the predictive capabilities of numerical forecasting can be significantly increased.

Under optional modes of operation it would be possible to make soundings with a grid spacing of 10 to 14 km over selected regions of the earth. For example, five soundings could be made in the partially clear eye of a hurricane every few hours, day and night, from birth to death. From these soundings the central pressure, a significant measure of hurricane strength, could be determined as the hurricane developes in the Atlantic and on its way to the U. S. coast. This high resolution capability would provide improved warning of hurricane destructive capability and provide an improved base of information for moving forward our understanding of hurricanes. Similar observations in the vicinity of jet streams could be used to estimate wind velocities in the jets. Other phenomena of mesoscale importance could be observed in similar detail at will.

Perhaps the best way to illustrate the great potential of the satellite sounding system described in this document is to show a series of photos taken from ATS-III on 28 September 1971 (Figure 1). On this day hurricane Ginger was present in the Atlantic and a tornado crossed NE Wisconsin. Enlargements of the regions containing these two storms are also shown. Superimposed on these enlarged photos are two sizes of squares. The largest (approximately the size of a GARP grid box) indicates the averaging area of soundings which would be available for the whole earth in about one hour. The small square (approximately 11 km on a side) shows the sounding detail that could be obtained for the hurricane area or the tornado area in about one hour when the sounder is used in a limited scan mode. Individual soundings at this resolution are available in only minutes. Thus the geostationary sounder presented in this document could provide an enormous improvement in our ability to observe small-scale severe weather phenomena.

The specific utility of geosynchronous sounding data has already been recognized by the scientific community. For example, Jastrow and Halem (1970) stress three uses for geosynchronous sounder data: (1) a supplement to polar orbiter data which improves wind estimates by 35%; (2) a backup to polar orbiter data which can provide wind errors as small as ∿1.5 m/s; and (3) fine time and space resolution data which would improve short range forecasts for small areas.

These views are also endorsed by the United States GARP Committee who state as recommendation No. 7 in the document Plan for U. S. Participation in the GARP Atlantic Tropical Experiment, "It would be desirable to have infrared temperature soundings from geostationary satellites, even if only on an experimental basis, since these would supply unique temperature and moisture data continuously in time. In addition, this IR sounder would complement the polar-orbiting IR sounders that are required for the First GARP Global Experiment (FGGE) in 1976."

The Joint Organizing Committee (JOC) has also stated that geostationary IR temperature soundings would be highly desirable for GATE in the report of the 5th Session at Bombay:

4.4.1.2 JOC also suggested the following additional observations as highly desirable for GATE:

> "Infrared temperature soundings, at least on an experimental basis from geostationary satellite, to significantly augment the aircraft observations by supplying valuable data, nearly continuous in time that would, for example, delineate temperature anomalies associated with the large wave-scale as well as the meso-convective scale phenomena."

In February 1971, the Tropical Experiment Board Report (see 4.6.1)

> "Acknowledged the importance of providing the observing capability required as recommended by the JOC for the full success of the experiment and stressed the need for a complete examination of the practicability of obtaining these types of observations."

The remarks by various bodies on the utility of a geostationary sounder related earlier tend to stress the applicability to problems in GATE and the FGGE, GARP. The great potential of the modified SMS in problems related to mesoscale phenomena could make substantial advances in satisfying another requirement for meteorological observations. These are discussed in a National Academy report, "The Atmospheric Sciences and Man's Needs" (1971) which stresses the great need to provide better predictions of severe weather as stated in their recommendation I-4:

> "In order to advance our understanding of mesoscale phenomena and to improve ability to forecast these phenomena, emphasis should be placed on research on fronts, jet streams, organized convection, and other phenomena of mesoscale."

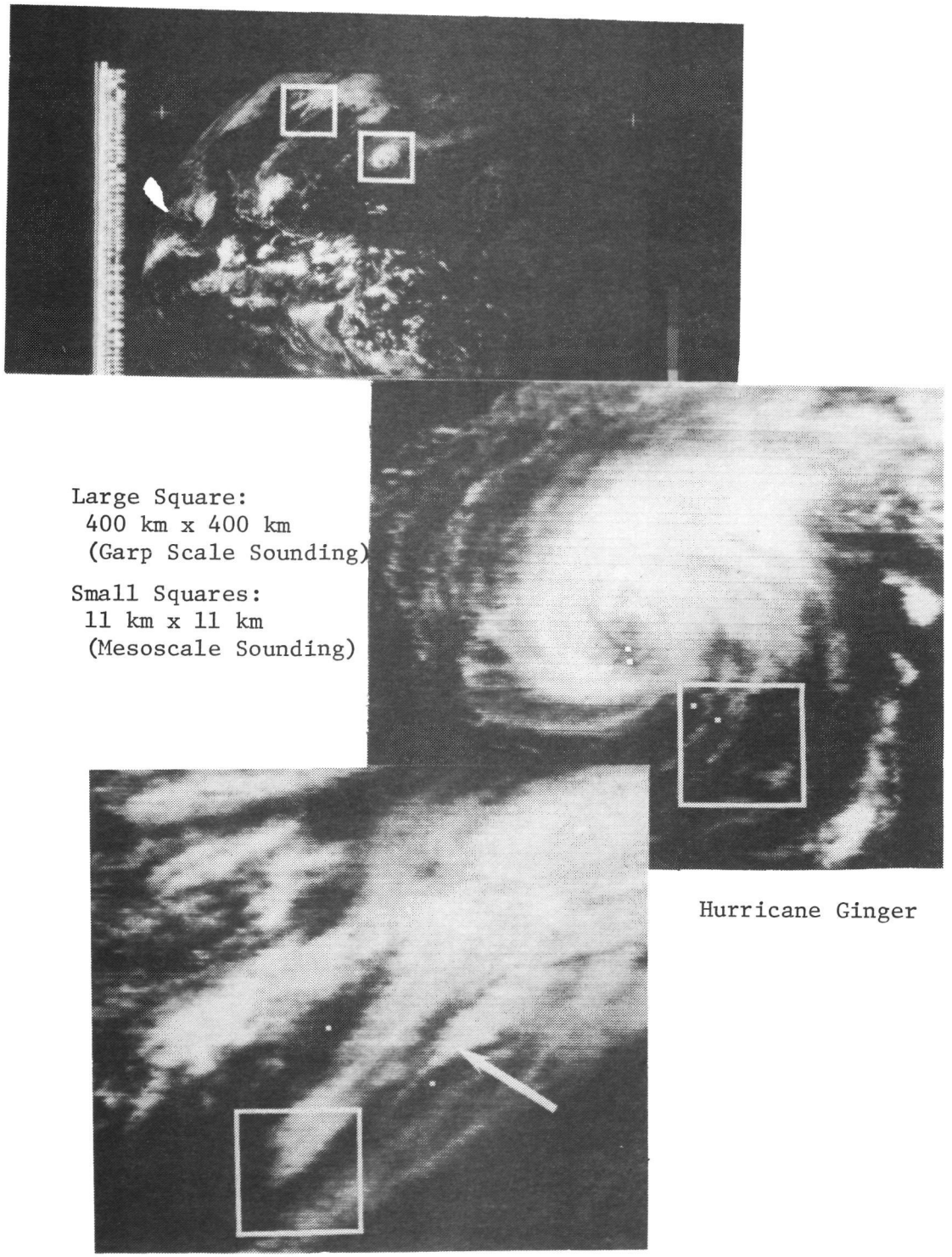

Figure 1. Spatial resolution capabilities of the SMS Sounder. Images are from ATS-3 (28 September 1971).

SMS MODIFICATIONS FOR SOUNDING

Only relatively minor modifications of the SMS system are required to schieve the highly desirable capability for vertical temperature and water vapor soundings of the atmosphere. This is so because the SMS (and the VISSR in particular) already contains most of the essential ingredients of a sounder (Figure 2). The large diameter telescope, the high efficiency radiative cooler, the data transmission system, and other components necessary for the measurement of surface temperatures are also capable of supporting vertical sounding instrumentation. The present IR filter used on SMS avoids effects of water vapor and carbon dioxide by selecting the wavelength range of 10.5μm to 12.6μm. By replacing this filter with a filter wheel which can select additional wavelengths sensitive to the effects of these atmospheric constituents it becomes possible to determine not only surface and cloud top temperatures, but also the three dimensional structure of atmospheric temperature and humidity.

Associated with this primary modification are several other changes which are also relatively minor. The essence of the entire set of modifications may be summarized as follows (see Figure 2):

1) The mounting of a twelve position filter wheel and stepper motor on the focus drive plate.

2) An increase in relay lens diameter (clear aperture) from approximately 0.72 in (1.83 cm) to 0.76 in (1.93 cm) and an increase in optical gain from 5.5 to approximately 7.0.

3) Replacement of the current two detector array with a six detector array with an extended cutoff wavelength and changing the IFOV from 0.25 mr to 0.30 mr.

4) Addition of four preamplifiers to obtain a total of six (one for each detector).

5) Modification of the analog switching which controls the IR data input to the VISSR MULTIPLEXER so that six detectors are sampled instead of two.

6) Appropriate additions to the CDA ground station so that sounder data can be stored and processed.

It is important to note that these modifications do not interfere with the visible and IR imaging functions of SMS. Use of a six detector array makes it possible to scan six IR imaging lines in one SMS rotation (without modification this would require six SMS rotations). Thus a complete 11μm IR image of the earth's disc is obtained by using only one rotation (or scan) out of every six. During the intermediate scans, (five of every six) other wavelength ranges are sampled by advancing the filter wheel to other positions. With this interlaced scanning method sounding measurements can be made without interrupting the 11μm IR imaging measurements.

The main body of this report details the design and performance specifications. Supporting research is discussed in the appendices.

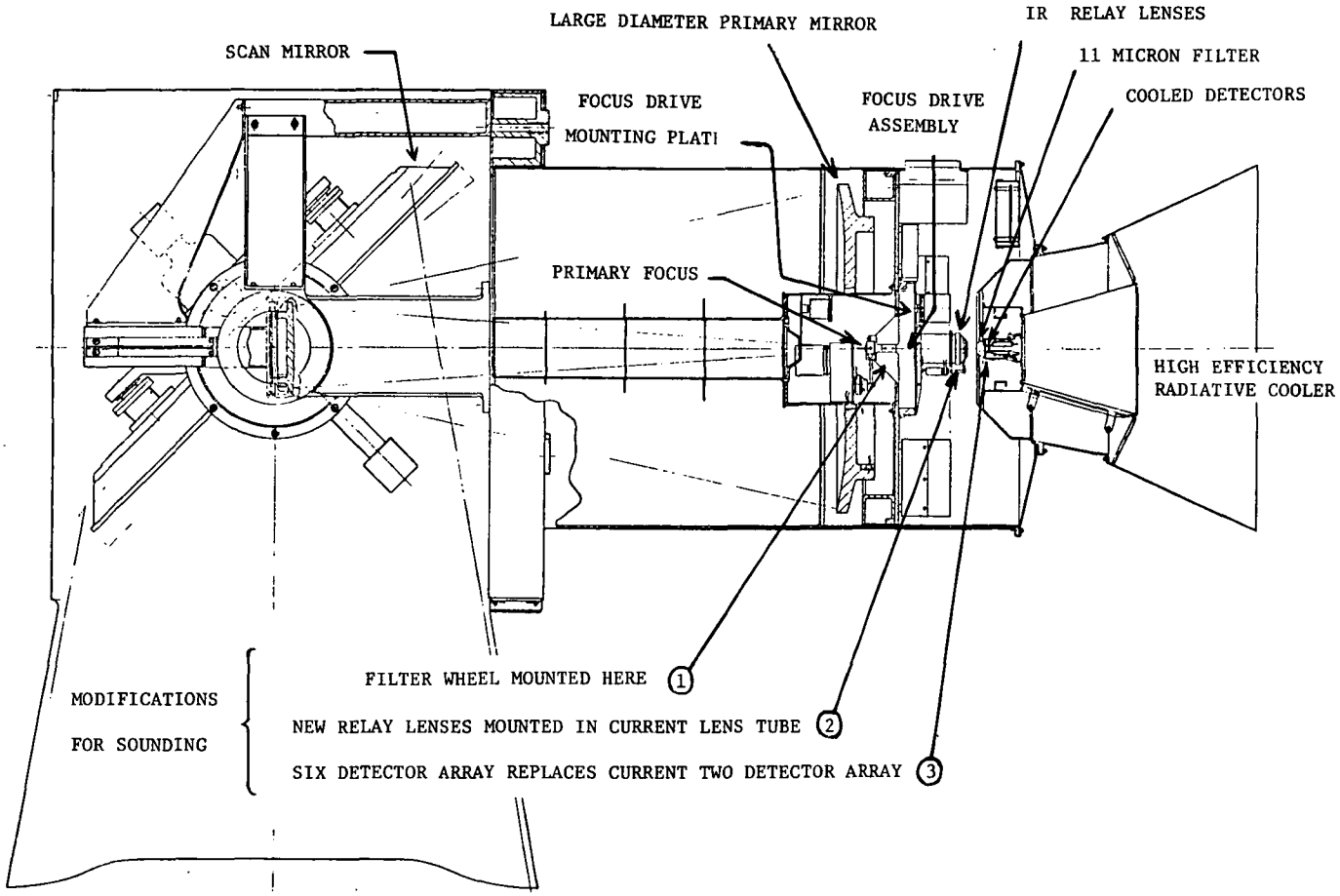

Figure 2. VISSR cross sectional diagram showing areas of modifications for sounding.

II. DESIGN SPECIFICATIONS

A VISSR SOUNDER retrofit can be accomplished in several different ways. The design specified in this section is selected on the basis of radiometric performance, cooling requirements, and simplicity. Making maximum use of current VISSR components and subsystems, the specified design obtains adequate sounding performance within the present capabilities of the VISSR radiative cooler without the complexities of either turreted lenses or pulsed-bias detectors. Minor modifications in five general areas of the SMS system are required for sounding:

1) IR OPTICS - introduction of a filter wheel and new relay lenses;

2) DETECTORS - replacement of the current two detectors (0.25 mr) with a six detector array (0.30 mr);

3) VISSR ELECTRONICS - addition of four new preamplifiers and a six position analog switch for the multiplexer input;

4) SMS/VISSR INTERFACE - a slight increase in command and housekeeping transmission; and

5) GROUND STATION DATA HANDLING - provision for storage of six IR scan lines and installation of sounder data processing system.

These modifications make possible vertical temperature and water vapor sounding without interfering with the visible and IR imaging functions of VISSR. Details of these modifications are specified in the remainder of this section. Operation and performance characteristics of the sounding instrumentation are treated in Sections III and IV respectively.

1. VISSR Sounder Optical Design

The basic components of the modified IR optical system consist of a filter wheel, relay lenses, and a calibration shutter. The way in which these components can be fitted within the present VISSR IR configuration (Figure 3(a)) is shown in Figure 3(b). Specific requirements for each component involved in the modification are listed below:

Filter Wheel: A twelve position filter wheel is required for the SMS sounder package. The approximate size of the wheel and the filter elements on it are shown in Figure 4. Its location near the prime focus (Figure 3) accounts for its relatively small size (approximately 2.5 inches in diameter). In this position filters are subject to diverging radiation from the f/ 7.17 primary. However, filters designed for operation with normally incident collimated radiation will perform with negligible degradation in this configuration (Baker, 1967).

Table 1 summarizes the spectral character of the twelve filters specified for the sounder. Channels 1 through 9 are used for vertical

(a) PRESENT VISSR IR CONFIGURATION

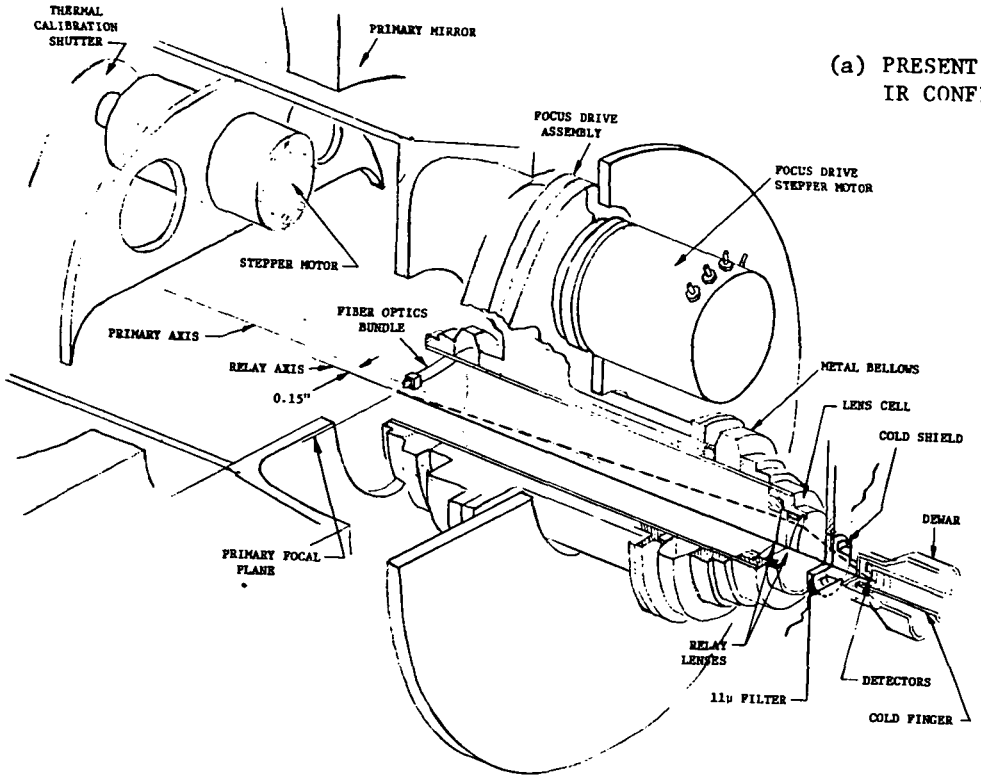

(b) VISSR MODIFIED FOR SOUNDING

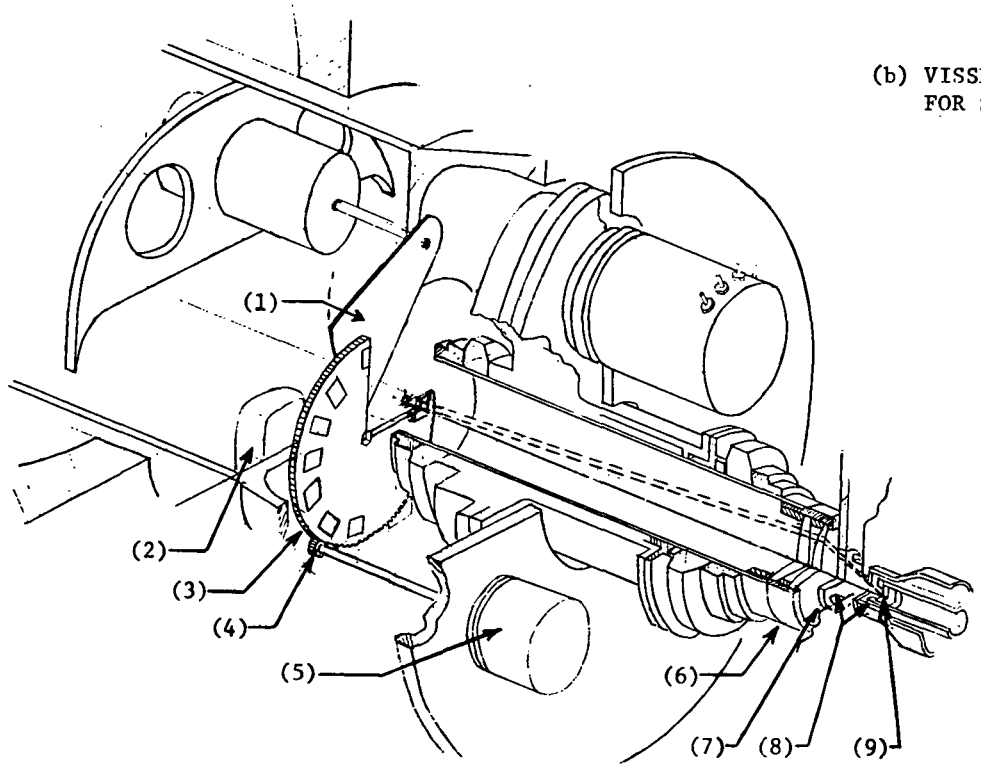

Figure 3. VISSR IR configuration as it now exists (a) and after modifications for sounding (b). Indicated modifications are: (1) thermal calibration shutter positioned between primary focal plane and filter wheel; (2) filter wheel bearing and failsafe mechanism, (3) twelve position filter wheel; (4) filter wheel drive gear; (5) filter wheel stepper motor; (6) new lens cell holding slightly larger and faster relay lenses; (7) ambient stage window replacing current 11 μm filter; (8) cold shields enlarged slightly; and (9) six 0.3 mr detectors replacing the two 0.25 mr detectors.

temperature sounding. Except for the 11μm window channel (#9) these are all located in the 15μm CO_2 band. Spectral channels were chosen on the basis of previous satellite sounding experience (Conrath, 1970; Wark, 1970) and with the help of optimization studies made by Michael Weinreb in cooperation with Smith, Wark and Fleming at the National Environmental Satellite Service. Although the specific set of temperature sounding channels specified here has not been optimized, it contains sufficient spectral redundancy to make this unnecessary.

Channels 10, 11 and 12 are used for correcting the CO_2 channels for water vapor absorption and for the determination of crude water vapor profiles. Channels 10 and 11 are the most tentative members of this set and require further study. Channel 12, located at the center of the strong 6.7μm water vapor band will be used to aid in the detection of cirrus clouds (Shenk, 1970).

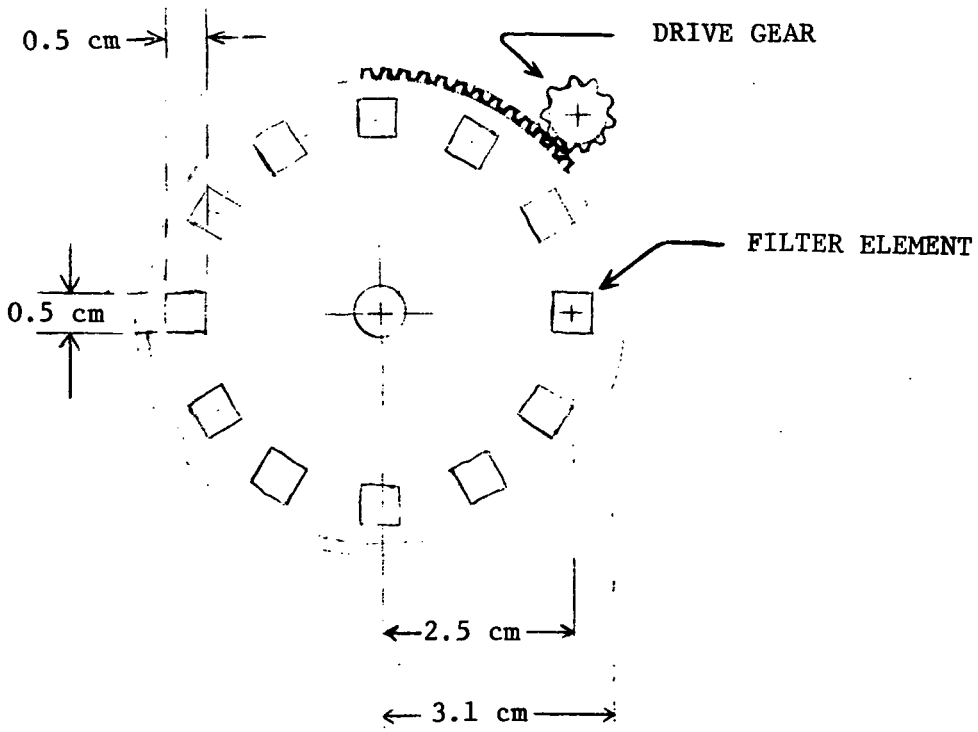

Figure 4. Twelve position filter wheel for the modified SMS.

Table 1

Spectral Channel	$\nu(cm^{-1})$	$\Delta\nu(cm^{-1})$	Filter Transmission
1	669	5	.35
2	680	20	.55
3	690	20	.55
4	700	20	.55
5	715	20	.55
6	735	20	.55
7	745	20	.55
8	760	20	.55
9	875	150	.65
10	1225	60	.75
11	1380	60	.75
12	1490	150	.75

A stepper motor is required for operation of the filter wheel (item (5) of Figure 3). It must be capable of advancing or reversing the filter wheel a maximum of three filter positions within 0.3 sec. (half the SMS rotational period). In the absence of a command signal the stepper motor must hold position. Specification of the stepping sequences required for interlaced sounding and IR imaging is made in Section III.

In the event of stepper motor failure a fail-safe mechanism must return the filter wheel to position 9 in order to insure a thermal imaging capability. This is referenced as item (2) in Figure 3.

Relay Lenses: The total relay lens system consists of the filter substrate, focusable components mounted in the lens cell (item (7) of Figure 3), a window mounted on the ambient cooler stage (item (8) of Figure 3), and a detector package window. Due to possible motion of the cooler as it reaches equilibrium the ambient stage window must be a plane parallel disc. All other components may be figured to some degree, although it would be desirable to have little curvature in the filter substrates and the major focussing power in the lens cell components. Final design configuration will be fixed by the performance requirements specified in Table 2.

The field coverage specified in the table will result in an increase in the maximum clear aperture diameter from the current 0.72 in (1.83 cm) to approximately 0.76 in (1.93 cm). This small increase in lens diameter can be accommodated easily by slight changes in the ring mounts of the lens cell (item (7) of Figure 3).

Suitable lens materials are germanium and IRTRAN VI (poly-crystalline CdTe). A combination of both will probably be necessary in order to approach achromatic performance. The use of IRTRAN VI is also desirable because it

Table 2

Parameter	Required	Comments
Image-Object Distance	5.556 ± .04"	(14.112 ± 0.1 cm)
Optical Gain	7.0	(increased from 5.5)
Field Coverage (diameter)	1.488 mr	.1707" at prime focus (.4336 cm)
Wavelength range	6.4μm - 15.0μm	
Diameter of 90% energy circle	≤ 0.25 mr	6.4μm to 13μm
	≤ 0.30 mr	13μm to 14μm
	≤ 0.35 mr	14μm to 15μm
Transmission (excluding filter)	≥ 0.75	6.4μm to 13μm
	≥ 0.62	13μm to 14.7μm
	≥ 0.49	14.7μm to 15μm

has a higher transmission at 15μm than does germanium. In order to achieve adequate performance over the entire wavelength range specified for the sounding optics it also may be necessary to deposit filters on corrective lens substrates.

The current VISSR focus drive assembly needs no modification to meet the sounding requirements. As with the present VISSR, focussing is required only to compensate for motion of the detector assembly as it cools to operating temperature, and should be required only a few times during the life of the satellite.

Calibration Shutter: This component is similar to present VISSR calibration shutter. The only substantial difference is in its location. The plane of this shutter is between the prime focal plane and the filter wheel (item (1) of Figure 3), while the current VISSR shutter is ahead of the prime focus (Figure 3(a)). The new position, which can be obtained by reversing the stepper motor in its mount, makes it possible to perform IR calibration at any time without obscuring the visible channels.

In normal operation the shutter blade would move under power into the relay optical train, remain for approximately 20° of an SMS rotation (or 0.033 sec out of 0.6 sec), and return under power to the retracted position. These events would take place, in response to a command pulse, between twenty-four and fifty times per earth frame at a rate of one event per SMS rotation, each event taking the place of one earth scan. The shutter would provide, together with the space view, a two-point calibration of the relay portion of the sounder and IR imaging detection systems: filters, relay lenses, and detectors would be calibrated as a unit.

Shutter blade emissivity should be 0.95 or greater. Shutter temperature should be monitored to within .05 K. Shutter drive and fail safe can be provided with a stepper motor and restraining spring to return the shutter blade to the retracted position when stepper motor power is removed (as with present VISSR). Under these conditions the shutter blade would not make a complete revolution.

It is possible to eliminate this component and its stepper motor by consolidating it with the filter wheel. This possibility should be investigated.

2. Detector Specifications

A single array of six square HgCdTe detectors is specified for both IR imaging and sounding. General requirements on the array and specific performance requirements for the individual detectors are specified in this section.

Detector Array: The IGFOV arrangement of the IR and visible channels is shown in Figure 5. Each IR detector has a square IGFOV of 0.30 mr on a side. The 0.192 mr spacing of the detectors normal to the scan direction is equal to the width of the VISSR scan mirror angular step. The IGFOV spacing along the scan direction is designed to obtain IGFOV registration between detectors, and it applies only for the sampling rate specified in Section II.3 (14.0 μsec between samples of the same detector, 2.0 μsec between samples of adjacent detectors, and a dwell time of 28.6 μsec). The six IR detectors sweep out six scan lines each SMS rotation, with an overlap of 36% between adjacent lines (compared to 23% for the current VISSR).

The physical dimensions of this six detector array can be obtained from the angular dimensions by multiplying by the ratio of the primary focal length to relay lens gain. As specified this ratio is 291.3 cm/7.0 = .0416 cm/mr. Thus each IR detector is 0.125 mm on a side.

Detector Performance Requirements: Recently, significant improvements have been made in the long wavelength performance of HgCdTe detectors. For example, Honeywell has made detectors with $D^*(15\mu m, f_c, 105\ K, 40°\ FOV) = 1.4 \times 10^{10}\ cmHz^{1/2}/watt$, with $f_c = 750$ Hz (Aldrich, 1970). The exceptionally good performance at the 105 K operating temperature substantially reduces requirements on the VISSR radiative cooler. The significant lowering of the 1/f to g-r crossover frequency f_c results in a sizeable reduction in noise equivalent bandwidth. This not only reduces the one sample NER, but also the fractional variance due to low frequency noise (see Appendix A). Texas Instruments is quoting performance figures somewhat better than Honeywell's even at a background field of view of 120°. Dissipation for these detectors varies from 1/2 mW to 2 mW for a detector 0.1 mm square. The following specification table has been formulated with these developments in mind (Table 3).

Table 3

Detector Parameter	Expected or Required
Operating temperature	105 K
Background temperature	300 K
Background aperture	≈70°FOV (exact value depends on final lens configureation)
Crossover frequency f_c	750 Hz
D*(λ = 14.95μm)	1.2×10^{10} cmHz$^{1/2}$/W (1.69×10^{10})
D*(λ = 14.0μm)	1.4×10^{10} cmHz$^{1/2}$/W (1.97×10^{10})
D*(λ = 11.0μm)	1.2×10^{10} cmHz$^{1/2}$/W (1.69×10^{10})
D*(λ = 8.0μm)	0.6×10^{10} cmHz$^{1/2}$/W (0.85×10^{10})
D*(λ = 6.4μm)	0.5×10^{10} cmHz$^{1/2}$/W (0.77×10^{10})
Dissipation	≤ 0.5 mW/detector
Responsivity	5000 V/W

Note: D* values are usually stated for the detector package as a whole, including the 29% transmission loss from an IRTRAN IV window. Corrected values are noted parenthetically.

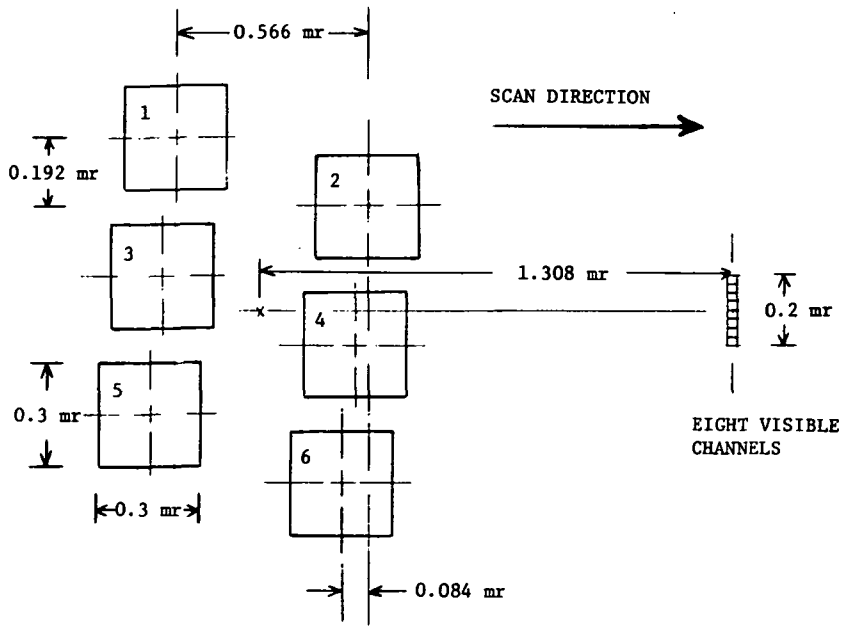

Figure 5. VISSR visible and infrared IGFOV arrangement for sounding.

3. VISSR ELECTRONICS

Although twelve spectral channels are sequenced in accumulating complete sounding information, only six detection and data transmission channels are required. The detection system requires four new IR channels and associated circuitry (as well as filter wheel logic and drivers). The four additional channels of data transmission can be obtained by replacing some of the sync bits with data. None of these changes will increase bit rates or communication bandwidth in the SMS/CDA link or require modifications in transmitters or receivers.

Additional Amplifiers and Multiplexing: Four additional low noise amplifiers, their pre-aliasing filters, four additional analog switches, and the associated wiring will be needed to carry the signals from the additional detectors to the multiplexer. The SMS already contains two IR amplifiers, filters, and analog switches for the existing IR imaging channels. Duplicates of these could probably be used for all six channels.

Sequencing and Control: New logic and power control must be added to step the filter wheel and operate the "redundant" or failsafe mechanism protecting the IR imaging capability. In either of the two auto sound modes (see Section III), it must generate the logic commands to obtain the proper combination of filters. In manual mode it must process separate commands relayed from the ground. Extra readouts to monitor the position of the filter wheel are required. These are:

1. Position of filter wheel
2. Manual or auto sounding
3. Auto sounding mode

Optimal Multiplexing and Data Format Modifications: The data system is presently configured to interlace the IR, visual, and sync information such that the IR samples are three times redundant, i.e., each of the two IR detectors are sampled three times per dwell time. This existing data format is displayed in Figure 6(a). Note that SYNC and $\overline{\text{SYNC}}$ bits are transmitted as often as the IR data (once every two data words).

The proposed reordering is shown in Figure 6(b). By reducing the SYNC and $\overline{\text{SYNC}}$ transmissions to once every seven words, it is possible to sample each of the six detectors of the modified VISSR at a rate of 2.05 samples per dwell time. In this case some of the highly redundant sync bits are replaced with additional data words.

Some changes in the multiplexer and demultiplexing hardware are required to obtain this twofold sampling redundancy. However, word structure, length, bit rates, and bandwidth are identical to the present system. The CDA ground station would need little hardward modification to receive the additional data, and only minor alterations in the computer software which stretches the IR imaging data for display. Sounding data would require additional storage until it could be relayed without interference with the stretched video (see Section II.5).

(a) EXISTING FORMAT
FOR SMS-A
(2 CHANNEL IR)

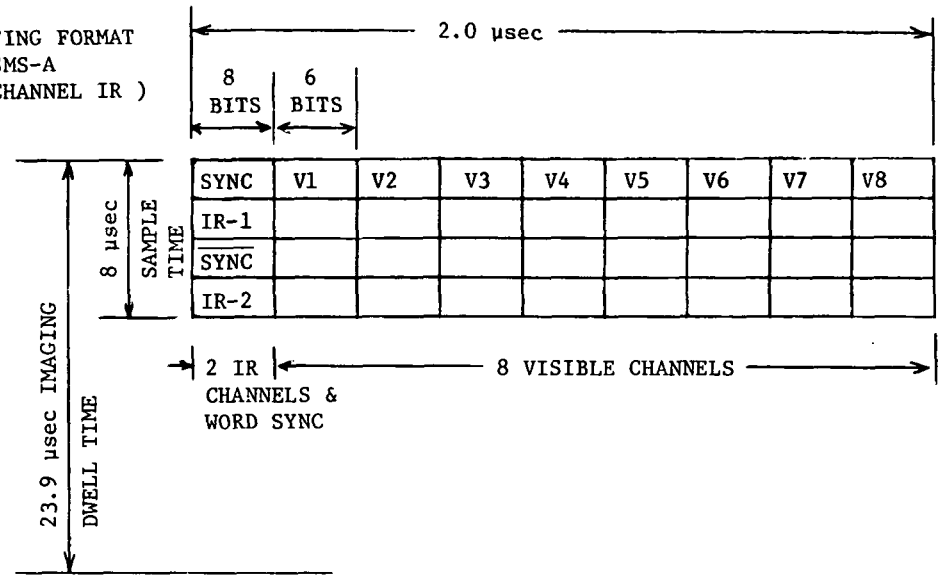

IR IMAGING: 2.98 SAMPLES/DWELL TIME
(0.25 mr IFOV) 0.084 mr/ SAMPLE @ 100 RPM

(b) PROPOSED FORMAT
FOR SMS SOUNDER
(6 CHANNEL IR)

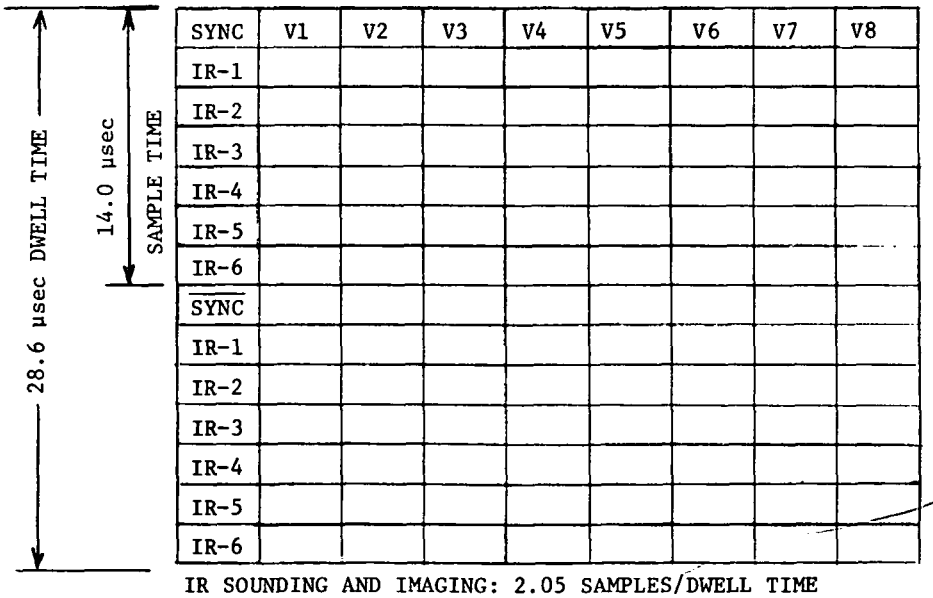

IR SOUNDING AND IMAGING: 2.05 SAMPLES/DWELL TIME
(0.30 mr IFOV) 0.146 mr/SAMPLE @ 100 RPM

Figure 6. 28 Mbps data formats for the SMS-CDA link: (a) present VISSR (b) VISSR modified for sounding.

4. Spacecraft/VISSR Interface

The additional IR detectors and the filter wheel will be near the spacecraft axis of rotation and should not greatly alter the dynamic balance. The VISSR electronics and multiplexing packages lie further off axis on the equipment platform, and may, after being modified, require some minor shifting of position to restore balance. Adequate room appears to be available. Only three other interface areas will require modification.

Command Capability: The present VISSR requires thirty-four discrete commands from the spacecraft command subsystem. Nine new commands are required, with 35-38 being stepping commands.

35.	Filter wheel	"STEP FORWARD"
36.	Filter wheel	"STEP REVERSE"
37.	Filter wheel	"REDUNDANT FORWARD"
38.	Filter wheel	"REDUNDANT REVERSE"
39.	Auto sound and imaging	"ON"
40.	Manual sound or imaging	"ON"
41.	Auto sound mode A	"ON"
42.	Auto sound mode B	"ON"
43.	Auto sound mode Q	"ON"

Extra commands other than #37 and #38 may be necessary to implement appropriate fail-safe requirements. For this reason it would be desirable to retain extra command space if at all possible.

Housekeeping Telemetry: Digital telemetry now occupies forty-six bits on VISSR. Seven more are needed, all of which must be sent for each spacecraft revolution. Convenience suggests placement of these bits in the line preamble or first data sample.

47-50	Filter wheel position (4)
51.	Auto sound on (1)
52-53.	Auto sound mode A, B or Q (2)

Timing Signals: A timing pulse or pulses must be provided at the appropriate time and spacecraft rotation angle to permit stepping the filter wheel prior to the next earth scan.

5. Ground Station Data Handling

The spacecraft used for sounding will perform more functions and collect more varied data than SMS-A. The total amount of IR data will not be increased very much (the total bit rate and bandwidth will see no increase), but the IR imaging will require reconstruction in the CDA computer from six detector channels rather than the existing two, while the IR sounding data requires an additional temporary storage capacity. No change is required in the CDA

visual channel data handling, and the stretched video link for both visual and IR imaging will be unchanged, so that no modification need be made at any DUS terminal unless sounder data is to be utilized. Sounding data will be relayed during the time interval between frames (between pictures).

CDA Demultiplexer and Line Stretcher: Minor modifications of the demultiplexer are required so that the data words replacing sync words are appropriately decoded (Figure 6(b)). The visual channel data handling is identical with that on SMS-A. The six IR channels require an extra buffer which is filled and emptied with six lines each revolution. It interfaces with a small and inexpensive digital storage disk rotating at a speed locked to the output bit rate of the CDA/DUS link. During the period between the end of one frame and the beginning of the next, the disk is read out and the sounding data relayed to the DUS. Figure 7 shows the areas requiring modification enclosed in a dashed line. The handling of IR imaging data will require the CDA computer to accept data from the input processor in six parallel channels once every six SMS revolutions, and process and read out one line of stretched video during each subsequent revolution. This will involve some software changes and an upgrading of I/O controller and computer interface capacity from two IR channels to six. Since imaging and sounding can be entirely separate functions, the two-point, one-point, and no interpolation option should be separately controllable for imaging and sounding.

DUS Modification: No modification of the existing imaging capability of the DUS terminals need be made. During frame retrace, the sounding data with proper channel identification and documentation can be received and shunted into a parallel channel to be stored for processing, if desired. Additional hardware is only required at those DUS stations which will use the sounder data.

Data Storage and Access: Two processes are necessary at the end of the data chain between VISSR and the inversion process which yields the atmospheric temperature and moisture soundings. The first is the collection and storage of the sensor data and the second is extracting the data of interest for processing. The second step has already been solved in the case of wind determination from ATS images by the Man-Computer Interactive Data Access System (McIDAS) developed at the Space Science and Engineering Center. This system avoids the very high cost of processing all of the data by placing an operator at a convenient place in the data stream where he can easily and quickly choose what data is to be processed. In the McIDAS system as applied to winds, the operator chooses candidate clouds whose displacements are then measured by a software program. This same system can be used to pre-process the data for sounding also. Instead of choosing suitable clouds we can choose suitable candidate clear areas. The criterion which determines whether the chosen area is clear enough and the actual inversion calculation can be done automatically in the computer.

This system allows great flexibility. The operator can choose the specific area or density of observations as will. For example, in the photo shown in the introduction the operator can choose to take several soundings

in the eye of the hurricane (which ought to allow one to obtain the central pressure) or he could choose the clear spots near the severe weather. This system allows one to obtain the data of interest without the horrendous "number smashing" required to process all the data.

The McIDAS system and how it can be applied to SMS data access is described further in Appendix D. While the approach to the data problem seems clear enough, this document does not contain a detailed description of a hardware specification needed to accomplish the task.

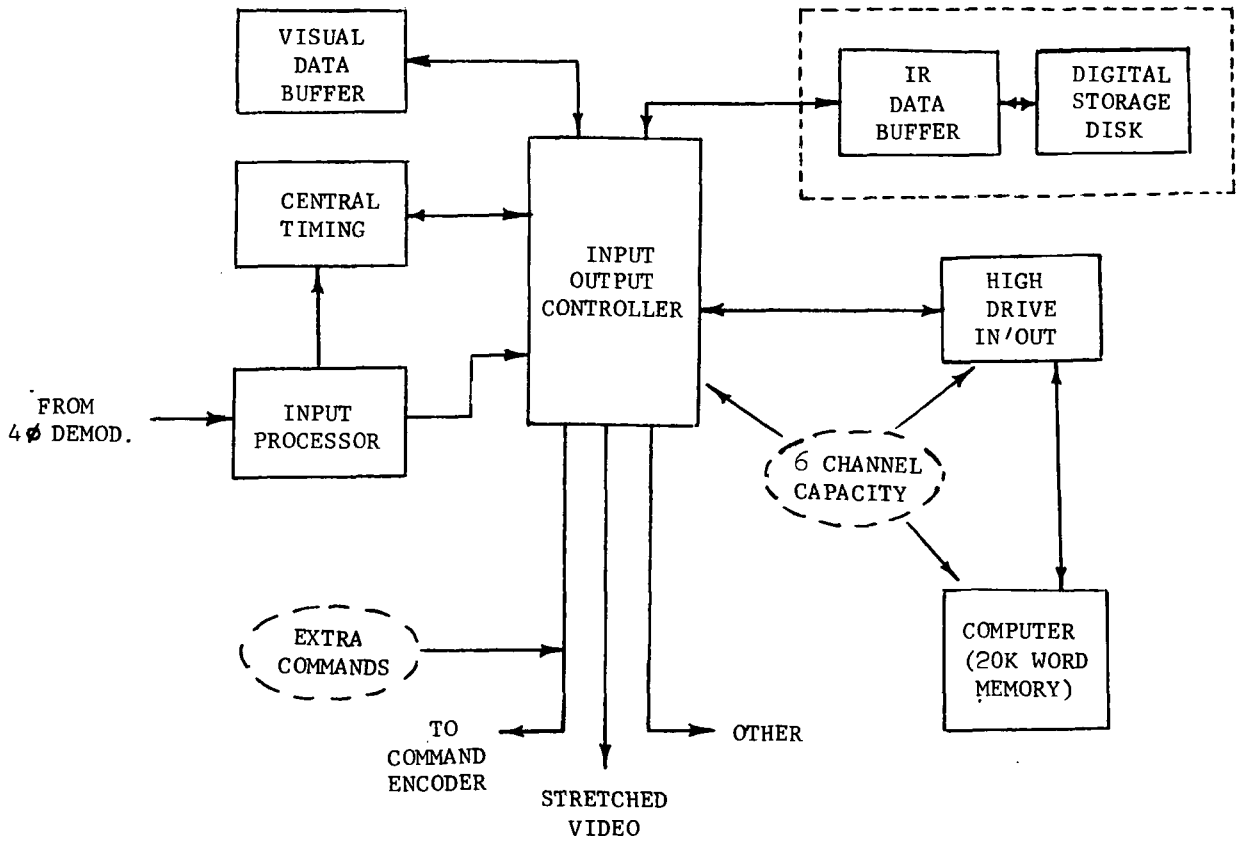

Figure 7. Line Stretcher Modifications

III. SMS SOUNDER OPERATION

The sounder instrumentation specified in Section II provides for a wide range of operational capabilities. Fundamental among these is the capability for interlaced sounding and IR imaging, with complete spatial coverage for each spectral channel. This requirement is met by a repeated six scan sequence of appropriate filter wheel steps. More general aspects of sounder operation deal with frame sequences and frame amplitudes as they relate to GARP scale and mesoscale sounding capabilities.

1. Sounder Scanning Sequences

Since a swath of six contiguous scan lines is swept out by the modified VISSR every SMS rotation, only one rotation of every six is required to achieve complete spatial coverage for a single spectral channel. Thus, during each frame of scans (a full frame consists of 1821 lines) complete coverage can be obtained for six different spectral channels. Since IR imaging is required for each frame, three automatically repeated six scan sequences are specified to obtain adequate sampling of all twelve spectral channels (only five sounding channels can be handled in one sequence).

Auto Sound Modes A and B: Each of these two scanning modes obtains complete IR imaging coverage and complete coverage for five other spectral channels as well, totalling eleven in all. Whichever mode is in effect is automatically repeated for the entire earth frame, at the completion of which another mode is initiated. In this manner complete spatial coverage for ten of the sounding channels is obtained every two frames of complete IR imaging data. Modes A and B alternate with mode Q to obtain twelve channel coverage, unless an external command selects a different sequence of operation.

The filter step sequences for modes A and B are presented in Table 4. In this table S+ and S- denote the internally generated VISSR filter wheel commands STEP +1 FILTER and STEP -1 FILTER, respectively. The manner in which this sequence of operations results in complete spatial coverage for both imaging and sounding channels can be seen in Figure 8. Note that imaging scan lines which register with a particular sounding scan line need not belong to the same six scan sequence. For example, detector #6 of scan #4 is in registration with elements on the line scanned by detector #1 of scan #1 of the next six-scan sequence.

Auto Sound Mode Q: The spectral channel (669 cm^{-1}) which is omitted from Auto Sound Modes A and B is sensitive only to upper atmospheric regions, which exhibit very slow variations with time. Accordingly, this channel (Q-branch) need not be sampled at the same time or frequency as other sounding channels, which respond to rapidly varying atmospheric regions. At whatever frequency meteorological requirements dictate this channel can be sampled by initiating Auto Sound Mode Q, specified by Table 4. The imaging-sounding interlace is similar to that obtained with Auto Sound Modes A and B except that only one sounding channel is sampled.

Table 4. Auto Sound Modes

Relative Scan No.	FW Steps prior to earth scan	Filter Position during earth scan	$\nu(cm^{-1})$	$\Delta\nu(cm^{-1})$
	AUTO SOUND MODE A			
1	S+,S+	1	875	150
2	S+,S+	3	680	20
3	S+,S+	5	690	20
4	S+,S+	7	700	20
5	S+,S+	9	715	20
6	S+,S+	11	735	20
	AUTO SOUND MODE B			
1	S+,S+,S+	1	875	150
2	S+	2	745	20
3	S+,S+	4	760	20
4	S+,S+	6	1490	160
5	S+,S+	8	1225	60
6	S+,S+	10	1380	60
	AUTO SOUND MODE Q			
1	S+	1	875	150
2	S-	12	669	5
3	NONE	12	669	5
4	NONE	12	669	5
5	NONE	12	669	5
6	NONE	12	669	5

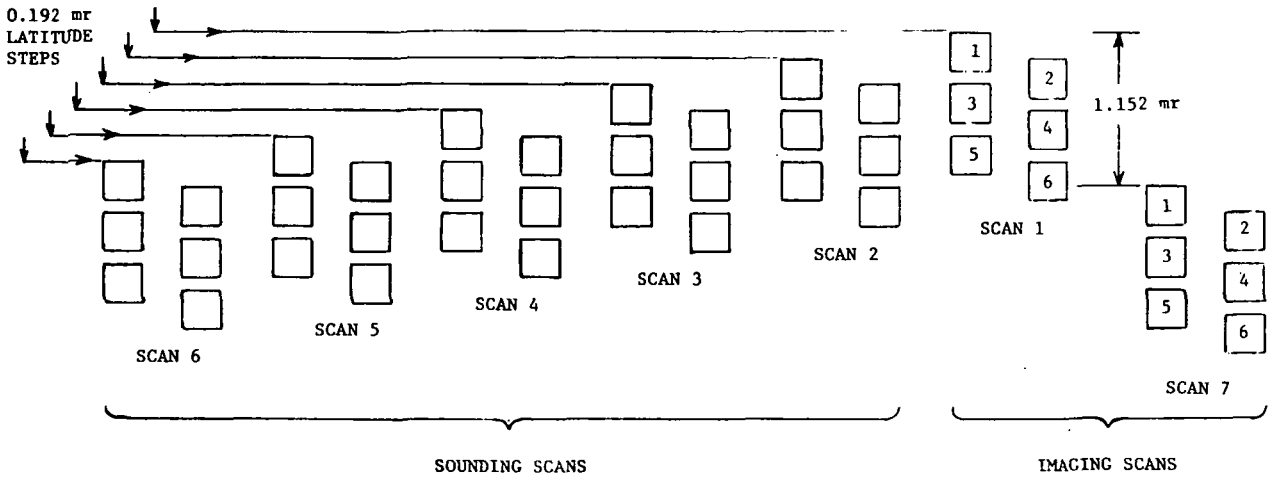

Figure 8. VISSR Sounder scan sequence. The repeated sequence of six scans achieves complete spatial coverage in five sounding channels and in the 11.5 μm imaging channel. Note, for example, the imaging coverage provided by scan #1 and scan #7 (actually scan #1 of the next six-scan sequence).

Command Mode: External commands to step the filter wheel can be used to override the automatic scan sequences followed in Auto Sound Modes A B, or Q. Two external commands are available: a positive and negative filter wheel step command. Automatic sequencing is terminated by any override command and does not resume unless initiated by the appropriate Auto Mode command.

2. In-Flight Calibration

A single calibration event consists of viewing a calibration shutter (see Section II) immediately after the end of DC restoration. The shutter view lasts as long as the scan of one frame line (0.033 sec) and substitutes for a line of earth sensing data. In this way a two-point calibration (shutter and space) can be made at any scan in the data frame, and the response to the calibration shutter is thus transmitted in the same way as the earth sensing data. Furthermore, because of the way in which sounding and imaging are interlaced, calibration of sounding channels need never interfere with the IR imaging function (or the visible imaging). The number and location of calibration events in the data frame depends on the mode of sounder operation.

Auto Calibration Modes: Whenever the sounder scan sequence is controlled by one of the Auto Sound Modes A, B, or Q, calibration of each spectral

channel in that mode is automatically made at the start of each data frame. The number of initial scans used for calibration depends on the noise equivalent radiance (NER) of the channels to be calibrated. The noise for spectral channels sampled during modes A or B is low enough (see Section IV) to require only four calibration events per channel, involving only four six-scan sequences out of approximately 304 in the complete frame. The first twenty-four lines of each data frame for each spectral channel are used for calibration in this case.

Automatic calibration sequencing is also obtained during operation in Auto Sound Mode Q. Calibration is initiated at the start of each data frame. The first six thermal lines (out of 1821) and the first 50 Q-branch lines of each of the five overlapping Q-branch data frames are used for calibration in this mode. Since Q-branch calibration requires approximately 105 calibration events (Appendix A) two complete earth frames in Auto Sound Mode Q are required to calibrate this channel once.

Command Mode Calibration: An external command for introducing the shutter can be used to initiate calibration instead of earth sensing during any SMS rotation. The calibration shutter is automatically retracted 0.033 sec following its introduction. If this command is used during any of the three Auto Sound Modes, automatic sequencing of filter wheel steps is not affected. If used in conjunction with override commands for filter wheel steps, automatic sequencing is terminated.

3. Sounder Event Timing

The timing of elementary events involved in sounder operation (relative to the SMS rotational period) is shown in Figure 9. It should be noted that not all the indicated events take place every rotation. The actual sequences of filter wheel steps and calibration shutter operations have been discussed already. The event timing presented is subject to modification as required by mechanical or electronic limitations.

4. Sounder Frame Sequences

Since only five different spectral channels (in addition to the 11μm window) are sequences in each of the auto sound modes A and B, two frames of data (one in mode A and one in mode B) are required to obtain complete spatial coverage for all eleven spectral intervals. Complete spatial coverage in the twelfth channel (the Q-branch) requires an additional frame in Auto Sound Mode Q. However, in mode Q the radiometric accuracy for a given averaging area is significantly inferior to that obtained in modes A and B. This disadvantage is compensated for by the slower time variations, larger scale spatial variations, and greater clarity of the atmospheric region sampled by the Q-branch filter.

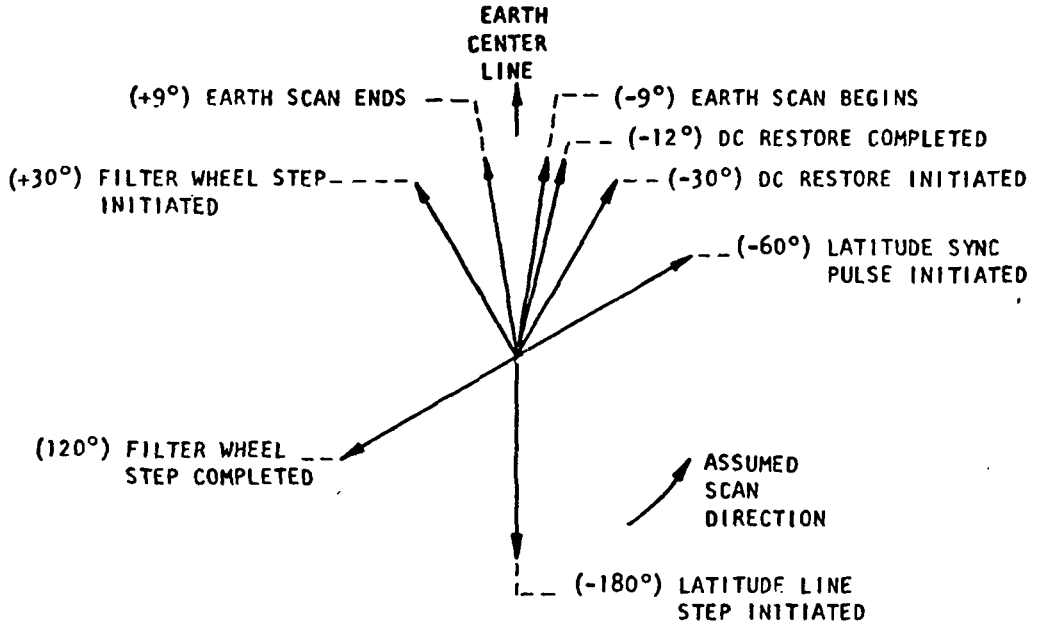

VISSR SOUNDER TIMING EVENT DIAGRAM (EARTH SENSING)

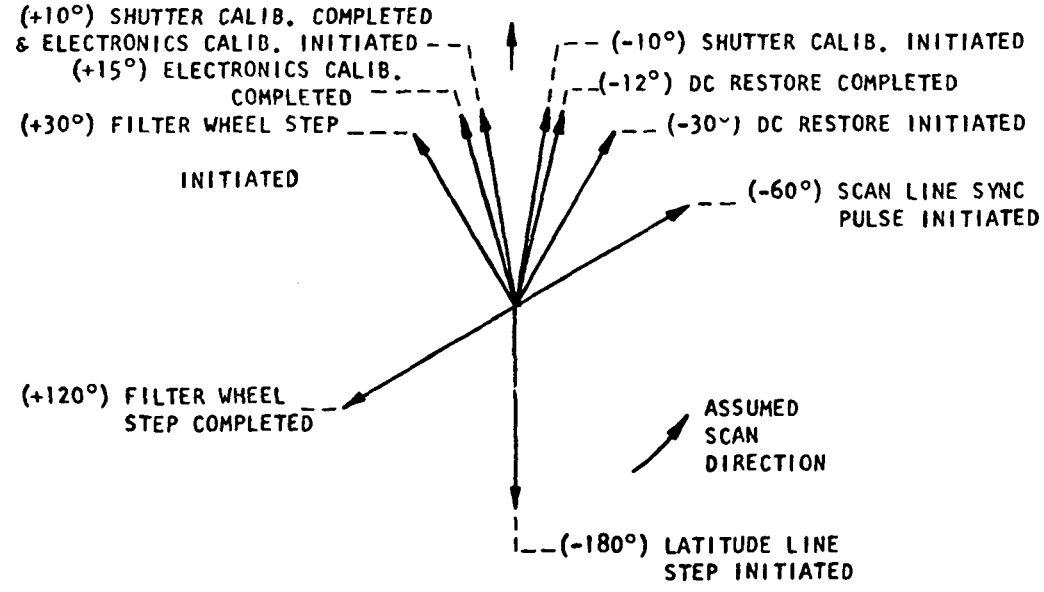

VISSR SOUNDER TIMING EVENT DIAGRAM (CALIBRATION)

Figure 9. VISSR Sounder timing event diagrams.

As shown in the next section (Section IV) if we assume that Q-branch radiances can be averaged over twice the time interval and four times the area of other spectral channels, then in all modes of operation the appropriate repeated frame sequence is just A B Q.

Operating with the A B Q sequence in the full frame mode (30 minutes per frame, complete coverage of the earth's disc), yields sufficient radiometric accuracy to make temperature soundings every hour and a half with a grid spacing of approximately 200 km under clear conditions and 400 km under very cloudy conditions (approximately 10% clear at sounder resolution). In both cases Q-branch radiances are obtained from three hour averages over 400 km x 400 km grid boxes.

5. Variable Frame and Mesoscale Operation

The current VISSR scanner is capable of operating with a reduced frame amplitude in two different modes: (a) single latitude scan repetition, and (b) variable amplitude scanning (with an amplitude of between eighteen and 1821 lines). The position of the reduced frame is selected by appropriate timing of the ground commands for execution. Any of the Auto Sound modes or the Command Mode of sounder operation can be used with the variable frame height option, except that the automatic calibration sequencing is aborted and calibration is made only by external command.

Since the rate of sampling per unit area within a frame is increased in direct proportion to the frame height reduction, it is possible to increase both sounding frequency and sounding resolution by sacrificing spatial coverage. With appropriate choices of frame amplitude, integration time, and averaging area it is possible to make useful atmospheric temperature soundings at almost any spatial resolution down to 10.7 km. A summary of the operational capabilities and trade-offs involved is presented in Figure 10. Each line displays the dependence of required integration time on the spatial resolution of the soundings for a given choice of frame amplitude. The left of each line is labelled by the frame amplitude and the right by the corresponding coverage (this is stated in km of latitude near the subsatellite point). The ABQ frame sequence was assumed for all amplitudes. This figure is based on the tabulated results of the next section (Section IV).

Note the substantial mesoscale capabilities afforded by the SMS sounder. Soundings every 10.7 km over a 45 km swath (chosen to intersect the eye of a hurricane, for example) can be made every 10 minutes. Soundings every 20 km covering the same area can be made with only four minutes of observations.

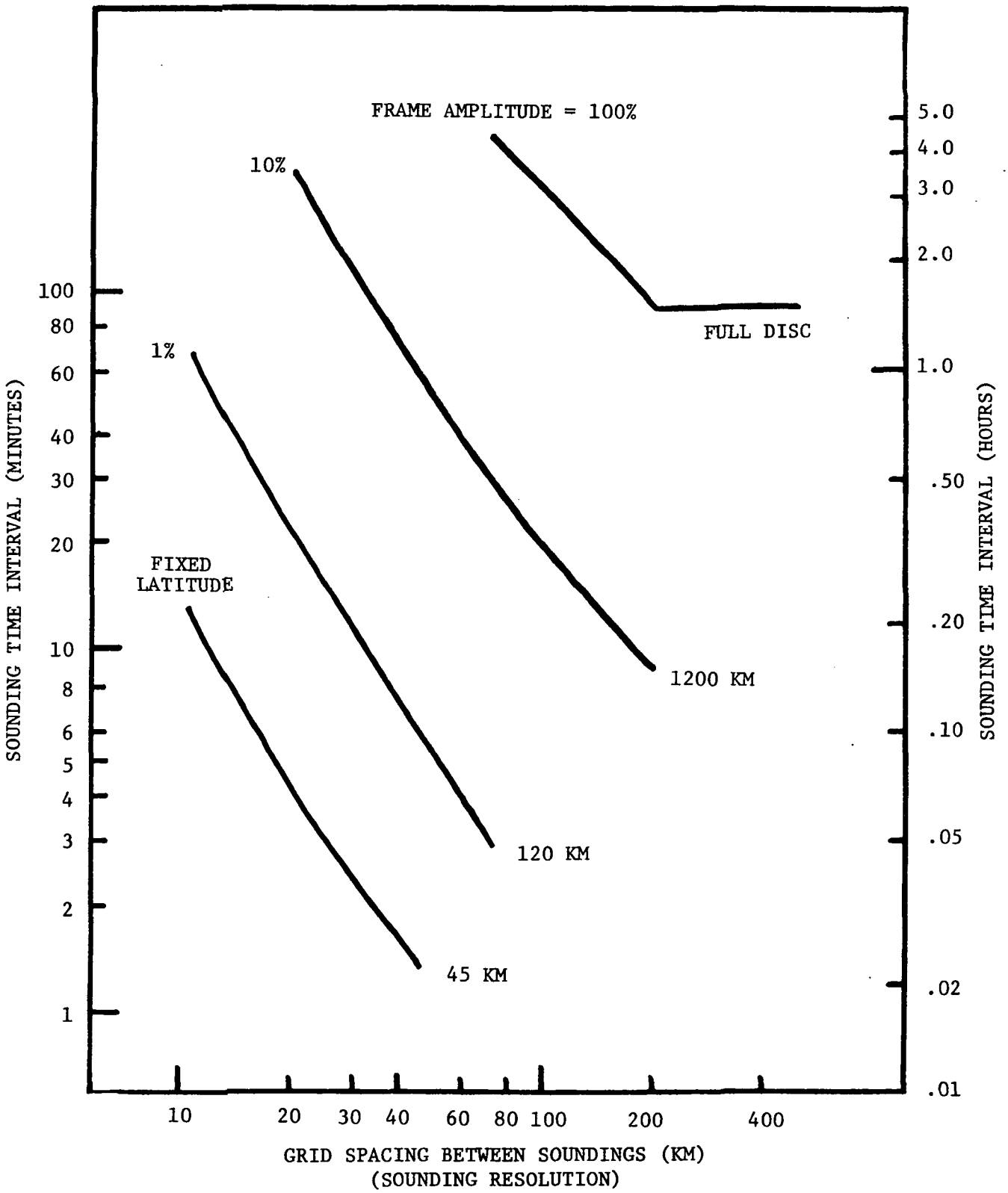

Figure 10. SMS Sounder operational capabilities. Each curve applies to a specific latitude coverage labelled on the left in percent of the full frame amplitude (1821 latitude steps of 0.192 mr each) and on the right in km of latitude near the subsatellite point.

IV. PERFORMANCE ANALYSIS

Adequate evaluation of the retrofit instrumentation specified in Section II requires an analysis of three major performance characteristics: the single sample Noise Equivalent Radiance (NER), the NER of spatial and/or temporal means of samples, and the heat load placed on the VISSR radiative cooler. The first two items are significant measures of the usefulness of the specified instrumentation, and the third is a significant measure of its feasibility.

1. Calculation of the One Sample NER

The Noise Equivalent Radiance (NER) is the spectral radiance of the scene which yields a signal equal in magnitude to the R.M.S. noise generated in the instrument. This is determined by instrument parameters according to the equation

$$NER = \frac{\gamma [A_d \Delta f_n]^{1/2}}{A_o \alpha^2 D^* \rho_\lambda \Delta \nu} \quad , \tag{1}$$

which makes use of the following notation:

γ = amplifier noise factor

A_d = detector area (cm^2)

Δf_n = effective noise bandwidth (Hz)

A_o = effective collecting aperture of optics (cm^2)

α = angular resolution (r)

D^* = specific detectivity ($cmHz^{1/2}/W$)

ρ_λ = net transmission of optics and filters

$\Delta \nu$ = spectral bandwidth (cm^{-1}).

The parameter units specified yield the NER in units of $W/(cm^2\text{-}cm^{-1}\text{-ster})$, which is converted to $erg/(sec\text{-}cm^2\text{-}cm^{-1}\text{-ster})$ by the multiplicative factor 10^7 erg/W-sec. The latter unit will be used here because of its popularity in the scientific literature on atmospheric temperature sounding. Equation (1) strictly applies only to flat field conditions. The effects of diffraction and prealiasing filters, which become important in the presence of clouds, are treated in Appendix C as part of the data handling problem.

Detailed calculations of optics transmission and NER are presented in Table 5 for three characteristically different cases: 1) imaging in 10.5μm to 12.6μm spectral region (160 cm^{-1} bandwidth); 2) sounding near 14μm (20 cm^{-1} bandwidth); and 3) Q-branch sounding at 14.95μm (5 cm^{-1} bandwidth). The optics transmission is based on AR coating and filter transmission characteristics quoted by the Optical Coating Lab Inc., Santa Rosa, California, and on published Ge bulk transmission properties (Collins, 1954). Transmission characteristics of AR coated IRTRAN VI were obtained from Eastman Kodak Company, Rochester, New York. The noise equivalent bandwidth (Δf_n) is calculated on the basis of a 1/f to g-r crossover frequency of 750 Hz, an effective lower cut-off of 2 Hz (see Appendix A for a detailed discussion of DC restore effects), and an upper cut-off of 17.45 KHz.

These results were obtained without including the probable improvements from the reduction of the detector effective black body background aperture as a result of the reflecting properties of the interference filters outside their passbands.

Results of NER calculations for all twelve spectral channels are individually summarized in Table 6. Also included in this table is the channel by channel performance for the two ends of a wide spectrum of data averaging capabilities. The two averaged data NER's tabulated are

a) The GARP Mean NER: For each spectral interval this is the NER of the average of all radiance measurements within a 400 km x 400 km area (57 lines of 37 IFOV's each are averaged). The analytical techniques used to estimate the noise standard deviation for this kind of data average are presented in Appendix A.

Full disc coverage (100% frame height) requires approximately 30 minutes per frame, including the time for forward scan, retrace and nutation damping. Since complete sampling of all spectral channels requires one frame each of Auto Sound Modes A, B and Q, the total time elapsed is thus 1.5 hours for each A B Q sequence.

b) The High Resolution NER: The highest resolution possible with the SMS sounder is 10.7 km x 10.7 km (0.3 mr square). By aborting the VISSR scan mirror latitude step, a swath of six lines (covering 45 km in latitude) can be repetitively scanned at a rate of 100 times per minute. Since each scan sequence of the three auto modes A B Q requires six scans, a total of 18 SMS rotations are required for a complete ABQ sequence. In order to obtain an NER adequate for sounding in each IFOV, 100 sequences are needed for time averaging. This takes a total of 1800 SMS rotations, or 18 minutes. Since only time averages are involved, the averaged samples have complete statistical independence (this is not true for spatial averages).

These two performance measures were included here to provide a complete twelve channel breakdown as a reference for the full discussion of data averaging performance capabilities. This subsequent discussion makes the simplifying assumption that all the sounding channels sequenced in mode A and B have essentially the same performance characteristics as the 715 cm^{-1}

Table 5

	Imaging	Sounding	Q-branch
Relay lens transmission	.75	.62	.49
Filter transmission	.65	.55	.35(1)
Primary transmission	.88	.88	.88
Net transmission	.43	.30	.15
ρ_λ	0.43	0.30	0.15
γ	1.3	1.3	1.3
$\sqrt{Ad}$ (mm)	0.125	0.125	0.125
Δf_n (KH_z)	24.25	24.25	24.25
A_o (cm^2)	1090	1090	1090
α (mr)	0.30	0.30	0.30
D*(cm $H_z^{1/2}$/W)(2)	(1.69×10^{10})	(1.97×10^{10})	(1.69×10^{10})
$\Delta\nu(cm^{-1})$	150	20	5(3)
NER (flat field) erg/(cm^2-sec-ster-cm^{-1})	.237	2.18	12.56

Notes: 1) Peak transmission with blocking out to 50μ.
2) The D* values no not include the usual window losses. These are accounted for in $\rho\lambda$.
3) *This is the half power bandwidth,* Requiring $\int \tau_\nu d\nu = \tau_{peak} \Delta\nu_{eff}$ we find $\Delta\nu_{eff} \simeq 8.1$ cm. This was determined from τ_ν curves of an OCL produced Q-branch filter used by NOAA.

Table 6 Sounding Performance Summary by Channel

Channel #	$\nu(cm^{-1})$	$\Delta\nu(cm^{-1})$	ρ_λ	D^*[1] $(10^{10} cmHz^{1/2}/W)$	One sample NER[2]	Required NER	GARP Mean NER, Full Disc Coverage, One Sequence of Modes ABQ (Total Time =1.5 HR)	High Resolution NER (11km x 11km), 45 km Latitude Coverage, 100 Sequences of ABQ (Total Time=18 min)
1	669	5	.15	1.69	12.56	.25	0.32[3]	.56[4]
2	680	20	.26	1.83	2.7	.25	0.15	.27
3	690	20	.28	1.83	2.54	.25	0.14	.25
4	700	20	.29	1.97	2.26	.25	0.12	.23
5	715	20	.30	1.97	2.18	.25	0.12	.22
6	735	20	.32	1.83	2.20	.25	0.12	.22
7	745	20	.33	1.83	2.13	.25	0.12	.21
8	760	20	.34	1.69	2.24	.25	0.12	.22
9	875	150	.44	1.69	.24	.25 (S)	0.013	.03
10	1225	60	.48	.85	1.05	.15	0.06	.11
11	1380	60	.51	.77	1.09	.15	0.06	.11
12	1490	150	.55	.70	.45	.10	0.025	.05

Notes: (1) D* values do not include window losses. These are incorporated into ρ_λ.

(2) NER values are in ergs/$(sec\text{-}cm^2\text{-}ster\text{-}cm^{-1})$.

(3) Two sequences of ABQ modes are required to reduce the Q-branch NER below the 0.25 limit (total time ≈ 3.0 hr).

(4) The usual procedure of averaging Q-branch radiances over twice the time interval and four times the area of the other channel averages yields an NER below the 0.25 erg/$(sec\text{-}cm^2\text{-}ster\text{-}cm^{-1})$ limit.

channel (a typical member of the set). Of course the substantially different performance characteristics of the Q-branch will be given the special consideration it requires.

2. NER of Data Averages

Because of the noise characteristics of the VISSR detection system the NER of a data average is usually greater than the one sample NER divided by the square root of the number of samples averaged. This depends in a complex way on the relative time and space locations of the samples averaged. The details of this behavior are presented in Appendix A. In the interest of simplicity, the present section provides only a summary of the application of these results.

Time and Space Averages in a Clear Atmosphere: As indicated in the previous section, appropriate choices of frame amplitude (latitude coverage), integration time, and averaging area, make possible useful soundings at almost any spatial resolution from 10.7 km (mesoscale) to beyond 400 km (GARP scale). The first step in calculating the sounder performance throughout this range is to determine the sampling requirements as a function of averaging area. Results of this determination are presented in Table 7.

In this table the NER of the area average (for one pass with complete coverage) is determined by the one-sample NER and the frequency spectrum of detector noise power (see Appendix A). Dividing this NER by the required NER and squaring yields the number of passes required in Auto Sound Modes A or B in order to insure that the combination of space and time averaging together yield an NER $\leq$ 0.25 erg/sec-cm^2-cm^{-1}-ster). In Auto Sound Mode Q the number thus determined must be divided by five because this mode selects the Q-branch filter five times for every FOV, whereas the other modes yield one measurement per FOV per spectral interval. As an example, consider the tabulated requirements for sounding a clear area 107 km x 107 km. In order to obtain the required NER in all channels it is necessary to have data from 2 passes in mode A, 2 passes in mode B, and 14 passes in mode Q, a total of 18 passes.

The Q-branch sampling requirement presented in the table is probably unrealistically severe in relation to the other channels. Since the Q-branch filter selects radiation from mainly above the tropopause, time variation of the corresponding radiances will be much slower than those emitted mainly from the troposphere (selected in modes A and B). Similarly, spatial variations will be more gradual. Although the precise nature of this difference is not known, it is probably reasonable to make the following assumption: determination of useful temperature soundings with spatial resolution Δx and time resolution Δt can be made from sets of spectral radiances with NER $\leq$ .25 erg/etc which are averaged within an area $(\Delta x)^2$ and for a time Δt except for the Q-branch which may be averaged within $(2\Delta x)^2$ and for a time $2\Delta t$. The required relative sampling rates implied by this assumption and Table 7 show that the optimum repeated sequence of auto sound modes for all averaging areas is A B Q, i.e., the same number of passes is required for each mode.

Table 7

FOV of Average (mr x mr)	Averaging Area (km x km)	lines x IFOV's/line	Typical Sounding Channel NER of Area Average	No. of passes in auto mode A or B required to Obtain NER < 0.25	Q Branch NER of Area Average	No. of Passes Required in Auto Mode Q
0.3x0.3	11x11	1x1	2.18	76	12.56	505
0.49x0.3	18x11	2x1	1.54	38	8.87	252
0.49x0.6	18x21	2x2	1.19	23	6.86	151
0.68x0.6	25x21	3x2	0.97	15	5.59	100
0.68x0.9	25x32	3x3	0.88	13	5.07	82
0.88x1.2	31x43	4x4	0.67	7	3.86	48
1.94x1.8	70x64	8x6	0.43	3	2.48	20
2.99x3.0	107x107	15x10	0.36	2	2.07	14
4.33x4.5	155x161	22x15	0.22	1	1.27	5
5.87x6.0	210x215	30x20	0.19	1	1.09	4
11.0x11.0	400x400	57x37	0.12	1	.71	2

A summary of the sounding performance for the ABQ frame sequence is presented in Table 8. The time required to obtain adequate sampling for temperature profile inversion is displayed as a function of the sounding resolution and latitude coverage desired. In this table the time required for a reduced amplitude frame is assumed to be equal to the full frame time (approximately thirty minutes) multiplied by the fractional frame amplitude, e.g. the 10% frame is assumed to require 3 minutes. The fixed latitude scan is exceptional in this respect because no retrace or nutation damping is involved.

Effects of Cloud Cover: For averaging areas containing clouds, only a fraction of the total number of samples can be used to determine clear column spectral radiances. For 75% cloud cover at the spatial resolution of the sounding channels, only 25% of the samples can be used directly (see Appendix C for indirect techniques and an expanded discussion of implementing direct techniques). However, the sounding performance under cloudy conditions is degraded more slowly than the loss of clear column samples would indicate. This comes about because many of the samples lost have little statistical independence and contribute very little to noise reduction even under clear conditions (see Appendices A and B for details).

An example of the effects of cloud cover on the NER for a GARP grid box (an averaging area of 400 km x 400 km) is shown in Figure 11. Results presented in this figure are based on the analysis of ATS data discussed in Appendix B.

3. Radiative Cooling Requirements

The six detectors specified for the SMS sounder increase the cold finger heat load, due to joule heating and lead conduction, from the current 0.4 mW to approximately 5.4 mW (assuming a joule heating of 0.5 mW per .01 mm^2), an addition of 5.0 mW.

If we assume a mean operating temperature of 87°K for the current VISSR (recent tests have actually shown 82°K performance) and a 1.5°K/mW rate of increase with additional heat load, we obtain a 94°K minimum mean operating temperature. Adding to this a 10°K safety factor, we obtain approximate operating temperature of 105°K without pulsed biasing of the detectors. This temperature (which was assumed in all performance calculations) is sufficiently low to insure adequate accuracy for sounding and IR imaging functions.

Table 8 Sounding Performance For The ABQ Frame Sequence

Approximate Grid Spacing of Determined Soundings	No. of ABQ Sequences Req. for Averaging	Time Required To Obtain Adequate Sampling				Auto Mode Q Passes Obtained In Twice This Time Interval	Minimum Grid Spacing Of Q-branch Radiances
		100% Frame Height	10% Frame Height	1% Frame Height	Fixed Latitude		
10 km	76			1.14 hr.	13.7 min	152	20 km
20 km	23		3.5 hr.	0.35 hr.	4.2 min	46	35 km
35 km	10		1.5 hr.	9 min	1.8 min	20	70 km
70 km	3	4.5 hr.	0.45 hr.	3 min		6	150 km
110 km	2	3.0 hr.	0.30 hr.			4	220 km
200 km	1	1.5 hr.	0.15 hr.			2	400 km

Notes: Adequate sampling times for a given grid spacing are fixed by the requirement that NER $\leq$ 0.25 erg/(sec-cm^2-cm^{-1}-ster) for all A and B channels. It is assumed that relevant Q branch radiances can be obtained from averages over twice the time interval and twice the grid spacing (four times the area).

Entries missing from the table in the time columns refer to conditions which are either impossible or of negligible utility.

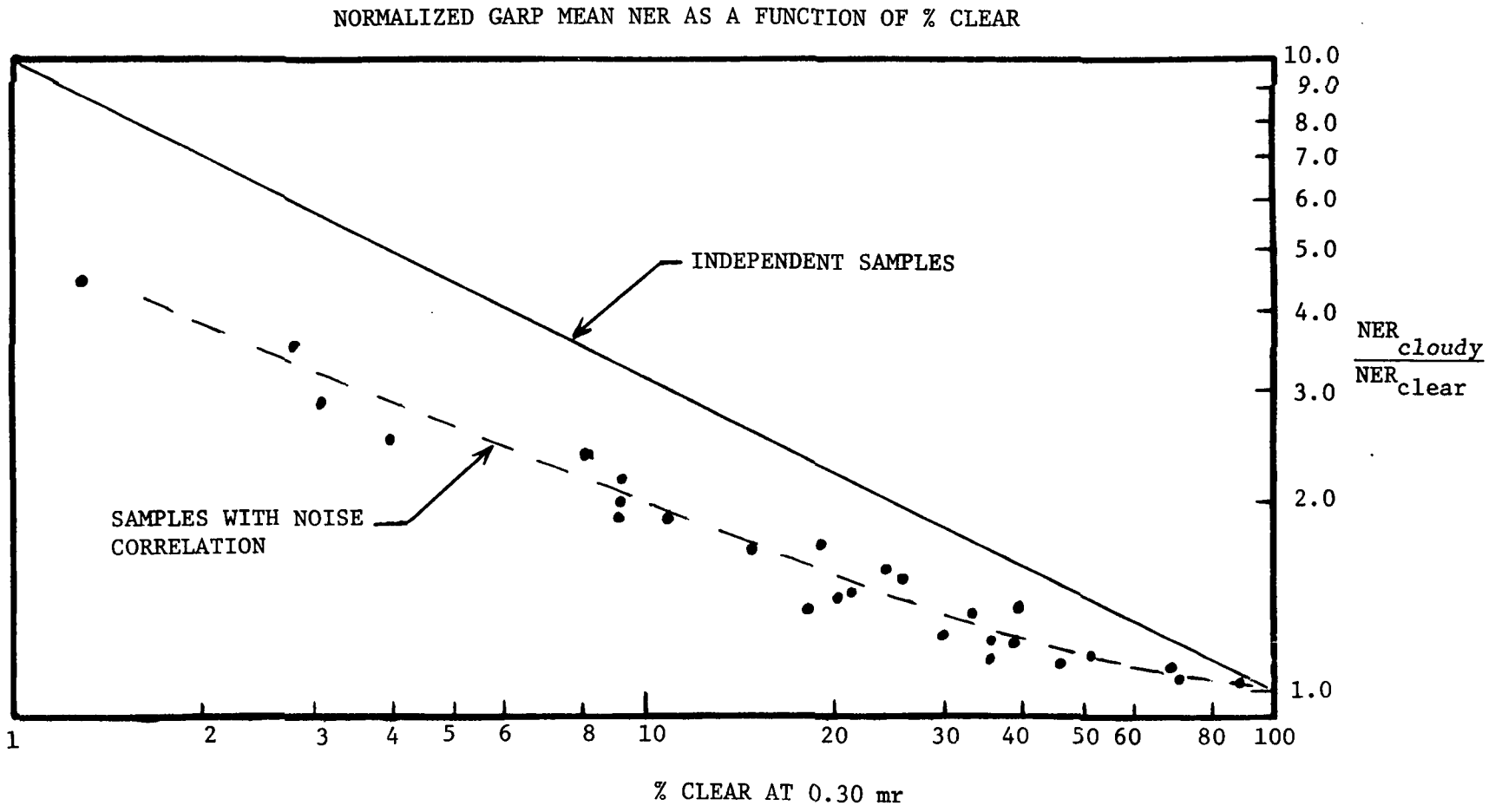

Figure 11. Effects of cloud cover on the NER of clear field data averages over a GARP grid box (400 km square). Results are normalized to unity for clear conditions. The plotted points are based on results in Appendix B, and the solid curve applies to independent sample averages (not the case for SMS).

APPENDIX A: NOISE AVERAGING STATISTICS

Temperature soundings of the atmosphere based on radiance measurements in the 15μm CO_2 band can be made only if clear column spectral radiances over the spatial regions of interest are determined within a standard error of 0.25 erg/(sec-ster-cm^2-cm^{-1}). Instrumentation specified for sounding from SMS can achieve this only by averaging many individual measurements, each with a standard error larger than that required for sounding. Thus it is important to determine precisely the effectiveness of such averaging procedures in reducing detector noise.

If all radiance measurements contained only random independent noise, then the standard error of the mean of N measurements, each with standard error σ, would be just $\sigma/\sqrt{N}$, a familiar result. However, since the infrared detectors in the specified configuration have substantial amounts of low frequency noise, samples taken every IFOV (i.e. at high frequency) will have noise components with significant correlation. This means that the standard error of the average of N SMS IR measurements will be larger than $\sigma/\sqrt{N}$. Determining how much larger is a relatively complicated procedure which must take into account the spectral distribution of detector noise power and the spatial distribution of the samples to be averaged. It is the subject of this appendix to describe the analytical methods used to treat this problem and to apply these techniques to appropriate aspects of SMS sounder performance analysis.

1. Detector Noise Characteristics

For the purposes of this discussion, detector noise can be completely described in terms of two related functions: the noise power spectral density which is given by

$$P(f) = \lim_{T \to \infty} \frac{2}{T} \left| \int_{-T/2}^{T/2} e(t)\exp(-2\pi ft)dt \right| , \qquad (2)$$

and the autocovariance function, defined as

$$C(\tau) = \lim_{T \to \infty} \frac{1}{T} \int_{-T/2}^{T/2} e(t)e(t+\tau)dt, \qquad (3)$$

where

f = frequency (Hz)

$e(t)$ = detector noise voltage at time t.

The autocovariance function can be related to the power spectrum through a cosine transform, i.e.

$$C(\tau) = \int_0^\infty P(f)\cos(2\pi f\tau)df . \qquad (4)$$

Equations (2) through (4) are the positive frequency versions of those given by Blackman and Tukey (Blackman, 1958).

Much of the subsequent discussion will be in terms of the RMS noise σ, and the signal variance, defined as

$$\sigma^2 = \lim_{T \to \infty} \frac{1}{T} \int_{-T/2}^{T/2} e(t)^2 dt. \tag{5}$$

The variance (or, in appropriate units, the noise power) is related to the noise power spectral density according to the equation

$$\sigma^2 = \int_0^\infty P(f)df, \tag{6}$$

where P(f)df represents the contribution to the signal variance from frequencies between f and f + df.

The approximate form for P(f) appropriate to detectors specified for SMS contains two components, each arising from independent processes. One part is independent of frequency and arises from generation-recombination noise (g-r noise). The second component is proportional to 1/f and arises from a number of sources. These are usually lumped together as "1/f noise." The frequency at which these two components are equal is called the crossover frequency, denoted by f_c. In practice, the detector signal will be filtered to eliminate all frequencies below f_{min} and above f_{max}. The effective noise power spectrum is thus given by

$$\begin{aligned} P(f) &= \frac{\sigma^2}{\Delta f_n}(1 + f_c/f), \quad f_{min} \leq f \leq f_{max} \\ P(f) &= 0, \qquad\qquad f < f_{min} \text{ or } f > f_{max} \end{aligned} \tag{7}$$

where Δf_n (the noise equivalent bandwidth) is determined through equation (6) to be

$$\Delta f_n = f_{max} - f_{min} + f_c \ln \frac{f_{max}}{f_{min}}. \tag{8}$$

The frequency constants appropriate to the HgCdTe detectors (used at 0.30 mr IFOV) and electronic filters specified for SMS are

$$\begin{aligned} f_c &= 750 \text{ Hz} \\ f_{min} &= .026 \text{ Hz} \\ f_{max} &= 17.45 \text{ KHz (0.30 mr IFOV)} \end{aligned} \tag{9}$$

It should be noted at this point that the approximate effect of DC restoration (to be discussed later) is to increase f_{min} to 2.0 Hz. However, for the present discussion the constants specified by (9) are appropriate.

2. Variance of Means: Theory

The expected variance of the means of samples of size N (containing N measurements) is defined as

$$\sigma_M^2 = E[(M-\mu)^2] = E(M^2) - \mu^2 \quad , \tag{10}$$

where E denotes expectation value, μ is the population mean, which is assumed to be zero for simplicity, and M is the sample mean

$$M = \frac{1}{N} \sum_{i=1}^{N} e(t_i) \quad , \tag{11}$$

where $e(t_i)$ is the detector signal at time t_i. Substituting (11) in (10), yields, after some manipulation,

$$\sigma_M^2 = \frac{1}{N^2} \sum_{i=1}^{N} \sum_{j=1}^{N} E[e(t_i)e(t_j)]. \tag{12}$$

For i = j the expectation of the product is just the population variance, i.e.

$$E[e(t_i)^2] = \sigma^2 \quad . \tag{13}$$

In general, we find that

$$E[e(t_i)e(t_j)] = C(t_j - t_i) \equiv C_{ij} \quad , \tag{14}$$

by definition (see equation (3)). Thus equation (12) can be rewritten as

$$\sigma_M^2 = \frac{1}{N} \sigma^2 + \frac{1}{N^2} \sum_{i-1}^{N} \sum_{j \neq i}^{N} C(t_j - t_i) \quad , \tag{15}$$

which shows directly the effect of noise correlation. If $e(t_i)$ and $e(t_j)$ were random independent variables then we would have $C(t_j-t_i) = 0$ for $t_i \neq t_j$ and the result $\sigma_M^2 = \frac{1}{N}\sigma^2$ would follow. Since $e(t_i)$ and $e(t_j)$ are not independent, a considerably different result is obtained (equation (15)).

For some applications, i.e. averaging all samples within a large time interval T, it is convenient to use an integral form for (15), namely,

$$\sigma_M^2 = \frac{1}{T^2}\int_t^{t+T} dt' \int_t^{t+T} dt''C(t'-t'') \qquad (16)$$

The function $C(\tau)$, which is central to this analysis, is shown in Figure 12 for the choice of constants specified by (9). $C(\tau)$ is obtained by numerical evaluation of equation (4). Also shown in Figure 12 is an approximation for $C(\tau)$, which is useful in applying equation (16), i.e.

$$C(\tau) \simeq \sigma^2 \frac{f_c}{\Delta f_n}[-\gamma - \ln 2\pi f_{min}\tau], \quad 2\pi f_{max}\tau >> 1 \ , \qquad (17)$$

where $\gamma = 0.577216$. For the constants of (9), this yields

$$C(\tau) \simeq [.0336 - .0273 \ln\tau]^2 \ , \quad (\tau \text{ in sec}). \qquad (18)$$

It should be noted that the techniques developed here can be applied not only to the determination of variance of means but also to the determination of variance of other linear combinations of data such as those involved in calibration. All that is needed is a specification of the space (or time) distribution of samples to be used.

3. Variance of Means: SMS Application

Temperature profiles determined from SMS sounder data will be based on averages of spectral radiance measurements over time and space. The spatial average generally consists of both measurements along scan lines (which have correlated noise) and also measurements on different scan lines (which have statistically uncorrelated noise). Typically, only measurements from clear FOV's will be used in the averages.

If N_L is the number of scan lines involved in the averages, N_k the number of measurements averaged on the kth scan line, and e_{ik} the error of the ith measurement on the kth scan line, then the expected variance of the mean of these measurements is given by

$$\sigma_M^2 = \sum_{k=1}^{N_L} \sum_{n=1}^{N_L} \sum_{j=1}^{N_1} \sum_{i=1}^{N_k} E(e_{ik}e_{jn})/N_{TOT}^2 \qquad (19)$$

where

$$N_{TOT} = \sum_{k=1}^{N_L} N_k \qquad (20)$$

is the total number of measurements averaged.

Since measurements on different scan lines ($k \neq n$) have no noise correlation, while measurements on the same scan line ($k=n$) do (equation (14)), it is found that

$$E(e_{ik}e_{jn}) = C_{ij}\delta_{kn}. \qquad (21)$$

Inserting this result in equation (19) reduces it to the form,

$$\sigma_M^2 = \frac{1}{N_{TOT}^2} \sum_{k=1}^{N_L} V_k \quad , \qquad (22)$$

where V_k, the expected variance of the sum of the N_k measurements on the kth scan line, is given by

$$V_k = \sum_{i=1}^{N_k} \sum_{j=1}^{N_k} C_{ij} \qquad (23)$$

Recall that $C_{ij} = C_{ji}$ since it depends only on the time interval between the ith and jth measurements.

To illustrate the application of these results, an example variance calculation will be made for three similar areas differing only in cloud cover. These are shown in Figure 13. The shaded boxes represent the clear FOV measurements from which average radiances are determined. Since there are only three distinct time intervals involved in this example, only three values of $C(\tau)$ are involved. These are listed in Table 9 for $f_{min} = .026$ Hz, $f_{min} = 2.0$ Hz (equivalent to DC restoration), and for the case of independent measurements (no noise correlation).

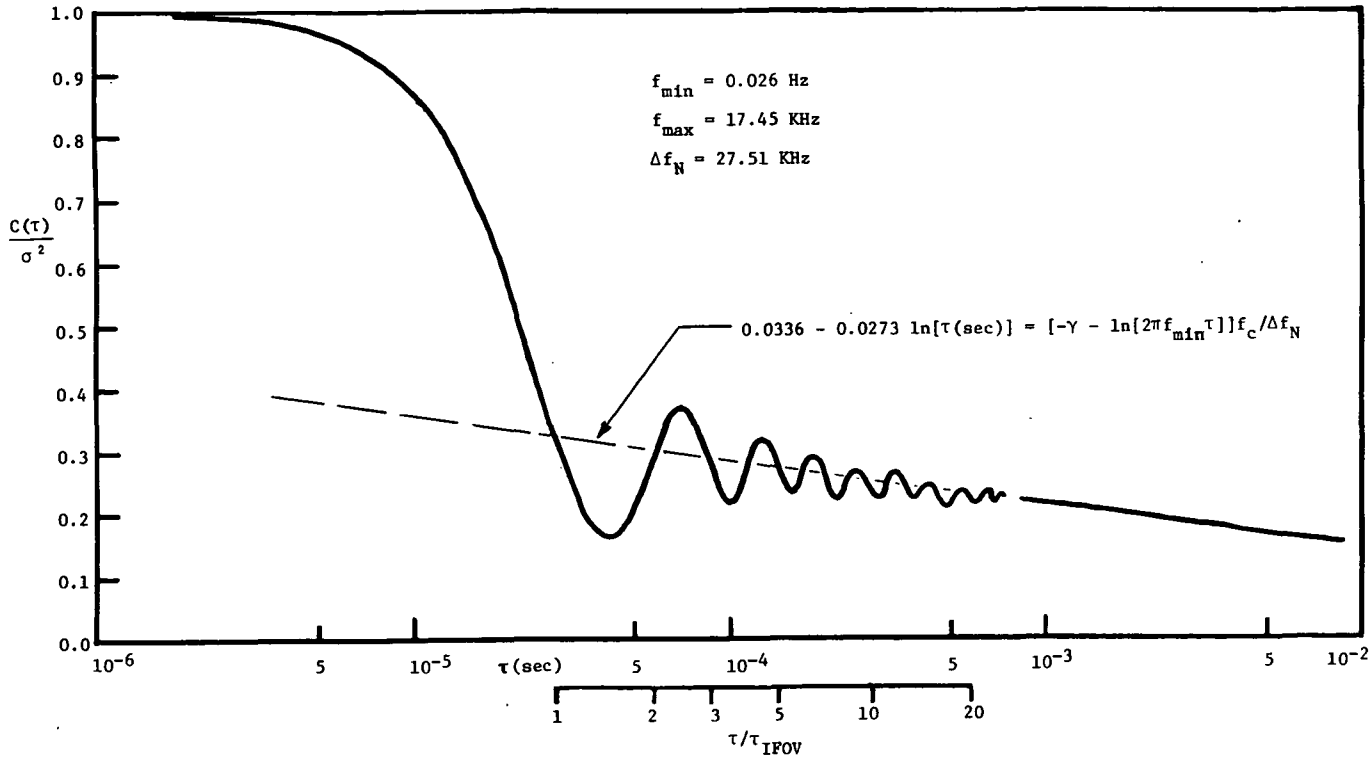

Figure 12. The autocovariance function for noise and filter characteristics applicable to the modified SMS.

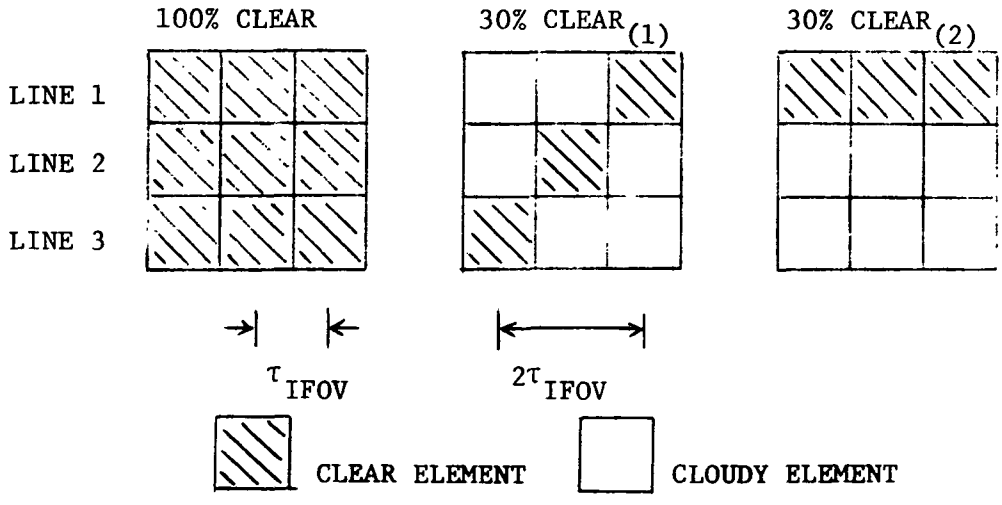

Figure 13. The three data grids used in example variance calculations of data averages.

Table 9 Autocovariance Values

	f_{min} = .026 Hz	f_{min} = 2 Hz (DC Restore)	Indep. Meas.
C(0)	1.0	1.0	1.0
$C(\tau_{IFOV})$	0.33	0.25	0.0
$C(2\tau_{IFOV})$	0.29	0.19	0.0

The variance (σ_M^2) calculations are summarized in Table 10. The line sum variances are calculated according to equation (23). For example, for line 1 of the 100% clear case this is determined as

$$V_1 = \sum_{i=1}^{3} \sum_{j=1}^{3} C_{ij} = 3\,C(0) + 4\,C(\tau_{IFOV}) + 2\,C(2\tau_{IFOV}),$$

whereas for the first 30% clear case the calculation yields the quite different result

$$V_1 = C_{33} = C(0).$$

Table 10 Variance Calculation Summary

Noise Situation	Case	V_1	V_2	V_3	N_{TOT}	σ_M^2
f_{min}=.026Hz	100% clear	4.92	4.92	4.92	9	0.18
	30% clear$_{(1)}$	1.0	1.0	1.0	3	0.33
	30% clear$_{(2)}$	4.92	N.A.	N.A.	3	0.55
f_{min}=2Hz (DC Restore)	100% clear	4.38	4.38	4.38	9	0.16
	30% clear$_{(1)}$	1.0	1.0	1.0	3	0.33
	30% clear$_{(2)}$	4.38	N.A.	N.A.	3	0.49
Uncorrelated Noise	100% clear	1.0	1.0	1.0	9	0.11
	30% clear$_{(1)}$	1.0	1.0	1.0	3	0.33
	30% clear$_{(2)}$	1.0	N.A.	N.A.	3	0.33

This example also illustrates the significance of the spatial distribution of cloud cover on SMS data averages: for the same percentage of cloud cover the expected variance strongly depends on where the cloud elements are located. The minimum variance is obtained when cloud elements are distributed equally over all scan lines. This comes about because of the relatively low statistical independence of the noise in measurements made along the same scan line.

Similar calculations have been applied to much larger averaging areas (400 km x 400 km GARP grid boxes) using a large sample of real cloud distributions determined from an analysis of ATS data. These results, which are presented in Appendix B, indicate a dependence of σ_M^2 on cloud cover which is relatively weak compared to that which would arise from data free of noise correlation

4. Variance of DC Restored Data

DC Restoration, as applied in SMS, is accomplished by an electronic feedback circuit which maintains the filtered detector response to space at a fixed voltage reference (usually 0 volts) prior to scanning the earth's disc. This results in the elimination of very low frequency noise components (effective f_{min} is increased from .026 Hz to 2 Hz) and references subsequent earth radiance measurements to an absolute calibration point, i.e. the spectral radiance of space.

An approximate mathematical equivalent of this procedure will now be described. The spectral radiance of the earth $I_E(t)$ at time t along a given scan line is determined from the error-free detector voltage $X_E(t)$ through the relation,

$$I_E(t) = \alpha(X_E(t) - X_4o) + I_4o, \tag{24}$$

where α is a proportionality factor and

I_4o = spectral radiance of space

X_4o = error free detector voltage response to space.

Note that equation (24) and the parameters involved do not contain errors.

The "measured" earth radiance with DC Restoration applied is given by

$$\tilde{I}_E(t) = \tilde{\alpha}(\tilde{X}_E(t) - \tilde{X}_4o) + I_4o \tag{25}$$

where the measured proportionality factor $\tilde{\alpha}$ (determined in reality by a two-point calibration) will be assumed insignificantly different from α. The remaining measured quantities in (24) are defined by

$$\tilde{X}_E(t) = X_E(t) + e(t) \tag{26}$$

$$\tilde{X}_{4o} = X_{4o} + \bar{e}_1 \tag{27}$$

where, for space response averaging from t_1 to t_2,

$$\bar{e}_1 = \frac{1}{t_2 - t_1} \int_{t_1}^{t_2} e(t')dt'. \tag{28}$$

We are, of course, assuming that $t > t_2$, i.e. DC Restoration is performed before the earth is scanned.

Making use of equations (24) through (28), we can write the difference between measured and actual earth radiances as

$$\tilde{I}_E(t) - I_E(t) = \alpha[e(t) - \bar{e}_1], \quad \text{(DC restore)}. \tag{29}$$

Taking the expectation value of the square of (29) yields the variance of the measurements $\tilde{I}_E(t)$. This takes the form

$$\sigma^2_{DCR} = \sigma^2[V_t + \bar{V}_1 - 2\bar{V}_{1t}], \tag{30}$$

where we define

$$V_t = E[e^2(t)] = \sigma^2 \tag{31}$$

$$\bar{V}_1 = E[\bar{e}^2] = \frac{1}{(t_2-t_1)^2}\int_{t_1}^{t_2} dt \int_{t_1}^{t_2} dt'C(t-t') \tag{32}$$

$$\bar{V}_{1t} = E[e(t)\bar{e}_1] = \frac{1}{t_2 - t_1}\int_{t_1}^{t_2} C(t-t')dt'. \tag{33}$$

Employing the approximation for $C(\tau)$ given in equation (18) in the integrals of equations (32) and (33), we find

$$\overline{V}_1 = \sigma^2[a + b\ln\Delta - \frac{3}{2} b] \tag{34}$$

$$\overline{V}_{1t} = \sigma^2[a - b + \frac{1}{\Delta} b(\delta\ln\delta - (\delta-\Delta)\ln(\delta-\Delta))] \tag{35}$$

where

$$\Delta = t_2 - t_1$$

$$\delta = t - t_1$$

$$a = .0336$$

$$b = .0273$$

For $\Delta = .03$ sec (the DC Restore time period), we find

$$\overline{V}_1 = 0.170\ \sigma^2, \quad \Delta = .03 \text{ sec.} \tag{36}$$

The term $\overline{V}_{1t}$ depends on δ which varies from $\delta \simeq \Delta$ to $\delta \simeq 2\Delta$, assuming that the earth scan begins shortly after the end of DC restoration. At the midpoint of the earth scan we find

$$\overline{V}_{1t} = 0.130\ \sigma^2, \quad \delta = 1.5 \tag{37}$$

and thus

$$\sigma^2_{DCR} = 0.91\ \sigma^2, \quad \delta = 1.5\ . \tag{38}$$

The variation of σ^2_{DCR} across the earth's disc is shown in Figure 14. (In equation (37), σ^2 is in units of spectral radiance squared, in which case $\alpha = 1$).

The effect of DC restoration on the variance of means of data can be found by making the replacement

$$C(t_i-t_j) \rightarrow C(t_i-t_j) - (\bar{V}_{1t_j} + \bar{V}_{1t_i}) + \bar{V}_1,$$

i.e. the right side replaces the left side in all variance calculations. The right side is plotted in Figure 15 for t_i and t_j corresponding to δ near 0.045 sec (midpoint of the earth scan). Also shown in Figure 15 is a plot of $C(\tau)$ for the lower cut-off $f_{min} \simeq 2$Hz. The similarity of the two curves is such that DC restoration may be approximated by increasing the lower cut-off frequency to 2Hz, although this is by no means exact.

5. Calibration Variance

Since DC Restoration determines the space reference in equation (24), only one more point (say at 300°K) is required to make a two-point radiance calibration of the SMS detection system. This can be achieved by exposing the detectors to radiation from a shutter (at ambient temperature) which is introduced into the IR relay optical train as required. This must be done in order to determine the proportionality factor α in equation (24). Suppose the detectors are exposed to space and then to the 300°K shutter. This single calibration event may be summarized by the following table:

Time Span	Scene	Voltage	Signal Handling
$-\Delta$ to 0	SPACE	$X_{4^o} + e(t)$	Averaging
0 to Δ	SHUTTER	$X_{300^o} + e(t)$	Averaging

The best estimate $\tilde{\alpha}$ for the proportionality factor α is thus

$$\tilde{\alpha} = (I_{300^o} - I_{4^o})/(\tilde{X}_{300^o} - \tilde{X}_{4^o})^{-1} \qquad (39)$$

where

$$\tilde{X}_{300^o} = \tilde{X}_{300^o} + \bar{e}_{300} \qquad (40)$$

$$\tilde{X}_{4^o} = X_{4^o} + \bar{e}_4$$

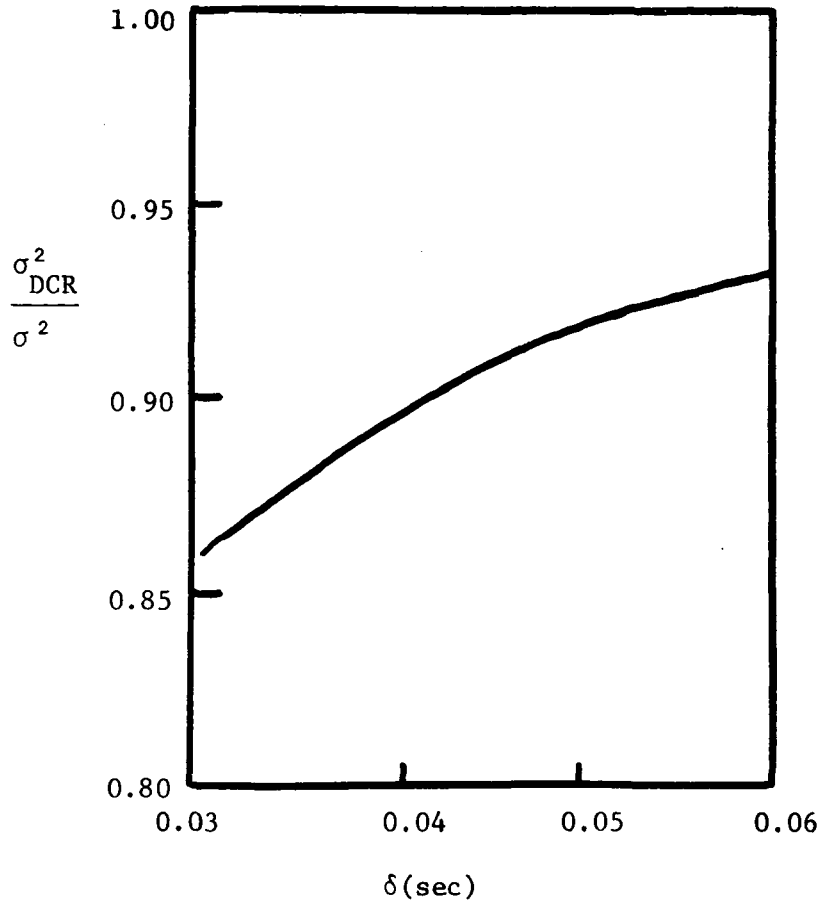

Figure 14. The ratio of noise variance with DC restoration to noise variance without DC restoration as a function of time along a scan (the earth scan starts at δ = 0.03 sec and ends at δ = 0.06 sec).

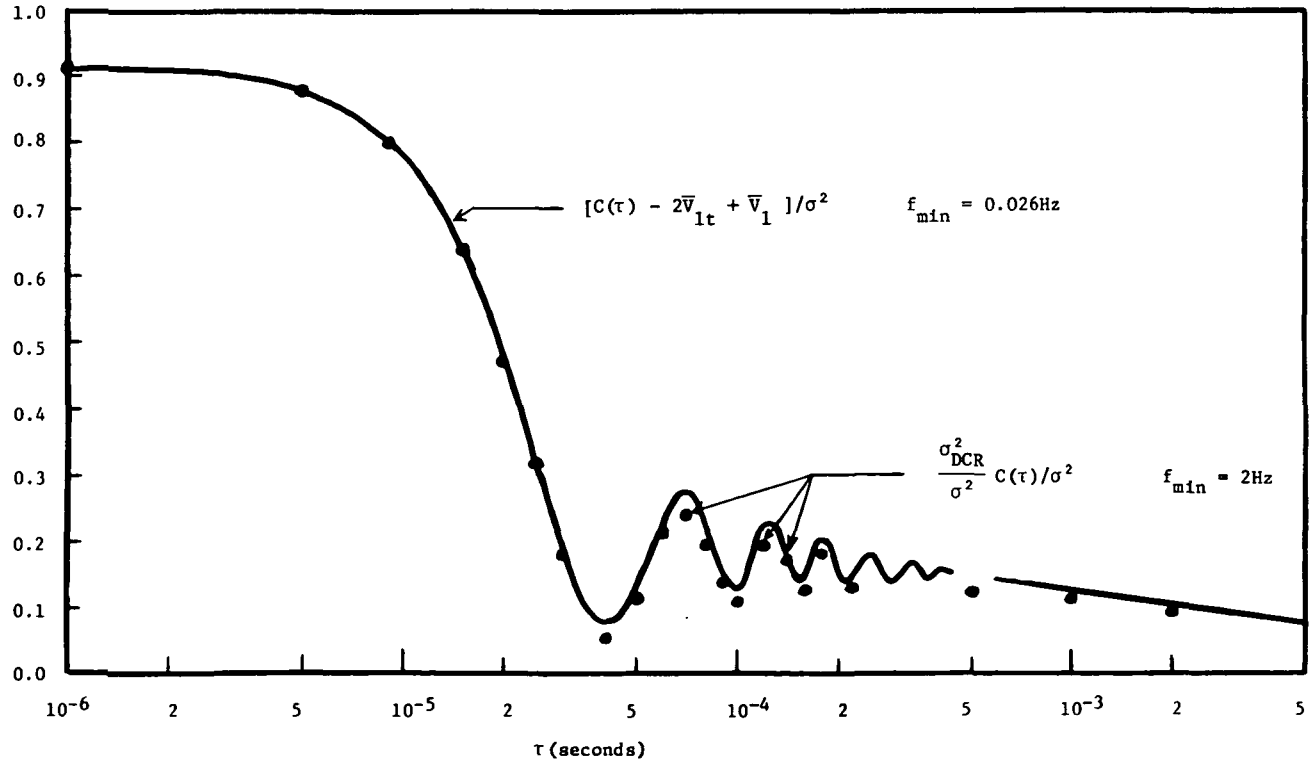

Figure 15. Comparison of $C(\tau)$ with DC restoration and $C(\tau)$ with f_{min} = 2 Hz.

$$\bar{e}_4 = \frac{1}{\Delta} \int_{-\Delta}^{0} e(t)dt \tag{42}$$

$$\bar{e}_{300} = \frac{1}{\Delta} \int_{0}^{\Delta} e(t)dt. \tag{43}$$

The average of the results of K calibration events reduces the error in $\tilde{\alpha}$ such that the contribution to radiance variance from calibration is given by

$$\sigma_c^2(K) = \frac{1}{K} E[\bar{e}_{300}^2 + \bar{e}_4^2 - 2\bar{e}_{300}\bar{e}_4]. \tag{44}$$

This term must be added to the right-hand side of equation (29) to yield the total signal variance (in radiance equivalent terms).

Applying the techniques already developed and the approximations (17) and (18) for $C(\tau)$, we find that

$$\sigma_c^2(K) = \frac{\sigma^2}{K} [-\frac{3}{2} \frac{f_c}{\Delta f_n} \ln 2\pi f_{min}] = 0.041\ \sigma^2/K \tag{45}$$

for the SMS sounder channels, as specified in this report. Within the approximations used, $\sigma^2_c(K)$ is independent of Δ. This is true for $\Delta >> 1/(2\pi f_{max})$. Equation (45) is useful in estimating the calibration frequency requirements for the SMS sounder.

The maximum radiance variance permitted by the requirements of inversion is $(.25\ \text{erg/etc})^2 = .065\ (\text{erg/etc})^2$. If we require that $\sigma_c^2(K)$ be only 10% of this total, then the number of calibration events needed is

$$K = .656\ \sigma^2/(\text{erg/etc})^2 \tag{46}$$

For most SMS sounding channels $\sigma^2 \simeq 5.0(\text{erg/etc})^2$, and for the Q-branch $\sigma^2 \simeq 160(\text{erg/etc})^2$. Substitution of these values into (45) shows that three or four events are sufficient for most channels and that one hundred five events are needed for the Q-branch calibration (669 cm^{-1}).

6. Correlated Noise Simulation

Many of the data handling algorithms studied for application to clear column radiance retrieval (Appendix C) are too complex to be simply evaluated

by methods described previously. In some cases only Monte Carlo techniques are practical. In the application of these techniques it is necessary to generate random noise with specific correlation properties and with a minimum of computer costs. This section describes the method that was developed to meet this need.

The method is designed to generate a string of random correlated numbers e_i, i-1,n which correspond to measurements at times t_i, i=1,n along a given scan line, and which satisfy the requirement

$$E[e_i e_j] = C_{ij} \equiv C(t_i - t_j) , \tag{47}$$

where, as before E denotes the expectation value.

The correlated numbers can be formed from a string of n uncorrelated random numbers r_i, i=1,n by linear combination, i.e.

$$e_i = \sum_{j=1}^{n} a_{ij} r_j . \tag{48}$$

Substituting (48) into (47) yields the following condition on the linear combination coefficients:

$$\sum_{j=1}^{N} a_{ij} a_{kj} = c_{ik} . \tag{49}$$

In forming a solution to equation (49) it is helpful to rewrite the problem in vector notation. The vectors are defined as

$$\vec{a}_i = (a_{i1}, a_{i2}, a_{i3}, \cdots a_{in}), \quad i=1,n. \tag{50}$$

The condition stated in equation (49) becomes

$$\vec{a}_i \cdot \vec{a}_k = C_{ik}, \quad (|a| = \sigma). \tag{51}$$

The simplest solution is to choose the $\vec{a}_i$ to be linearly independent in the following manner.

$$\vec{a}_1 = (a_{11}, 0, 0, \ldots, 0)$$

$$\vec{a}_2 = (a_{21}, a_{22}, 0, \ldots, 0)$$

.

.

.

$$\vec{a}_k = (a_{k1}, a_{k2}, \ldots, a_{11}, 0, \ldots, 0)$$

$$\vec{a}_n = (a_{n1}, a_{n2}, \ldots, a_{n,n-1}, a_{nn}). \qquad (52)$$

The $n(n+1)/2$ non zero coefficients can be uniquely solved by applying the $n + (n^2+n)/2$ independent conditions of equation (50).

Once the a_{ij} coefficients are determined for the appropriate $C(\tau)$, they can be used repeatedly to convert strings of computer generated random numbers to strings of correlated random numbers through equation (47).

APPENDIX B: CLOUD DISTRIBUTION STUDIES

Radiometrically sounding the atmosphere for the temperature profile requires a knowledge of the clouds which may be within the field of view. The simplest method is to sound only in areas that are clear; however, the most interesting meteorological information is in regions of weather development which involve clouds. Therefore, looking between the clouds in cloudy regions is desirable.

A study was undertaken to examine cloud distributions using reflected radiance measurements from the ATS satellites (Stamm, 1970). The first portion of this appendix describes the study of fractional cloudiness as a function of spatial resolution.

As work progressed toward developing a feasible sounder for SMS, it became apparent that a description of only the percent clear area within a cloudy region was insufficient. A more complex analysis including detector noise statistics was required. Thus a new study of ATS data was undertaken and makes up the second part of this appendix. Similar studies of a small number of cases based on high resolution Gemini photographs are discussed in Appendix C.

Finally, the three-dimensional distribution of clouds determined from AFGWC and ITOS data is discussed.

1. Fractional Cloudiness as a Function of Spatial Resolution: ATS Data

The purpose of the first ATS data cloud study was to find the percentages of selected cloudy areas of the earth that are cloud-free at various spatial resolutions. The criterion was made that if any ATS sample was determined to contain clouds (i.e., the radiance was over a predetermined threshold), then all fields of view of any size containing this sample would be considered cloudy. The data grids were approximately the size of a GARP grid.

An example of the data is given in Figure 16. It shows the clear area vs. resolution normalized to percent clear area at 4.6 km for an extratropical front over northwestern United States on 23 April 1968 at 1714:10 GMT. Numbers indicate percent clear area at 4.6 km resolution, which is somewhat less than the true clear area percentage. In general, areas that are highly cloudy at small fields-of-view (IFOV) increase in cloudiness faster with increasing IFOV than less cloudy areas. However, this figure shows that although the warm sector has fewer clouds than the frontal band at 4.6 km resolution, its percent clear area decreases faster with reduced resolution. This is because the clouds in the warm sector are a more irregular mixture of different types making the holes between the clouds smaller. Other cloud types investigated included cumulus and cumulonimbus over the Amazon, the intertropical convergence zone, and subtropical high pressure zone cumulus and stratus. Cloud types on 20 January 1968 at 1911:31 GMT were also investigated.

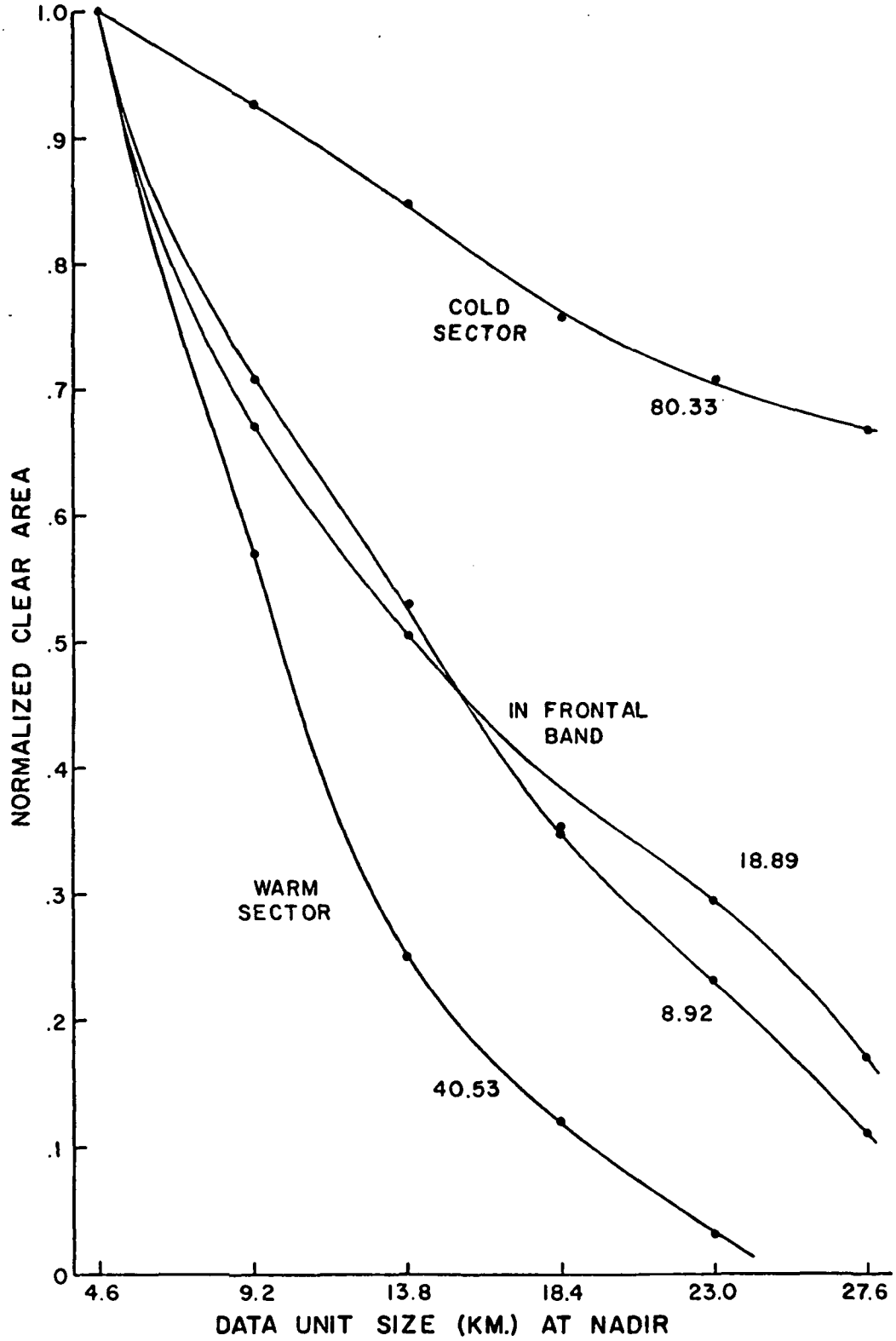

Figure 16. Normalized clear area as a function of spatial resolution for selected ATS data.

The conclusion of this study is that, assuming only a small number of detectors is available, 0.4 mr is a good IFOV size for temperature sounding from geosynchronous altitude.

2. Statistical Frequency of GARP Grids as a Function of Cloud Cover

Once a good spatial resolution had been determined for cloudy areas, it was desirable to find out how much of the earth was cloudy. The 20 January 1968 ATS-III photograph was divided into 652 GARP-sized grids (400 km). Training on the few areas of this photograph which had been previously investigated, an estimate was made of the percent of clear area within each grid. The results are given in Figure 17(a). The numbers give the percent of the total number of grids within each category. On this particular day, there was more cloud area than clear area. The main conclusion to be drawn from this is that less than 20% of the grids are difficult to sound (i.e., are over 80% cloudy).

Additional statistics were obtained for the 23 April 1968 case, for which 143 GARP-sized grids were analized by computer to determine the percent clear at ATS resolution (see next section). The results are given in Figure 17 (b). These results are not completely representative since clear regions were purposely not analized.

3. Effects of Cloud Cover and Sounder Resolution on Clear Field Averages

It is established in Appendix A that the minimum variance of a data mean is obtained when the samples used are equally distributed among all the scan lines intersecting the averaging areas. This would be the case if clouds were in streaks going north-south. East-west streaks would have the opposite effect and averaging of clear IFOV's would produce less noise reduction. In order to determine the effects of averaging in a large number of realistic cases, ATS-3 data was selected for analysis. 23 April 1968 at 1714:10 GMT was chosen because it had been previously studied (Stamm, 1970). The half earth photo was divided into GARP sized grids (400 km across). A large number of the grids fell into two natural regions which were analyzed separately: 1. United States and Canada (32 grids). 2. Atlantic Ocean (45 grids).

Each of the grids contained 84 ATS lines and 252 ATS samples per line. The grids were subdivided in 3 ways in order to simulate 3 different instantaneous fields of view (IFOV): 1) 1 line by 3 samples (0.125 mr) giving 84 x 84 or 7056 IFOV's per grid; 2) 2 lines by 6 samples (0.25 mr) giving 42 x 42 or 1764 IFOV's per grid; and 3) 3 lines by 9 samples (0.38 mr) giving 28 x 28 or 784 IFOV's per grid. From a plot of relative radiance vs. sample number, a cloud threshold value was chosen for each grid corresponding to a radiance just above the signal (including noise) of the ocean or land (see Stamm, 1970). The percent of the 21,168 samples in each grid with radiances below the cloud threshold was then counted to determine the percent clear at ATS resolution.

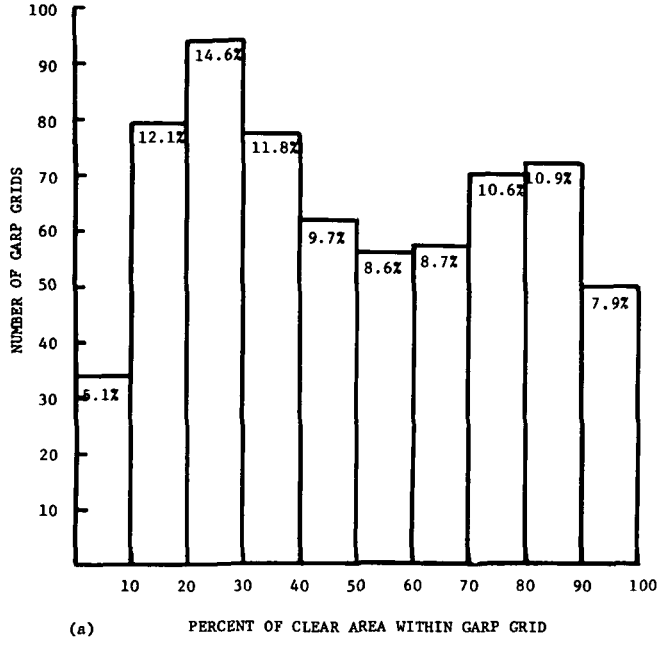

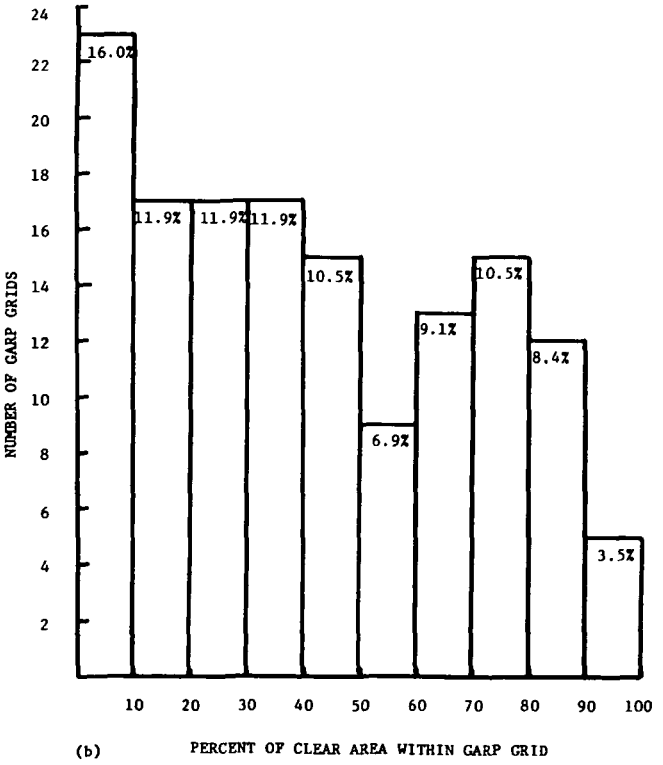

Figure 17. Frequency of GARP grids as a function of cloud cover derived from ATS data: (a) visual estimates using 20 January 1968 ATS III photograph; (b) computer analysis using 23 April 1968 ATS III data.

If any of the samples in the sounding IFOV had a radiance above the cloud threshold, the whole IFOV was considered cloudy. The percent of the IFOV's within a grid which were entirely clear was calculated and called percent clear at sounder resolution. This was done for each of the 3 resolutions. Figure 18 shows an example of a grid (0.38 mr resolution) in which each entirely clear IFOV is marked with an X.

The noise within the samples along a single line of data is not independent; it depends on the time relationships among the "clear" samples (see Appendix A). Thus the reduction in variance obtainable by averaging the entirely clear IFOV's along a line was calculated for each line of IFOV's in each grid from the relative time spacing of the clear IFOV's. Since the noise from data on different scan lines is independent, the noise for the individual lines could be combined in a weighted average to get the mean noise for the grid. The standard deviation (square root of variance) to the data mean for the grid pictured in Figure 18 was determined to be 11.5% of the single samples standard deviation.

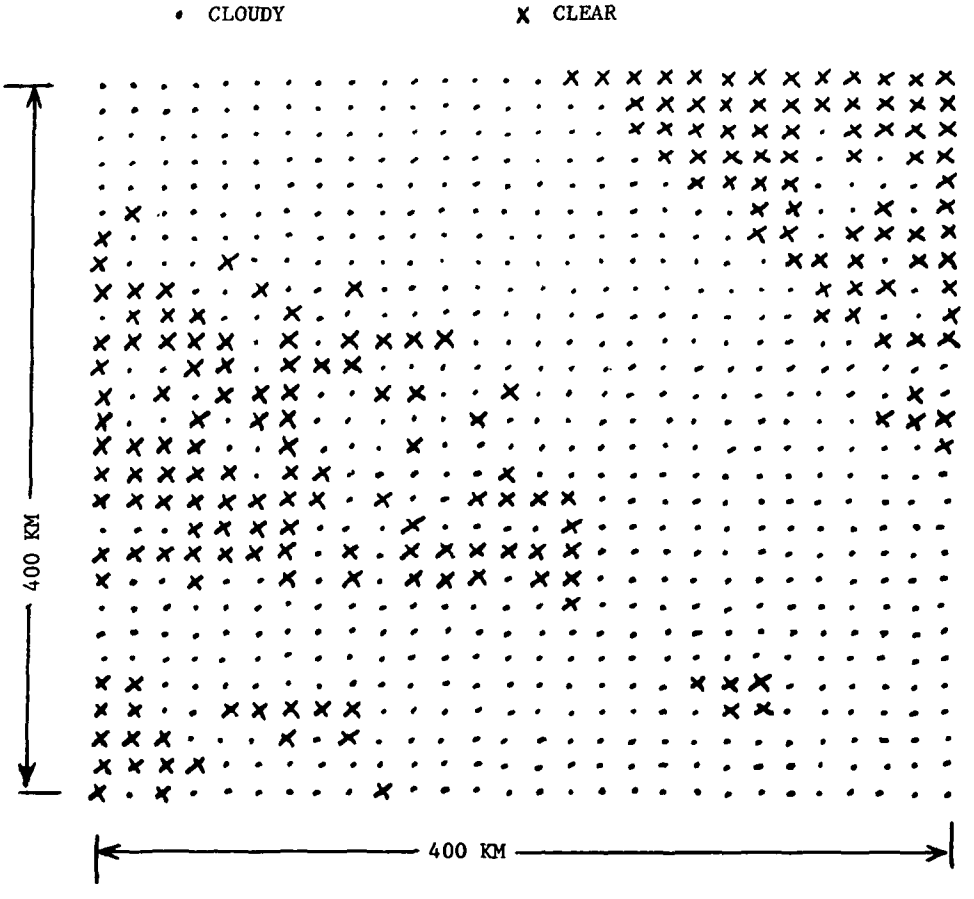

Figure 18. An example of the ATS derived cloud grids used in calulating noise in area averages of clear column radiances.

Figures 19 and 20 show the results of the analysis of the 32 land grids and 45 ocean grids respectively. The ratio of the standard deviation of the clear IFOV mean (σ_M) to the standard deviation of single measurements (σ) is plotted vs. the percent clear at ATS resolution for each of three different resolutions. The dashed lines indicate what the ratio would be for independent samples for the three resolutions. The location and scatter of the points are essentially the same both over land and over water. It should be noted that the dependence on cloud cover is considerably less in the real case than it is for independent samples. In other words, cloudy situations are degraded much less from the independent sample case than clear situations.

In order to meet the GARP requirement of an error less than 0.25 erg/(sec-cm^2-cm^{-1}-ster), the following standard deviation ratios (σ_M/σ) are required: 0.167 (0.38 mr), 0.093 (0.25 mr), and 0.036 (0.125 mr). These ratios can be doubled if four complete coverages are averaged. The following table summarizes the 77 grids analized. (Unsoundable means no clear IFOV's at that resolution).

Percent of Grids

	0.38 mr	0.25 mr	0.125 mr
Soundable in:			
1 Coverage	69%	53%	25%
4 Coverages	88%	87%	83%
Unsoundable	5%	$2\frac{1}{2}$%	0%

The higher resolution (0.125 mr) has a greater noise reduction (ratio of averaged standard deviation to single IFOV standard deviation is less), but the original single IFOV standard deviation is greater. These two effects almost exactly cancel if the total detector area is kept constant. Under this constraint, which is nearly equivalent to constant detector dissipation, four detectors at 0.125 mr are available for every detector at 0.25 mr. But only two are needed to duplicate the area coverage. (All of this ATS analysis assumes complete area coverage for each resolution). Therefore, since the sounder will be stepping a constant amount (0.192 mr) regardless of sounder resolution, and since only two of the four detectors will be needed for complete coverage, the total area will be scanned twice at 0.125 mr for every scan at 0.25 mr.

If the lens speed and the noise equivalent bandwidth Δf_N are kept constant, the noise of a single detector is inversely proportional to the square root of the detector area; thus the noise for the 0.125 mr detector should be twice the noise of the 0.25 mr detector. On the other hand, for independent samples, the noise reduction due to averaging is inversely proportional to the square root of the number of samples. Since, with the 0.125 mr detectors, there are four times as many samples as

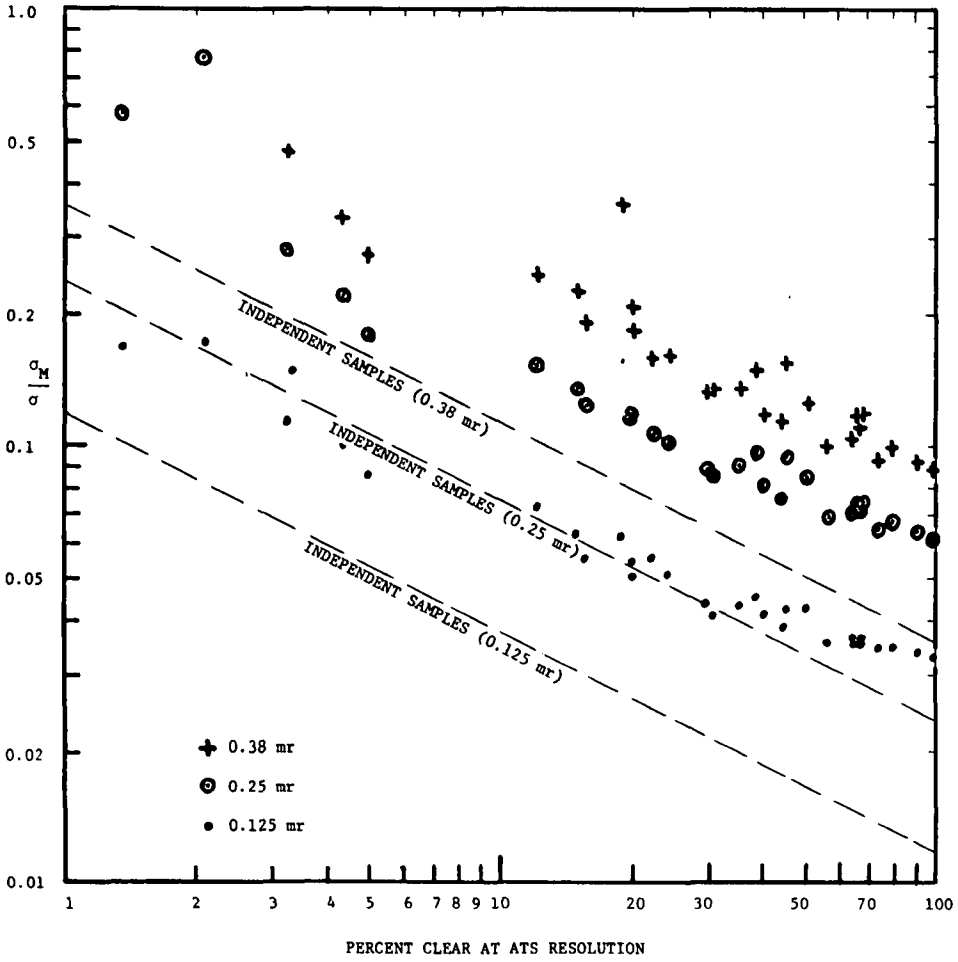

Figure 19. Effects of cloud cover on the ratio of the standard deviation of the clear IFOV mean to the standard deviation of single samples. Results are from an analysis of 32 ATS III-derived GARP grids over the U.S. and Canada.

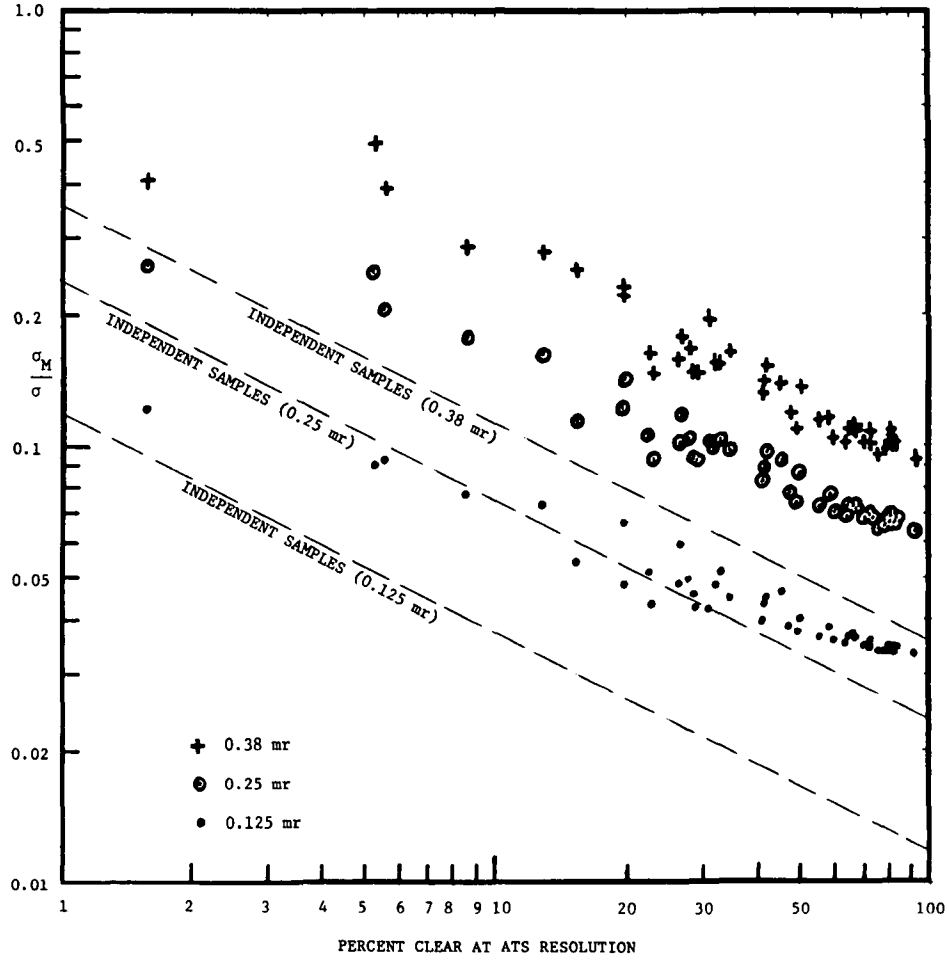

Figure 20. Same as Figure 19 except that 45 ocean grids were analyzed.

with the 0.25 mr detector, the total averaged noise should be the same. The real (non independent) case is shown in Figure 21 where the ratios of standard deviation reduction (i.e. square root of noise reduction) at the various resolutions is displayed as a function of cloud cover. The real situation, including the change in Δf_N and in averaging characteristics with resolution, is not far from the independent sample case described above even for very cloudy situations.

The conclusion of this analysis is that, within the range studied, the resolution does not make too much difference provided that the total detector area is kept constant and provided that extremely cloudy cases are not considered. The lower resolution (0.38 mr) is slightly better for completely clear areas and the higher resolution (0.125 mr) is better for cloudy situations. Since cloudy situations are more difficult to sound, the resolution should be made as small as possible consistant with the equal detector area requirement. This is, the limit depends on the number of detectors possible (determined by detector leads, construction, and telemetry channels).

4. Three-Dimensional Distribution of Cloud Openings

The previous discussion assumes that all soundings require clear fields of view all the way to the ground. However, if only low clouds are present, the channels which sense the atmosphere above these clouds can still operate. Hence, a new study was undertaken in March 1971 to determine cloud spacings as a function of altitude. The first data to be analyzed were "three-dimensional Nephanalysis" maps produced by Air Force Global Weather Central. These maps are an aggregation of surface, radiosonde, aircraft, and satellite measurements. Cloud top heights are given every 100 n. mi. (Coburn, 1970).

After a preliminary hand analysis involving the drawing of contours on the maps, the cloud top altitudes were put into a computer. An area roughly 6000 by 4000 km over North America and the Atlantic Ocean and a similar size area over the North Pacific, both containing large cyclones, were chosen. Using squares 100, 200, 300, and 400 nmi on a side as resolution elements, the percentages of these resolution elements within the large area, which were clear down to a given altitude were determined. Figure 22(a) shows these percentages vs. resolution. The altitudes correspond roughly to 1000, 750, 500, 300, and 200 mb. The figure also shows the situation twelve hours later. Since a cloudy region was picked in the first place, it is logical that the cloudiness would decrease with time.

In order to obtain higher resolution data, the second phase of the three-dimensional cloud statistics study involved the analysis of ITOS infrared (11μm) imagery for 27 April 1971 at night. The area encompassed a large frontal system over the midwestern United States at about 1100 GMT. The data was in the form of a polar stereographic map with 2048 by 2048 data samples per hemisphere. The ground resolution of the data ranged from 4 mi at the equator to 8 mi at the pole. In the vicinity of the frontal system, the resolution was between 6 mi and 7 mi. The frontal system was

divided into thirty regions that were forty data samples on a side. This amounted to about 400 km or a GARP-sized grid.

The data was given in terms of temperature. In order to translate this into cloud top altitudes, the radiosonde soundings for 27 April 1971, 1200 GMT were used. Using the soundings in and near each region, the minimum, maximum and weighted average (more significance given to the soundings in the center of the region) of the temperature at each level were determined.

As with the "three-dimensional nephanalysis" maps study, the purpose was to find the percent of the area with cloud tops above a given altitude: that is, the percent of area unusable for sounding down to that altitude. Again, the various resolutions were simulated by combining the data elements, and a resolution element was considered cloudy if any of the data elements within it were cloudy. Figure 22(b) shows the change in cloudiness for various resolutions and levels for a typical cloudy region in the frontal system. The X indicates the cloudiness when the average temperature was used for the level, and the error bars indicate the results with the minimum and maximum temperatures.

The conclusion is that holes between clouds are larger and represent a greater percentage of the area at high altitudes than at low altitudes. Therefore, more of the samples are usuable at high altitudes. In fact, the Q-branch can be thought of as being entirely clear.

One difficulty with trying to determine cloud top altitudes from a single channel of infrared radiation is that the average temperature of a scene is found. Examination of high resolution Gemini and Apollo photographs shows that there are many cases of cloud clusters where the size of individual clouds is considerably less than the IFOV of ITOS, Nimbus, ATS, or even the SMS infrared imaging channels. This means that the cloud temperature is averaged with the ground temperature between the clouds, giving an apparent cloud top height less than the true height. This effect should be investigated more thoroughly.

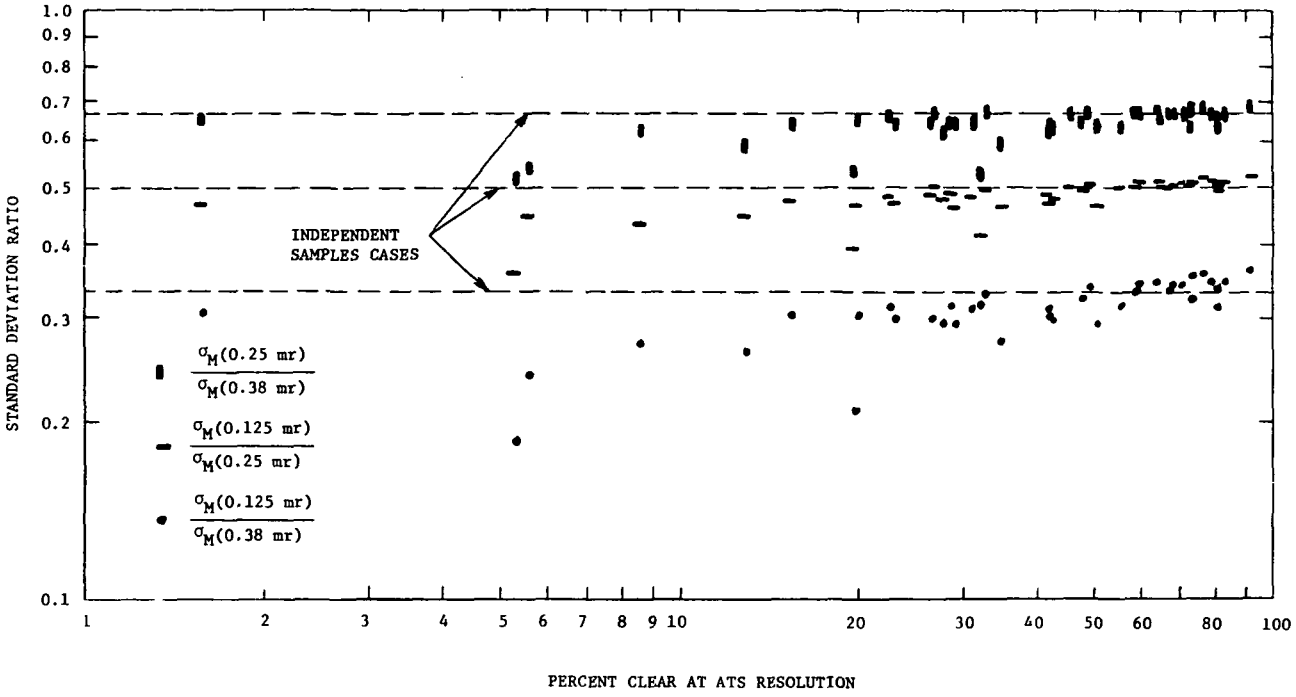

Figure 21. Ratios of standard deviations at three resolutions for GARP sized grids over the Atlantic Ocean from ATS III, 23 April 1968 171410 Z.

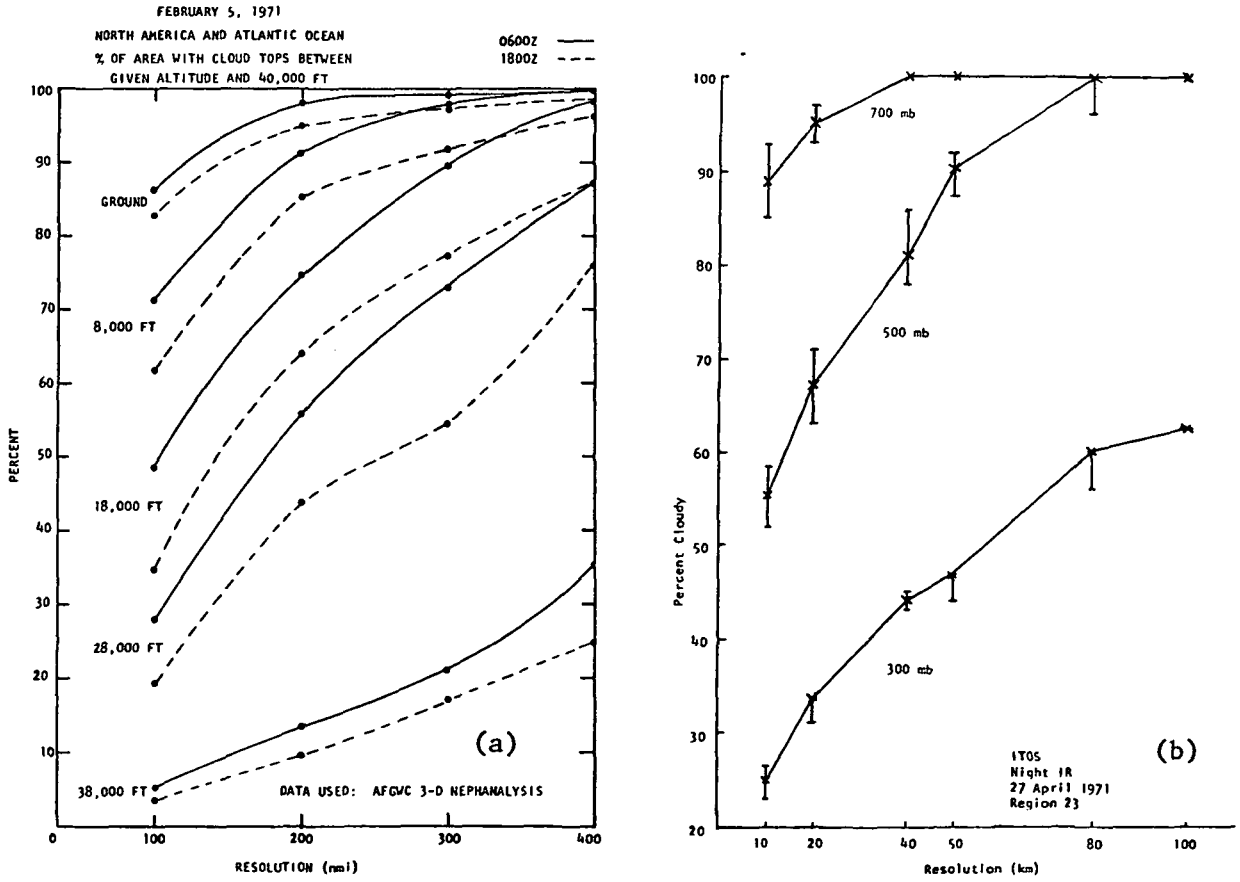

Figure 22. Percentage of clear area down to a fixed level as a function of level and resolution: (a) based on AFGWC 3-D Nephanalysis maps for North America and the Atlantic Ocean 5 February 1971; and (b) based on ITOS Night IR data for 27 April 1971.

APPENDIX C: CLEAR COLUMN RADIANCE RETRIEVAL

Radiometric soundings of atmospheric temperature and water vapor profiles are based on sets of clear column spectral radiances, i.e. radiances that would be observed in a clear (cloud free) atmosphere. Determining these radiances requires either the rejection of all data contaminated by the presence of clouds (using only data from clear FOV's) or the correction of cloud-contaminated data to eliminate the effects of clouds. The first approach is most practical for high resolution sensors which can make measurements in clear regions between clouds, and the second method is most practical for low resolution sensors which usually make measurements containing some cloud contamination.

The 0.3 mr resolution specified for the SMS sounder places it in a middle ground with regard to choosing the optimum retrieval techniques. A study of their dependence upon the size and distribution of cloud elements relative to the FOV size and upon the noise characteristics of the detection system reveals that, while clear field of view (CFOV) techniques can produce usefully accurate clear column radiances, a definite improvement frequently can be made using cloud correction techniques.

The remainder of this appendix is divided into two major sections: (1) a discussion of the available methods of clear column radiance retrieval and their inherent difficulties; (2) simulation studies of retrieval accuracy including the effects of cloud variability and instrumental degradation.

1. A Survey of Clear Column Radiance Retrieval Methods

Two general methods are of interest: clear-field-only (CFOV) techniques which have the central problem of determining which IFOV's are clear, and projection techniques which extrapolate clear radiances from sets of cloud contaminated radiances.

Clear Field Averaging: For a given averaging area containing clouds it is frequently possible to obtain sufficient radiometric accuracy for sounding by averaging measurements made in the holes between clouds (see Appendix B). The main requirement for application of this method is a reliable means for determining which IFOV's are clear and which are not. The procedures used depend on the spectral channel for which the clear column determination is required and on the availability of SMS imaging information. A basic summary of procedures is provided by the following:

a) IR Window Channel Histogram Analysis: The SMS infrared imaging channel has the highest radiometric accuracy of all (NER $\simeq$ 0.25 erg/sec-cm^2-sec-ster)), and yields approximately 2000 observations per GARP grid. This large number of samples, together with a low NER per sample (see Section IV) makes possible straightforward application of well-developed techniques of histogram analysis (Smith, 1970) to determine the clear column

spectral radiance in this channel. Quoting from Smith's paper we find that

> "The method accounts for atmospheric attenuation and instrumental noise and also objectively discrimates cloud-free from cloud-contaminated observations."

This technique works best when cloud-free holes are large compared to the field of view. As the holes shrink to a size comparable to the field of view, the frequency of partially contaminated fields of view becomes large enough for the analysis to fail (Shenk, 1971). At this point instrument noise and "cloud noise" become inseparable by histogram analysis. Such cases must either be rejected or be treated by different methods.

b) Clear Field Determination Using Visible Data: The very high resolution (.025 mr) visible imaging channels on SMS can be used to detect the presence of clouds in sunlit regions. Since there are 144 of these high resolution samples within a sounding field of view (0.30 mr), the determination of clear sounding areas should be accurate; the whole field of view can be rejected as cloud-contaminated if any of the visible elements have a radiance greater than a certain threshold. Implementation of this technique is discussed in Appendix D. This approach can be used for all spectral channels (IR window and sounding).

c) Clear Field Determination Using IR Imaging Data: This technique makes use of IR imaging data to determine clear FOV's observed in the sounding channels. The infrared imaging field of view which has a radiance less than a specified threshold would be classified as cloud-contaminated. The threshold would be chosen large enough to eliminate any significant contamination due to overlaps of clear radiance noise and partially-cloudy radiance noise. This would not bias radiances in the sounding channels since the noise overlap would not be correlated with that in the infrared imaging channels.

The performance of these techniques is noticably impaired by diffraction and scanning effects which result in a field of sensitivity which is considerably larger than the geometrical field of view. Since the fractional number of fields which are clear rapidly decreases with increasing FOV, the requirement for complete clarity out to a distance substantially beyond the geometrical FOV limits can result in rejection of a significant number of otherwise useable measurements, depending on the distance required to obtain a negligible level of sensitivity. An amplified discussion of this problem is included with the discussion of computer simulation.

Projection Methods: These methods make use of a linear relationship between spectral radiances in two different channels and a knowledge of the clear column spectral radiance in one of them (usually an infrared window channel) to determine the clear column spectral radiance in the other by extrapolation.

For a single FOV partially filled with clouds of a single type, the observed radiances in the two channels (I_{ν_1} and I_{ν_2}) are related to the fractional cloud cover N according to the equations

$$I_{\nu_1} = N\, I_{cd,\,\nu_1} + (1-N)\, I_{cl,\nu_1} \tag{53}$$

$$I_{\nu_2} = N\, I_{cd,\,\nu_2} + (1-N)\, I_{cl,\nu_2}. \tag{54}$$

where I_{cd,ν_1} and I_{cd,ν_2} are the spectral radiances coming from the cloud and I_{cd,ν_1} and I_{cl,ν_2} are the spectral radiances of the clear atmosphere. Following Smith's assumption (Smith, 1969) which states

$$I_{cd,\nu} = \varepsilon_\nu\, I^*_\nu + (1-\varepsilon_\nu)\, I_{cl,\nu} \quad (\varepsilon_\nu = \text{cloud emissivity}), \tag{55}$$

equations (53) and (54) can be rewritten as

$$I_{\nu_1} = N^*_{\nu_1}\, I^*_{\nu_1} + (1-N_1^*)\, I_{cl,\nu_1} \tag{56}$$

$$I_{\nu_2} = N^*_{\nu_2}\, I^*_{\nu_2} + (1-N_2^*)\, I_{cl,\nu_2}, \tag{57}$$

where I_ν^* is the radiance that would arise from an opaque cloud at the same level as the true cloud and $N_\nu^* = \varepsilon_\nu N$ is the effective cloud amount. If the cloud is a grey emitter, i.e. $\varepsilon_{\nu_1} = \varepsilon_{\nu_2}$, then $N^*_{\nu_1} = N^*_{\nu_2} = N^*$ and the effective cloud amount can be eliminated from (56) and (57) to obtain

$$I_{\nu_2} = m\, I_{\nu_1} + b \tag{58}$$

where

$$m = (I_{\nu_2}^* - I_{\nu_2,cl})/(I_{\nu_1}^* - I_{\nu_1,cl}) \tag{59}$$

$$b = I_{\nu_2}^* - m\, I_{\nu_1}^*$$

The main point of equation (58) is that the two spectral radiances are linearly related; plotting I_{ν_2} against I_{ν_1} for different effective cloud covers yields a straight line similar to that shown in Figure 23. It is assumed in this figure that the cloud level (and thus $I_{\nu_1}^*$, $I_{\nu_2}^*$) and grey emissive properties are the same for all points. Note that equation (58) applies only to the line segment, as indicated in the figure.

The usual checkerboard technique of clear column radiance determination uses two pairs of measurements in different but geometrically adjacent FOV's to determine the straight line (not the segment), and independent knowledge of I_{cl,ν_1} to determine how far the line should be projected to obtain I_{cl,ν_2}. This procedure is illustrated in Figure 24. The effect of measurement errors is also indicated. Obviously the error in the projection increases as the distance (in radiance) between the two measurement pairs decreases. For this reason only measurements from fields with substantially different degrees of cloud cover can be treated with any significance in the determination of clear column radiances. It is also clear from the figure that the projection error is decreased when the projection distance is small, i.e. when one radiance pair is near to the point $(I_{cl,\nu_1}\ I_{cl,\nu_2})$.

The reason for using only geometrically adjacent fields is to increase the probability that the same cloud type is present in both fields. If this were not a concern it would be better to fit all observations in the entire averaging area to a straight line and make just one projection. The effect of multiple cloud types on the checkerboard method is illustrated in Figure 25.

If two cloud types are present within the grid and each IFOV contains one type or the other (but not both) all points in the $I_{\nu_2} - I_{\nu_1}$ plot will lie near either of two straight lines. (Radiances from IFOV's which contain both cloud types will lie between the two lines). Every time a field containing a small amount of warm cloud is paired with a field containing a large amount of cold cloud, a positive bias error occurs in the projection (type 1 bias). Every time a field containing a large amount of warm cloud is paired with a field containing a small amount of cold cloud a negative bias error results (type 2 bias). Since warm clouds are usually smaller than cold clouds, the type 1 bias has the higher probability.

When the sensor accuracy is high, the IFOV small, and only adjacent pairs used, a histogram of the checkerboard determinations of I_{cl,ν_2} shows the characteristics displayed in Figure 26. Obviously a good estimate of I_{cl,ν_2} can be obtained from the peak of the histogram. In this case, which can be duplicated by SMS through time averaging over restricted regions, the type 1 bias is separable. However, when radiance measurement accuracy is relatively low (as it is for the SMS sounder in a single pass mode) the histogram peak at I_{cl,ν_2} is spread over a large region of radiance and is not

The main point of equation (58) is that the two spectral radiances are linearly related; plotting I_{ν_2} against I_{ν_1} for different effective cloud covers yields a straight line similar to that shown in Figure 23. It is assumed in this figure that the cloud level (and thus I_{ν_1}*, I_{ν_2}*) and grey emissive properties are the same for all points. Note that equation (58) applies only to the line segment, as indicated in the figure.

The usual checkerboard technique of clear column radiance determination uses two pairs of measurements in different but geometrically adjacent FOV's to determine the straight line (not the segment), and independent knowledge of I_{cl,ν_1} to determine how far the line should be projected to obtain I_{cl,ν_2}. This procedure is illustrated in Figure 24. The effect of measurement errors is also indicated. Obviously the error in the projection increases as the distance (in radiance) between the two measurement pairs decreases. For this reason only measurements from fields with substantially different degrees of cloud cover can be treated with any significance in the determination of clear column radiances. It is also clear from the figure that the projection error is decreased when the projection distance is small, i.e. when one radiance pair is near to the point (I_{cl,ν_1} I_{cl,ν_2}).

The reason for using only geometrically adjacent fields is to increase the probability that the same cloud type is present in both fields. If this were not a concern it would be better to fit all observations in the entire averaging area to a straight line and make just one projection. The effect of multiple cloud types on the checkerboard method is illustrated in Figure 25.

If two cloud types are present within the grid and each IFOV contains one type or the other (but not both) all points in the I_{ν_2} - I_{ν_1} plot will lie near either of two straight lines. (Radiances from IFOV's which contain both cloud types will lie between the two lines). Every time a field containing a small amount of warm cloud is paired with a field containing a large amount of cold cloud, a positive bias error occurs in the projection (type 1 bias). Every time a field containing a large amount of warm cloud is paired with a field containing a small amount of cold cloud a negative bias error results (type 2 bias). Since warm clouds are usually smaller than cold clouds, the type 1 bias has the higher probability.

When the sensor accuracy is high, the IFOV small, and only adjacent pairs used, a histogram of the checkerboard determinations of I_{cl,ν_2} shows the characteristics displayed in Figure 26. Obviously a good estimate of I_{cl,ν_2} can be obtained from the peak of the histogram. In this case, which can be duplicated by SMS through time averaging over restricted regions, the type 1 bias is separable. However, when radiance measurement accuracy is relatively low (as it is for the SMS sounder in a single pass mode) the histogram peak at I_{cl,ν_2} is spread over a large region of radiance and is not

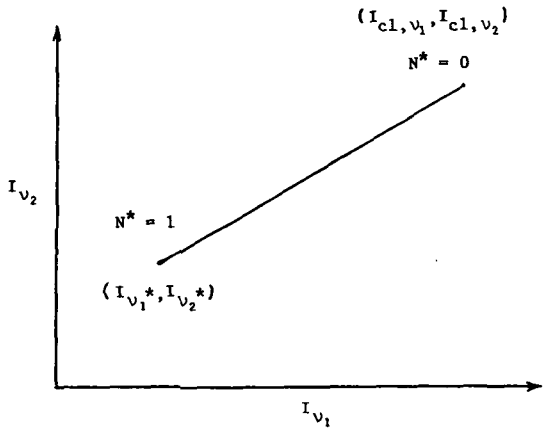

Figure 23. A plot of the linear relation between I_{ν_2} and I_{ν_1} for a single cloud level and type for effective cloud covers between N*=1 (opaque cloud filling the FOV) and N*=0 (completely clear FOV).

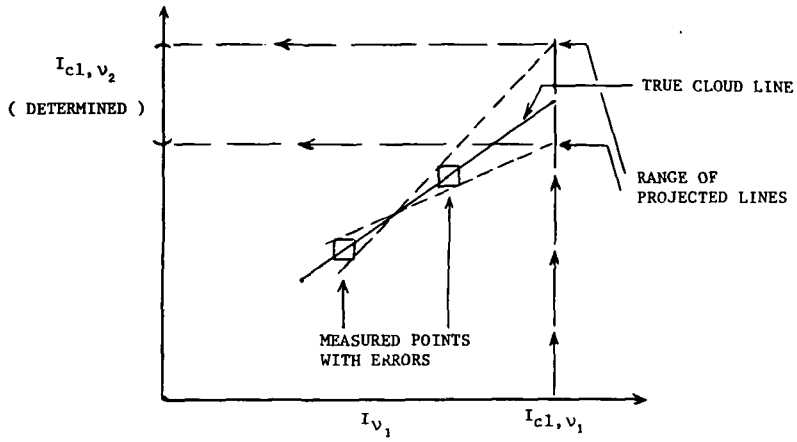

Figure 24. An illustration of projection errors for a single pair and a single cloud level.

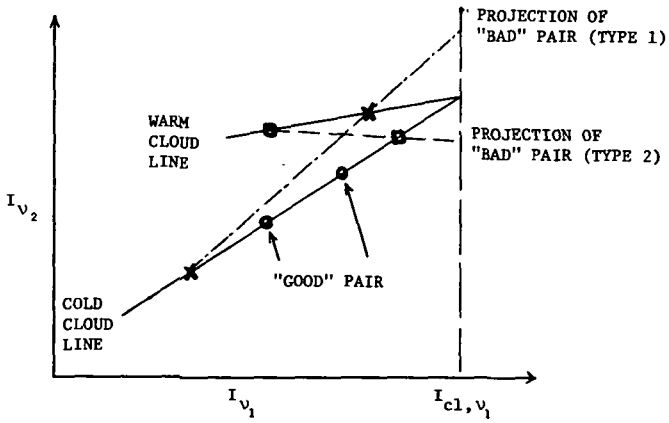

Figure 25. An illustration of bias errors in the presence of multiple cloud levels.

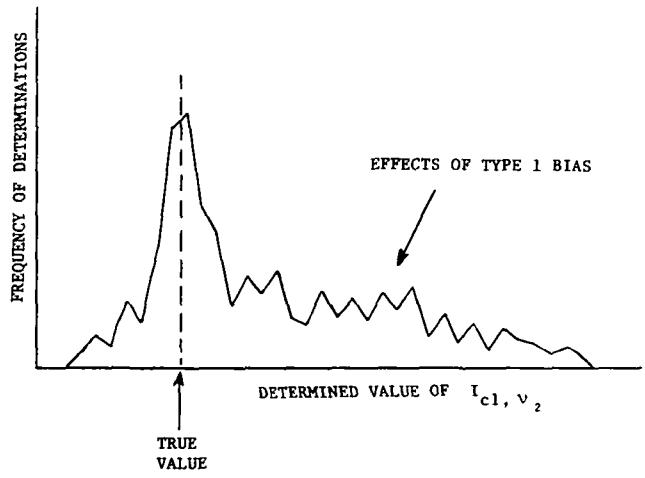

Figure 26. A typical histogram of paired-field projections.

easily separated from the determinations with type 1 bias. In neither case is it possible to directly average the clear column determinations to obtain an unbiased estimate.

Bias effects can be eliminated from the checkerboard technique if paired fields can be checked for cloud type differences before a clear column determination is made. In this case only fields which have the same kind of cloud contamination would be used. A test for this condition can be made with observations in two window channels, each in a different spectral region. In the case of Nimbus F and proposed ATS-G sounders, window channels at 4μm and 11μm are used for this purpose.

With these two channels it is possible to check for emittance "greyness" and cloud height variations in each pair of fields (Smith, 1969). This cannot be done with SMS sounder data because the sounder has no capability for 4μm measurements. However, in the case of SMS, other techniques are available for checking cloud characteristics.

High resolution visible window channel data can also be used effectively for this purpose. For radiatively black clouds (according to Fujita (1967), these include fog and stratus 0.3 km or deeper, thick cirrostratus and altostratus deeper than about 0.7 km, and convective clouds) the N* value is equal to the fractional cloud amount N. Since there are 144 SMS visible imaging FOV's for each sounding FOV the fractional cloud amount N can be determined easily: for each sounding FOV N would be just the number of cloudy imaging FOV's divided by 144. The visible channel radiance can also serve as a check on cloud thickness which is a strong influence on cloud albedo. A comparison of the visible channel determination of the cloud cover ratio between two candidate fields with the IR window channel determination

$$\frac{N_1}{N_2} = \frac{I_1 - I_{c1}}{I_2 - I_{c1}} \tag{60}$$

will reveal cases which do not satisfy the conditions of: (1) black clouds, and (2) all clouds at the same height. When the two ratios disagree the pair would be rejected.

A new projection technique which does not use geometrically paired fields has been developed for SMS application. This technique minimizes bias errors by making use of the tendency for low clouds to be small relative to high clouds. When this is the case, radiances from fields containing warm clouds tend to group in the high radiance region of the $I_{\nu_2} - I_{\nu_1}$ plot, whereas fields containing cold clouds tend to group in the low radiance region. Plots of all fields in averaging area show characteristics similar to Figure 27. By fitting a straight line to the high radiance region only, it is possible to isolate, for the most part, warm clouds from cold. Projecting this line to I_{c1,ν_1} then determines I_{c1,ν_2}.

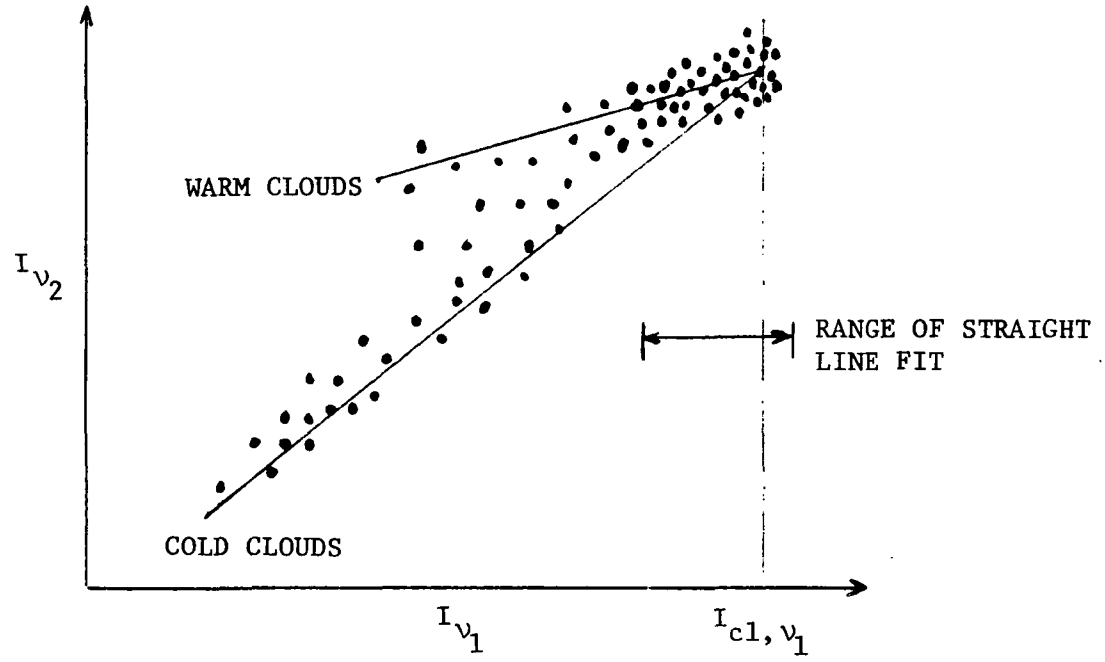

Figure 27. An illustration of conditions for which the straight-line fit projection method can be used to isolate cloud populations. Plotted points are typical high resolution measurements pairs for a complete GARP sized grid.

2. Computer Simulation of Retrieval Methods

In order to evaluate, under realistic conditions, the performance of various algorithms for determining clear column radiances, a computer simulator was developed. It's use and operation are summarized by the following sequence of steps:

1) Very high resolution satellite photographs (usually from Apollo or Gemini) are converted to high resolution (typically 0.1 mr) grids of alphanumeric characters. Each character describes the height, emissivity, and amount of cloud in the corresponding high resolution FOV. These classifications are made with the help of conventional radiosonde data. The characters are punched on cards and serve as the simulator input.

2) Average radiances are calculated for each sounding field of view from the input grid classifications and the known sounding appropriate to the input grid. These averages account for scanning and diffraction effects by means of a spatial weighting function.

3) Random correlated noise is added to each of these radiances to form simulated SMS measurements.

4) The retrieval algorithms are then used to reduce the simulated measurements to mean clear column spectral radiances for the grid.

5) The algorithm performances are evaluated by comparing the retrieved radiances with the known input radiances.

Many repetitions of steps (3) and (4) are required to obtain statistically sound evaluations.

The effectiveness of the simulator depends on the accuracy of the instrumental simulation and on the accuracy and representativeness of the scene simulation (i.e., the input grid). Only the first of these is computerized.

Simulation of Instrument Behaviour: Noise characteristics and spatial weighting characteristics are the two most important items of instrumental behaviour that require simulation. The first of these is thoroughly discussed in Appendix A. The second requires explanation.

In the case of an ideal diffraction-free step scan radiometer the detector output is proportional to the direct average of the scene radiance over the geometrical field of view of the detector. In the case of the SMS radiometer the detector output is filtered so that each measurement is an unequally weighted time average of the field swept out by the detector FOV. In addition, diffraction effects reduce the detector response to scene radiances within the IGFOV and increase its response to scene radiances outside the IGFOV. Both effects can be simultaneously described by a spatial weighting function $\phi(x,y)$ which is defined so that the detector response $I(t)$ at time t is given by

$$I(t) = \int_{-\infty}^{\infty} dx \int_{-\infty}^{\infty} dy\ \phi(x-x_o(t),\ y-y_o(t))\ I_s(x,y) \tag{61}$$

where x and y are coordinates of the scene and $x_o(t)$ and $y_o(t)$ are the scene coordinates of the spatial weighting peak at time t. This point follows the scanning IGFOV but lags behind because of the prealiasing filter at the detector output. Since the detector response $I(t)$ must equal the scene radiance I_s when the scene is flat, $\phi(x,y)$ must satisfy the normalization condition

$$\int_{-\infty}^{\infty} dx \int_{-\infty}^{\infty} dy\ \phi(x,y) = 1. \tag{62}$$

The net spatial weighting function can be calculated from the impulse response function $R(t)$ and the diffraction weighting function $D(x,y)$ according to the following equation

$$\phi(x,y) = N \int_{-\infty}^{\infty} dx'\ R\ \frac{(x-x')}{v}\ D(x-x',y), \tag{63}$$

where v is the scene velocity of the detector IGFOV, and

$R(\frac{x-x'}{v})$ = the fraction of the filter output at time $\frac{x}{v}$ due to detector input at time x'/v.

$D(x-x',y)$ = the fractional energy emitted by the scene from (x,y) which falls on the detector while its IFOV is centered at (x',y).

N = a normalization factor adjusted so that $\phi(x,y)$ satisfies equation (62).

It is assumed that the detector IFOV scans in the positive x' direction.

The impulse response function is calculated from the characteristics of the prealiasing filter. This is assumed to be a five-pole Chebychef filter with

a) Linear Phase, 0.5° ripple

b) -3 dB frequency = 17.45 KHz

c) Pole locations (normalized so that the -3 dB radian frequency = 1 rad/sec)

$P_1 = -.70557$

$P_{2,3} = -0.67745 \pm j\ 0.94007$

$P_{4,5} = -0.54117 \pm j\ 1.82565$

The impulse response function is obtained from the equation

$$R(t) = \frac{1}{2\pi} \int_{-\infty}^{\infty} H(j\omega) e^{j\omega t} d\omega \tag{64}$$

where

$$H(p) = \text{const.}/[(p-p_1)(p-p_2)(p-p_3)(p-p_4)(p-p_5)]. \tag{65}$$

Results of this complex integration are shown in Figure 28. Both time and angle axes are included for reference. Note that the filter output at time t=0 is mainly determined by signals input at a time 24 μsec earlier and entirely unrelated to signals input at times $t \geq 0$ (the future does not influence the present).

The diffraction weighting function is calculated from the equation

$$D(x,y) = \int_{A_d} d\xi' d\eta' I_d\ ([(\xi(x)-\xi')^2 + (\eta(y)-\eta')^2]) \tag{66}$$

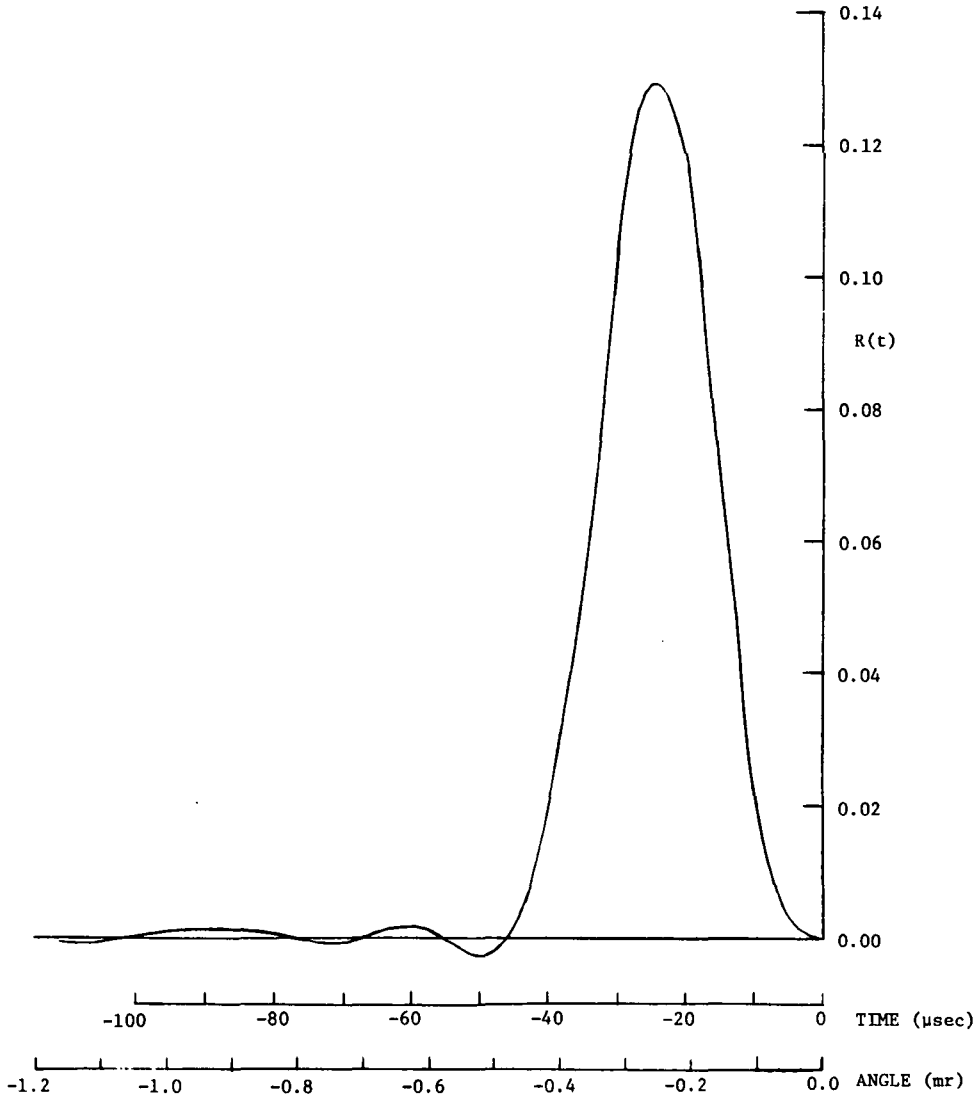

Figure 28. Impulse response function R(t) as a function of time and angular scan coordinates. Negative values refer to time and angle previous to the current IGFOV center.

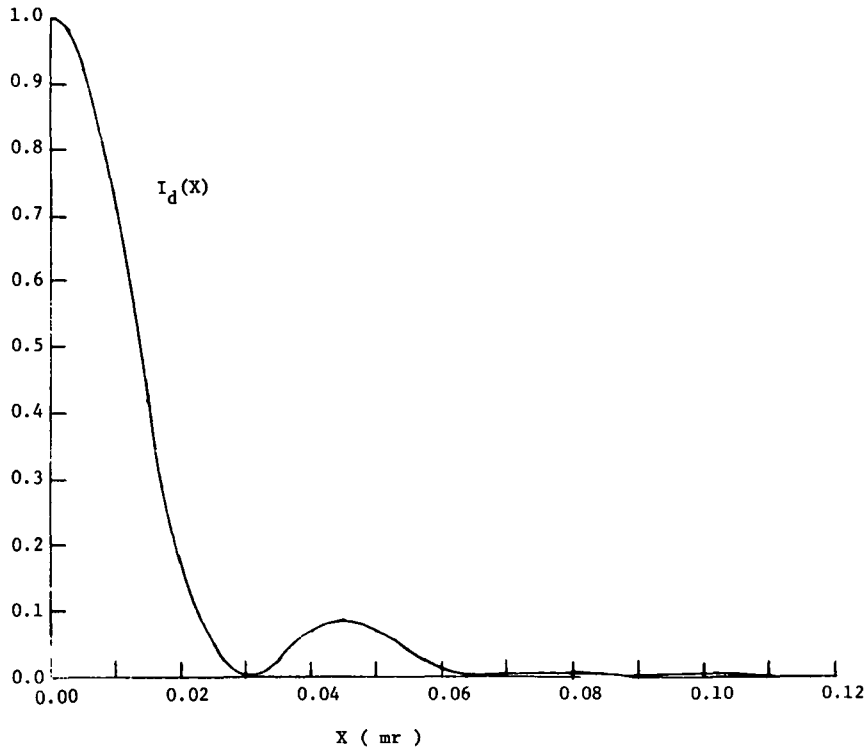

Figure 29. The normalized diffracted intensity $I_d(r)/Io$ for SMS (at 11.5 μm) as a function of r the angular distance from the projected center of the pattern.

where the integral is taken over the detector area A_d; $\xi(x)$ and $\eta(y)$ are projections on the focal plane of the scene position (x,y); and $I_d(r)$ is the diffracted intensity on the focal plane at a distance r from the geometrical projection of a point source in the scene. The diffracted intensity is that of an annular aperture and is given by (Born, 1965)

$$I_d(r) = \frac{I_o}{(1-\varepsilon^2)^2} \left[\left(\frac{2J_1(\rho)}{\rho}\right) - \varepsilon^2 \left(\frac{2J_1(\varepsilon\rho)}{\varepsilon\rho}\right)\right]^2 \qquad (67)$$

where

ρ = 2π a sin r/λ

a = outer aperture radius

λ = wavelength of diffracted radiation

ε = obscuration ratio (inner aperture radius = εa)

J_1 = the first order bessel function

I_o = the intensity at the center of the pattern (r=o).

A plot of this function for λ = 11.5μ is displayed in Figure 29. A cross section of the resultant diffraction weighting function D(x,y) for a detector 0.3 mr square is plotted in Figure 30. This cross section represents the intersection of D(x,y) with a plane passing through the center of the IFOV (x=0, y=0), perpendicular to the x,y plane and parallel to one of the four detector edges. The horizontal coordinate is measured in milliradians from the center of the IGFOV. Of the energy emitted by sources near the center of the IGFOV and collected by the sounder optics approximately 93% strikes the detector surface; from sources 0.3 mr from IGFOV center the fraction is down to 0.9%.

Integrating the impulse response function over the diffraction weighting function according to equation (63) yields the net spatial weighting function of the SMS sounder, i.e. (x,y). Figure 31 displays the central cross section of this function which is parallel to the scan direction. The cross section perpendicular to the scan direction is identical to the diffraction weighting function shown in Figure 30. The dotted curves display the spatial weighting that would apply to a diffraction-free radiometer with detector response numerically averaged (not electronically filtered) over a time interval equal to the dwell time τ_{IFOV}. The ideal radiometer response goes to zero outside the 0.3 mr x 0.6 mr field scanned by the IGFOV in the time τ_{IFOV}, while the actual instrument has some response to sources considerably outside this region.

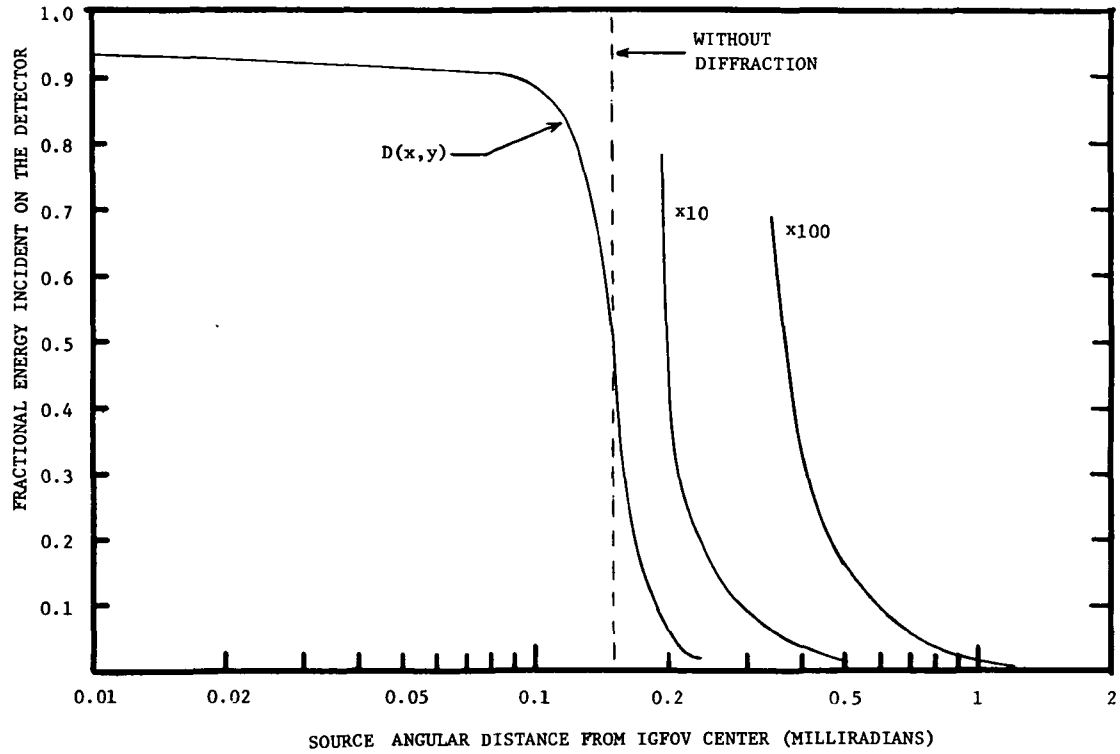

Figure 30. A cross sectional plot of the diffraction weighting function for an 0.30 mr detector. The cross section shown is taken through the IGFOV center.

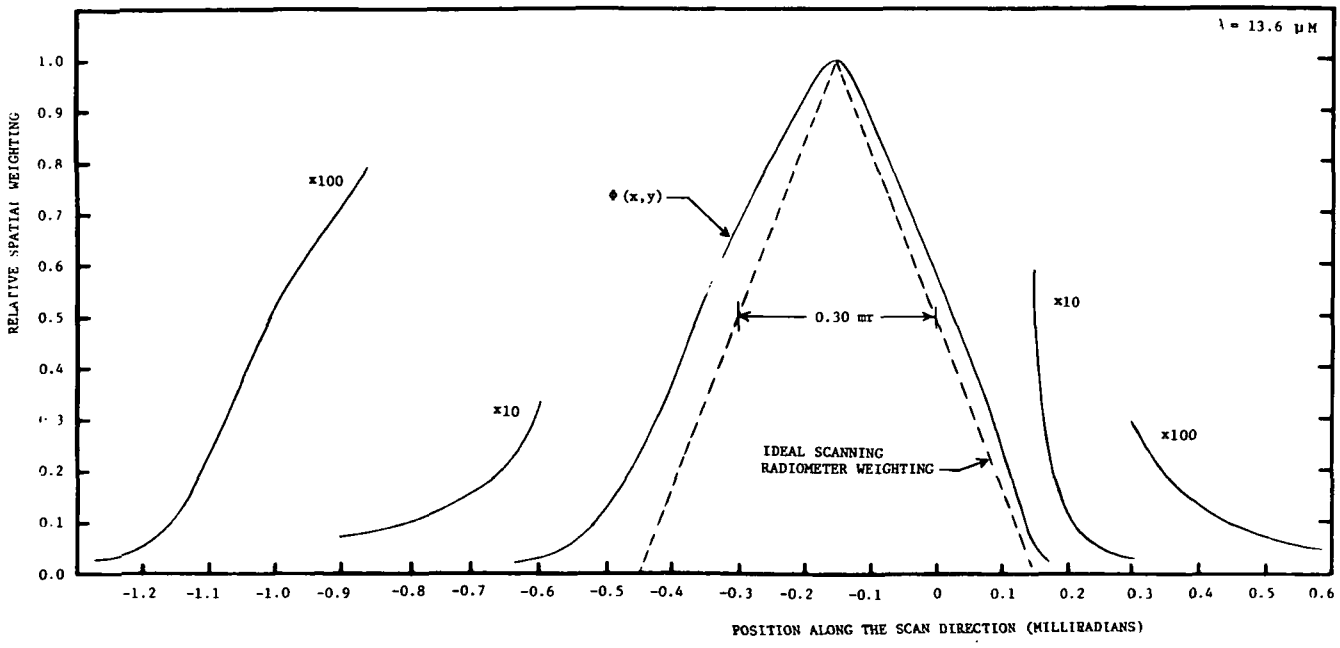

Figure 31. The net spatial weighting function $\phi(x,y)$ as a function of angular position along the scan direction and passing through the center of the IGFOV.

Although the limits of the averaging integrals in equation (61) are infinite, a practical set of finite limits is necessary for the computer simulation. These were chosen to be $^{+0.7}_{-1.0}$ mr along the scan direction (relative to the position of the weighting function peak) and ± 0.7 mr normal to the scan direction. Approximately 99% of the energy falling on the detector comes from sources within these limits. The remaining 1% comes from sources spread out over an extremely wide field and cannot be practically included in the simulator. It should be noted, however, that in extreme situations this 1% contribution could lead to a bias error which is larger than the NER required for inversion. Further mention of this effect will be made in the discussion of simulator results.

Cloud Grids: Although the computer simulator is capable of handling a wide variety of input data grids, at this writing only two such grids have been extensively used. These are both derived from Gemini photographs and cover an area approximately 400 km square. The cloud characteristics of these two grids are summarized in Table 11.

These grids contain a number of the problem situations which can cause algorithms to fail: many cloud elements smaller than the detector IFOV, multiple cloud types at different altitudes within the grid, many cases of different cloud types within the same sounder IFOV, clouds of different emissivities, and a relatively small percentage of clear sounder IFOV's. A notable exception is the variation of emissivity among clouds at the same level, although this latter factor is only significant for algorithms employing more than one window channel. In connection with this it must be noted that no specification of the visible channel cloud albedo is made in these grids; nor are visible channel radiances ever calculated by the computer simulator.

Algorithms Used by the Simulator: Taking into account the simulator limitations a selection of clear column radiance retrieval methods was made among those specified in Section 1 of this appendix. The SMS simulator was programmed to employ six different algorithms. These are:

1) CFO-VIS: Clear fields only are averaged to obtain clear column radiances. The clarity of a field is determined by the high resolution visible channel data.

2) CFO-IR: All FOV's which have an IR window radiance greater than a chosen cut off value (usually near the clear column window radiance) are assumed clear and sounding channel radiances from those FOV's are averaged.

3) PFOV-VIS: The ratio of fractional cloud covers in pairs of neighboring fields are determined by high resolution visible channel data. Each pair for which this ratio or its inverse lies between 0.0 and 0.6 are employed in the paired field of view (checkerboard) method to obtain a clear column radiance determination. These determinations are combined with the CFO-VIS results in a weighted average to obtain a best estimate for the grid.

Table 11 Cloud Grid Characteristics

Parameter	Mexico Grid	Canary Islands Grid
Percent clear at		
Gemini Resolution	82%	73%
Percent clear at		
Sounder Resolution (0.3 mr)	40%	23%
Cloud Types (Level, Emissivity)		
Type 1	700 mb, 1.0	800 mb, 0.8
Type 2	400 mb, 1.0	350 mb, 0.85
Type 3	400 mb, 0.3	
Percentage of total		
cloud amount		
Type 1	39%	48%
Type 2	48%	52%
Type 3	13%	

4) PFOV-IR: This method is similar to the previous one, with the important exception that the effective cloud cover ratios are determined using the IR window channel measurements.

5) PFOV-IR+VIS: This is a combination of the previous methods which uses only paired fields for which both the visible channel determination and the IR channel determination of the cloud cover ratio are in agreement.

6) LINE FIT: This projection technique is best described with reference to Figure 27, section 1 of this appendix. A straight line least squares fit is made to the (I_{ν_1}, I_{ν_2}) measurements pairs which correspond to FOV's with with window channel radiances (I_{ν_1}) greater than a given threshold. This line is projected to $I_{\nu_1} = I_{\nu_1,clear}$ to obtain the clear column sounding channel radiance $(I_{\nu_2,cl})$.

All of these techniques except (1) and (3) require a knowledge of the clear column window channel radiance. Simulation of histogram techniques for this determination show that the high radiometric accuracy of the IR window channel makes this process almost trivial. It should also be noted that techniques (1), (3) and (4) are only applicable to sunlit regions of the earth, while the others do not have this restriction.

Selected Simulator Results: No simulator tests have been made with 0.3 mr resolution specified for the sounder. However, tests at 0.4 mr and at 0.2 mr can be interpolated to approximate the behaviour at 0.3 mr. Among the many test conditions studied with the simulator, three are particularly important in algorithm evaluation:

1) IDEAL SCAN: This is the condition appropriate to the ideal step-scan diffraction free radiometer. The spatial weighting function in this case is constant over the IGFOV and zero outside. This situation serves as a reference point in assessing the effects of instrument degradation.

2) NORMAL WEIGHTS (0.4 mr): In this case the spatial weighting function includes diffraction and scanning effects as discussed previously, except for modifications appropriate to the 0.4 mr resolution of the sounding channels, and the 0.2 mr resolution of the IR imaging channel.

3) NORMAL WEIGHTS (0.2 mr): Conditions are as described for (2) except that both sounding and imaging channels have the same spatial resolution of 0.2 mr.

In all three cases tests were made with data sets corresponding to complete non-overlapping coverage, and with a sounding channel which is strongly affected by the presence of clouds (735 cm^{-1}). The raw results are presented in Table 12.

Table 12 Raw Simulation Results

	Ideal Scan 0.4 mr $\sigma_s = 1.0$ $\sigma_w = 0.56$ (0.2 mr)		Normal WTS 0.4 mr $\sigma_s = 1.0$ $\sigma_w = 0.56$ (0.2 mr)		Normal WTS 0.2 mr $\sigma_s = 3.0$ $\sigma_w = 0.56$ (0.2 mr)	
	RMS	BIAS	RMS	BIAS	RMS	BIAS
CFO - VIS	0.13	+.02 (1)	0.52	+.02	0.40	-.05
	(0.11)	(+.02) (2)	(0.44)	(-.13)		
CFO - IR (cutoff=CR)	0.16	+.02	0.21	-.02	0.24	-.07
	(0.11)	(+.03)	(0.36)	(-.04)		
CFO - IR (cutoff=CR-σ_n)	0.12	-.01	0.20	-.13	0.24	-.13
	(0.10)	(+.01)	(0.31)	(-.06)		
PFOV - VIS (direct average)	0.75	+.74	0.59	+.58	0.34	+.30
	(0.37)	(+.36)	(0.33)	(+.25)		
PFOV - IR (weighted average)	0.22	-.07	0.17	-.12	0.18	+.01
	(0.07)	(-.00)	(0.21)	(-.03)		
PFOV - IR + VIS (weighted average)	0.14	+.03	0.22	+.16	0.27	-.13
			(0.36)	(-.05)		
LINE FIT (cutoff=80% CR)	0.13	+.07	0.14	-.05	0.22	-.08
			(0.26)	(+.05)		
LINE FIT (cutoff det. by fit std. dev.)			0.17	-.08	0.25	-.14

Notes: (1) Bias errors of magnitude less than about 0.03 are insignificant at the level of accuracy of these tests. A bias error is considered positive if the determined clear column radiance is greater that the true value. (2) Numerical values in parentheses apply to the Mexico Grid; all others apply to the Canary Islands Grid.

The results tabulated are radiance errors (RMS and BIAS) which result from the algrothm determination of mean clear column radiance for the grid. The column headings note the values of σ_s (the sounding channel one-sample flat-field NER) and σ_w (the window channel one-sample flat-field NER).

The direct average PFOV-VIS method strongly shows the type 1 bias discussed in section 1 of this Appendix. Direct averaging in the PFOV-IR mode also shows this strong bias. However, if the individual determinations combined in the average are weighted according to the inverse of their expected variances, the type 1 bias is effectively suppressed. (The PFOV-VIS method with weighted averaging was erroneously omitted from the tests).

The effects of realistic weighting functions can be seen by comparing the first column of Table 12 with the third. The substantial degradation of CFO-VIS method results from small number of fields which are absolutely clear out to the limit of the weighting function sensitivity. The relative degradation at 0.2 mr (after dividing by $\sigma_s = 3.0$) is less because the spatial weighting function is more compact. Methods which show the smallest degradation are the PFOV-IR and LINE FIT methods. The slightly poorer performance of the PFOV-IR+VIS method compared to the PFOV-IR alone results from its very high pair rejection rate. In requiring visible and IR effective cloud cover ratios to agree closely, this method accepts only a third to a fifth of the samples accepted by the PFOV-IR method. This results in an improvement in quality of the data averaged but a much too large reduction in quantity. A better choice of the required level of agreement should result in substantially improved performance.

It is interesting to note the performance quality of the CFO-IR algorithm. In spite of an inherent tendency toward a negative bias as the cut-off is moved to lower radiances (see section 1), its performance is comparable to that of the PFOV-IR and the LINE FIT methods, even with the simulated instrument degradation.

In order to interpolate results for the specified sounder resolution of 0.3 mr it is necessary to normalize the raw results of Table 12. The normalization reduces all results to those which would obtain for the same number of scan lines and the same single sample radiance at all resolutions. Normalized results are presented in Table 13. Linear interpolation is used to obtain the normalized 0.3 mr results. Multiplying these by the typical sounder NER of 2.2 erg/(sec-cm^2-cm^{-1}-ster) yields the expected performance of the algorithms for the specified sounder. The deduced performance for the best algorithms is very nearly equal to the 0.3 mr performance estimated on the basis of the CFO method for an ideal sounder (0.19 erg/(sec-cm^2-cm^{-1}-ster) for the Canary Island Grid). Thus the projection techniques with the presence of instrument degradation are able to duplicate very closely the performance of the CFO method under ideal conditions and justify the use of the latter method, in earlier parts of this report, to estimate sounder performance characteristics.

Table 13: Normalized Simulation Results and Expected 0.3 mr Performance

	Mean Clear Column Radiance RMS Noise Normalized to the Same Number of Scan Lines and Unit Single Sample NER				
	Ideal Scan 0.4 mr	Normal WTS (0.4 mr)	Normal WTS (0.2 mr)	Interpolated Results (0.3 mr)	Expected NER for 0.3 mr (Canary Islands)
CFO - VIS	.09	.37	.13	.25	.55
CFO - IR (cutoff = CR)	.11	.15	.08	.12	.26
CFO - IR (cutoff = CR - σ_w)	.08	.14	.08	.11	.24
PFOV - VIS (Direct Ave)	.53	.42	.11	.27	.59
PFOV - IR (weighted-Ave)	.16	.12	.06	.09	.20
PFOV - IR + VIS (weighted Ave)	.10	.16	.09	.13	.29
Line FIT (cutoff = 80% CR)	.09	.10	.07	.09	.20
Line FIT (cutoff Det by fit Std Dev)		.12	.08	.10	.22

APPENDIX D: APPLICATION OF McIDAS HARDWARE TO SMS SOUNDER DATA PROCESSING

Four requirements are paramount in the satellite data storage and access system:

1) Small amount of raw data storage: The huge volume of data from SMS leaves only two choices in handling. The data are either quickly processed in near real time at a rate faster than it was collected, or data are thrown away. The sounder data are only a fraction of the imaging data, but the principle is the same. We cannot afford to invest in a continuously growing backlog of unprocessed data.

2) Real time processing: Sounding data are most valuable for forecasting, and decline in usefulness if they must be stored for very long. Further, data which can at least be preprocessed to reduce volume at an early stage will reduce total subsequent processing.

3) Time domain access: The chief value of geosynchronous satellite data lies in the fact that the same portions of the earth are observed twenty-four hours a day. The advantages of observing a dynamic system continuously in time are self-evident. Unfortunately the data are not received in time-sequenced subsets centered on a single geographical point of interest. We get a serial bit stream containing data from the whole earth at once, line by line. Due to small fluctuations in spacecraft position and attitude, the points of interest are never in the same place in subsequent frames. The problem thus reduces to one of selection of the proper data from a much larger quantity of extraneous information.

4) Human judgment: No set of computer algorithms or electronic circuits can completely replace the need for human judgment. While simple, repetitive decisions may be transferred to computers and hardware, a less costly, less time-consuming, and initially more effective approach would be to permit a human observer to control data selection and processing without himself becoming a bottleneck in the flow of data. An effective means of interaction between man and data must be available.

These requirements have been satisfied in the McIDAS data storage and access system developed by SSEC for use in the GATE program to measure winds from cloud displacements. The step from selecting clouds to selecting areas suitable for sounding is trivial.

The system incorporates a low resolution analog disk interfaced to a small computer and TV monitor (see Figure 32). Raw data are received and broken into TV frame-sized segments which are stored in analog form on the videodisk. At the same time, the full resolution data in digital form are transferred to digital tape or drum to await processing by a large computer. The analog data are stored on the disk by channels in time sequence, allowing display frame by frame like a motion picture. The operator, with the aid of a joystick cursor, indicates the approximate position of an area of interest. No measurements are made from the TV screen. The display hardware converts

the cursor position to a set of approximate coordinates which allow the larger computer at some later time to extract from the full data tape the region of interest. The operator has full access to all the data in visual form in TV frame-sized segments at full or reduced resolution. All data are viewed in either single-frame or time-lapse sequencing, giving full visual access to the time domain. The operator may limit himself to simple data selection or rejection, or choose to become involved in more complex decision-making, leaving the simple and repetitive tasks to the computer. While present computer output is directed to a printer or plotter, it could also be displayed on the TV screen for a final quality control check.

Figure 32 shows the modifications required to handle SMS data with McIDAS type hardware at the CDA or DUS. The single disk video recorder now used for ATS data must be modified to have multiple disks and parallel heads sufficient to handle all channels as the data arrives. The digital computer tape now being used would be replaced by digital videotape to get greater storage surface, greater bandwidth, and faster access. This still merely serves as a buffer for raw data. Ideally, one might record on one machine, and playback on the other so that no taped data need be removed and stored.

Editing, preprocessing and quality control could also be done using a small- or medium-sized computer. The only need for a large computer is in generation of actual wind data sets and soundings. At this point, the data volume will have been considerably reduced by the prior selection and editing processes, and what data remain have a very high ratio of information to volume.

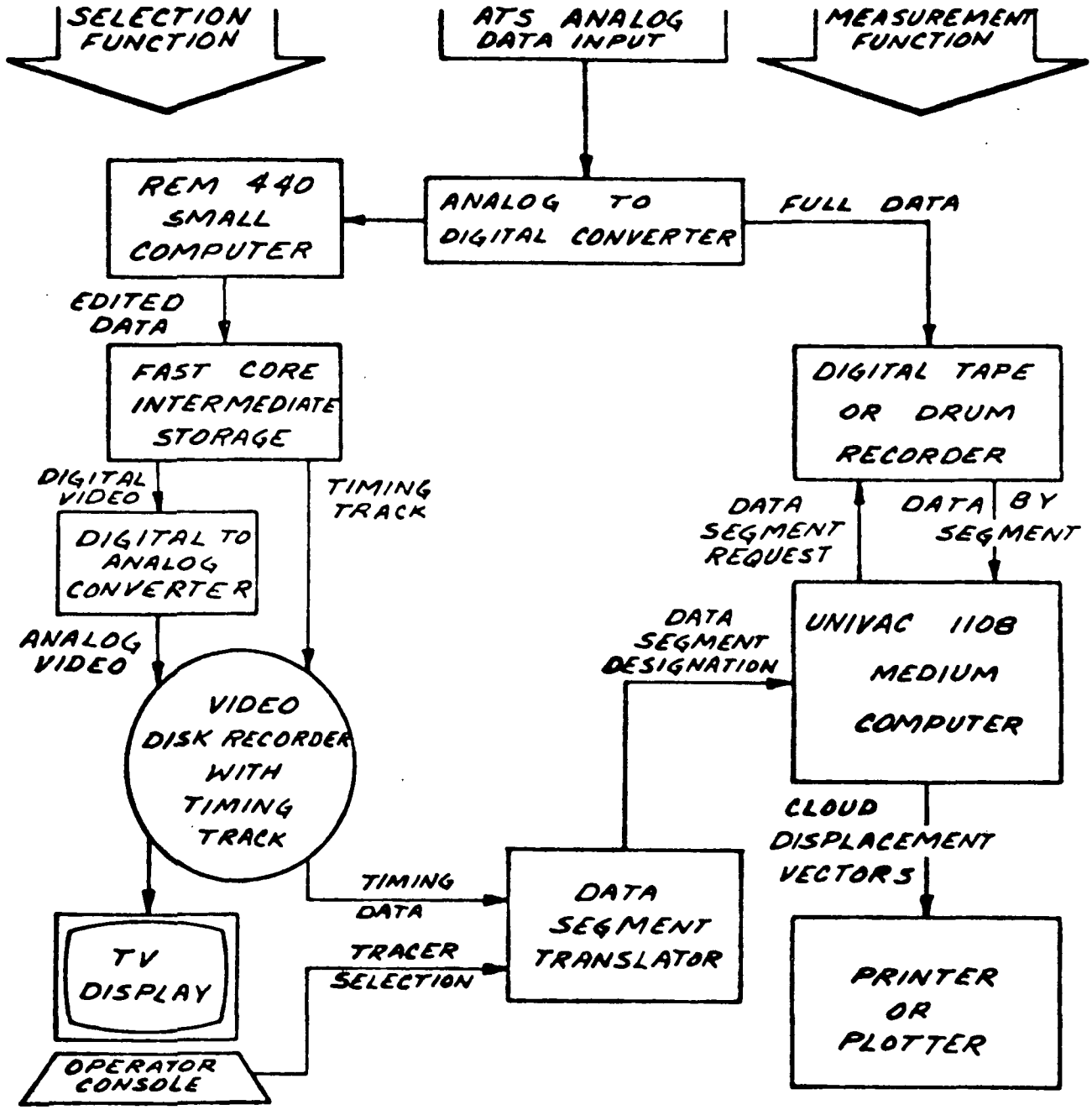

Figure 32. The prototype McIDAS system developed by SSEC uses an operator to select individual tracer clouds from a TV picture and a computer to perform precision cloud displacement measurements. All video equipment is assembled from standard commerical TV components. The system is designed to produce 20 highly accurate cloud displacement vectors per minute at a cost of about 10 cents per wind.

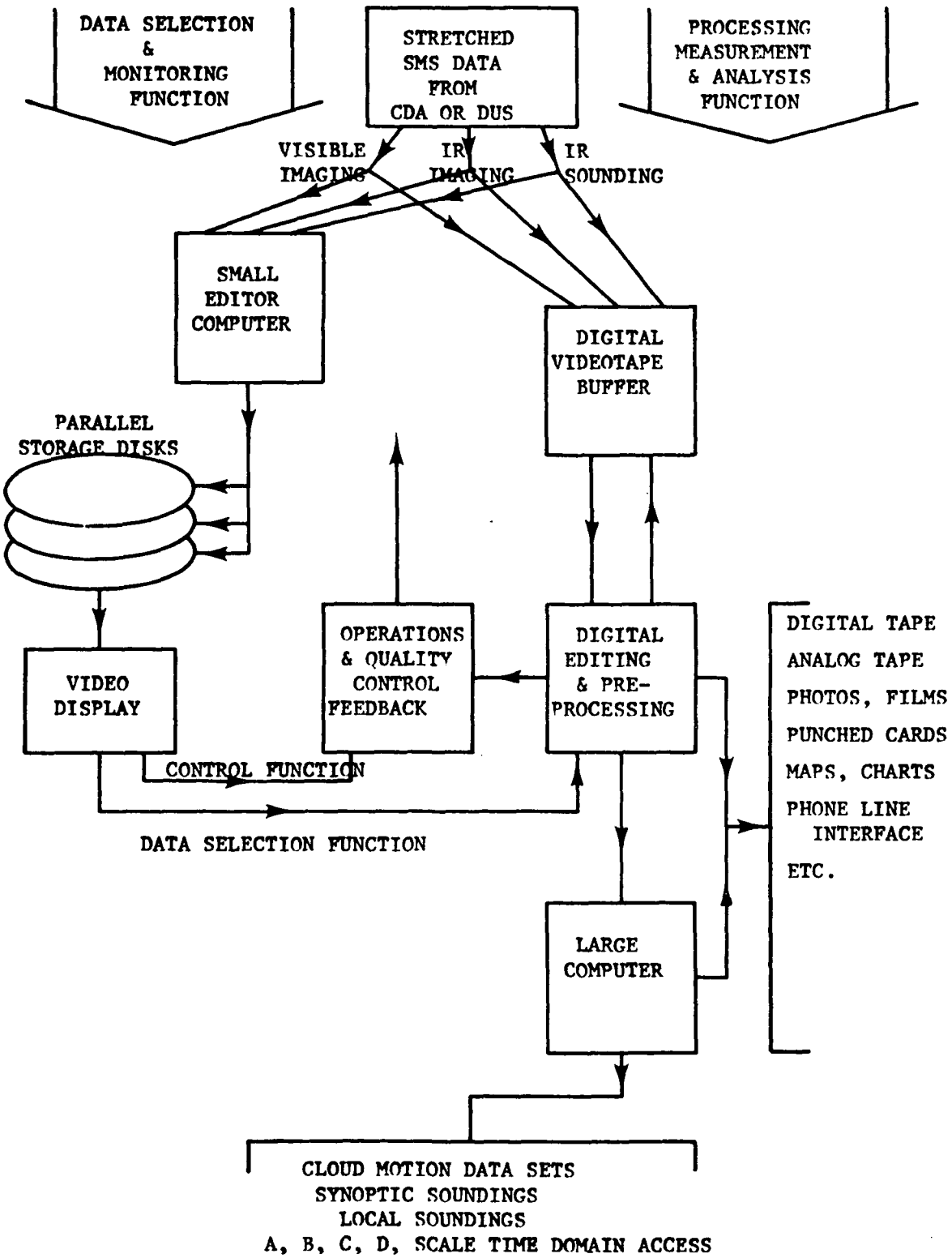

Figure 33. An expanded McIDAS system for SMS sounder data handling.

REFERENCES

Aldrich, N. C. and B. L. Musicant, November 1970: "Infrared Photodetectors (15.5 Micron Mercury Cadmium Telluride Photodetectors for Operation at 105°K)." Honeywell Radiation Center, Lexington, Massachusetts.

Baker, M. L. and V. L. Yen, August 1967: "Effects of the Variation of Angle of Incidence and Temperature on Infrared Filter Characteristics." Applied Optics, Vol. 6, No. 8, pp. 1343.

Blackman, R. B. and J. W. Tukey, January 1958: "The Measurement of Power Spectra from the Point of View of Communications Engineering," Part 1. The Bell System Technical Journal, Vol. 37, No. 1, p. 185.

Coburn, A. R., 15 March 1970: "Three Dimensional Nephanalysis." AFGWC Technical Memorandum, p. 70-79.

Collins, R. J. and H. Y. Fan, 15 February 1954: "Infrared Lattice Absorption Bands in Germanium, Silicon, and Diamond." Physical Review, Vol. 93, No. 4.

Conrath, B. J., R. A. Hanel, V. G. Kunde and C. Parbhakara, 1970: "The Infrared Interferometer Experiment in Nimbus 3." J. Geophys. Res. Vol. 75 (30), p. 5831.

Fujita, T. and H. Grandoso, November 1967: "A Proposed Method of Estimating Cloud-Top Temperature, Cloud Covers, Emissivity, and Cloudness From Short- and Long-wave Radiation Data Obtained by Medium-Resolution Scanning Radiometers." SMRP Research Paper No. 48, University of Chicago.

Jastrow, R. and M. Halem, June 1970: "Simulation Studies Related to GARP." Bull. Am. Meteor. Soc., Vol. 51, No. 6, p. 490.

Shenk, W. E. and V. V. Salomonson, 1970: "A Multispectral Technique to Determine Sea Surface Temperature Using Nimbus 2 Data." Goddard Space Flight Center, Greenbelt, Maryland.

Shenk, W. E. and V. V. Salomonson, 1971: "A Simulation Study Exploring the Effects of Sensor Spatial Resolution on Estimates of Cloud Cover from Satellites," NASA TN D-6247.

Smith, W. L., 1969: "The Improvement of Clear Column Radiance Determination with a Supplementary 3.8μ Window Channel." NESC TM 16.

Smith, W. L., P. K. Rao, R. Koffler and W. R. Curtis, August 1970: "The Determination of Sea-Surface Temperature from Satellite High Resolution Infrared Window Radiation Measurements." Monthly Weather Review, Vol. 98, No. 8, p. 604.

Stamm, A. J. and T. H. Vonder Haar, June 1970: "A Study of Cloud Distributions Using Reflected Radiance Measurements from the ATS Satellites." J. Appl. Meteor., Vol. 9, No. 3, p. 498.

Wark, D. O., August 1970: "SIRS: An Experiment to Measure the Free Air Temperature from a Satellite." Applied Optics, Vol. 9, No. 8, p. 1761.

ACKNOWLEDGEMENTS

The authors of this report are pleased to recognize supporting contributions to this effort by other members of the SSEC staff. Excellent technical support was given by Professor R. J. Parent, who made many useful suggestions and criticisms. Able programming support came from Ralph DeDecker and Subhash Dandage.

For their efforts in preparation of the final manuscript, special thanks go to Tony Wendricks for drafting work, to David Cadle for photographic reproductions, and to Debbie Czerwonka who typed the preliminary and final versions of the text.